NASA Contractor Report 179594

# LIFE PREDICTION AND CONSTITUTIVE MODELS FOR ENGINE HOT SECTION ANISOTROPIC MATERIALS PROGRAM

Second Annual Status Report

G.A. Swanson, I. Linask, D.M. Nissley,
P.P. Norris, T.G. Meyer, and K.P. Walker

Contract NAS3-23939
April 1987



NASA

TABLE OF CONTENTS

TABLE OF CONTENTS (continued)

LIST OF ILLUSTRATIONS

LIST OF ILLUSTRATIONS (continued)

LIST OF ILLUSTRATIONS (continued)

LIST OF ILLUSTRATIONS (continued)

LIST OF ILLUSTRATIONS (continued)

LIST OF TABLES

LIST OF TABLES (continued)

# SECTION 1.0

# INTRODUCTION

One of the more important recent developments in gas turbine blade materials has been the introduction of directionally solidified and single crystal castings. Among the advantages of these materials are:

- Substantially increased high temperature creep and stress rupture strengths and enhanced oxidation/corrosion resistance due to the elimination of grain boundaries
- Increased low cycle fatigue life because the elastic modulus in the direction of solidification is lowered and thermally induced stresses are reduced
- Higher melting temperature and greater heat treatment flexibility resulting from the elimination of grain boundary strengthening elements.

This casting process has matured to the level where it is now routinely used in the production of commercial and military aircraft jet engine turbine blades. Unfortunately, metallurgical and processing advances have not been matched by corresponding advancements in the knowledge and understanding of the mechanics of these materials, their failure mechanisms, and methods for life predictions. In order to realize the full potential of these materials, it is necessary to have a complete knowledge of the full envelope of life limiting parameters. Anisotropy introduces many life prediction questions especially for stresses which are not parallel to the direction of solidification. Oxidation resistant coatings add another layer of complexity to these questions. All of these issues are addressed in this NASA Hot Section Technology (HOST) program.

The program consists of a base program which covers a duration of 42 months, and two optional programs which are to be exercised at the discretion of NASA. In the base program, a primary and alternative coated single crystal material, operating at relevant turbine airfoil temperatures, are being investigated. In Option 1 which has been exercised by NASA, the same two single crystal materials, in an uncoated condition and operating at root attachment temperatures and notched conditions, will be studied. In Option 2 a directionally solidified or recrystallized material, in coated and uncoated conditions, would be studied at temperatures occurring at the airfoil and root attachment, respectively.

In the base and optional programs, candidate constitutive and life prediction models are being developed concurrently. Laboratory specimens, which will be tested under a variety of mechanical and thermal load histories, will provide data for the final model selections. The models will be incorporated into a computer code which will be checked for operability on a representative turbine blade section.

The first year effort of the contract involved materials selection, specimen preparation, basic material tests, literature searches of appropriate constitutive and life prediction models, initial formulation of constitutive models, and initial constitutive and fatigue tests. The results of the first year effort are reported in the First Annual Status Report, NASA CR-174952 (Reference 1).

The results of the second year effort are presented in this report. During this period, constitutive tests of the overlay coating and the primary single crystal material were continued. Previously selected candidate constitutive models were evaluated using the data. For the coating, two models which include a back stress formulation were continued for further development. For the single crystal, development of "microscopic" and "macroscopic" constitutive models are in the final stages.

Level I fatigue tests of coated single crystal specimens were completed and Level II tests started. The tests are designed to provide data for initial evaluation and development of life prediction models respectively. Coating cracking data were obtained along with specimen life data. Initial evaluation of life prediction models was conducted.

During the following year, development of the constitutive models will continue with emphasis on applicability to thermomechanical fatigue conditions. Level II tests will be continued in order to increase the life prediction data bases. Evaluation and development of life prediction models for the coating and single crystal material will be conducted using the data.

## SECTION 2.0

## TASK I - MATERIAL/COATING SELECTION AND ACQUISITION

PWA 1480 and Alloy 185 were previously selected as the primary and secondary single crystal materials respectively to be evaluated in this program (Reference 1).

PWA 1480 was the first superalloy specifically designed for use in single crystal form and was developed with the goal of achieving an optimum balance of creep strength, thermal fatigue strength, and oxidation and hot corrosion resistance. PWA 1480 is the most widely used single crystal alloy in gas turbine engines today and the most advanced turbine airfoil material utilized in Pratt & Whitney production engines. PWA 1480 was certified for commercial use in the JT9D-7R4D/E engine in late 1981 and has since been certified for use in the JT9D-7R4G/H, PW2037 and PW4000 engines.

Two heats of PWA 1480 were procured for this program from the Howmet Turbine Components Corporation, Alloy Division, Dover, New Jersey. The primary heat, identified by Howmet as 200A14824, has been designated P9866. The secondary heat, identified by Howmet as 200B14773, has been designated P9867.

Alloy 185 exhibits greater creep anisotropy than PWA 1480 as a result of its higher hardener content compared to PWA 1480 and different structure. Consequently, its selection as the secondary single crystal material makes possible testing the range of applicability of the constitutive and life prediction models developed in this program (Reference 1).

A single heat of Alloy 185 was procured for this program from the Howmet Corporation, Alloy Division. This heat, identified by Howmet as 242A15847, has been designated P9921.

Nominal compositions for PWA 1480 and Alloy 185 along with actual compositions of the procured heats are listed in Table I.

The directional solidification casting process was employed to cast cylindrical single crystal bars of both selected alloys with nominal 15.2 cm (6.0 in) length and 2.54 cm (1.0 in) and 1.59 cm (0.625 in) diameters. The primary growth direction was controlled to produce <001>, <111>, <011> and <123> oriented bars. The castings were solution heat treated, followed by a rigorous evaluation to ensure that only quality castings are used for specimen fabrication (Reference 1).

Two coatings were selected for this program to be representative of those employed on actual turbine blades operating in gas turbine engines: PWA 286 overlay coating and PWA 273 outward diffusing aluminide (Reference 1). The general coating compositions and application processes are summarized in Table II. Typical microstructures are illustrated in Figure 1.

Table I

Single Crystal Superalloys

| Alloy | Heat Code | Alloy Composition (Weight Percent) Elements Ni | Cr | Co | Ti | Al | Ta | W | Mo | C |
|---|---|---|---|---|---|---|---|---|---|---|
| PWA 1480 | Nominal | Bal* | 10.0 | 5.0 | 1.5 | 5.0 | 12.0 | 4.0 | -- | -- |
| | P9866 (Heat A) | Bal* | 10.35 | 5.5 | 1.44 | 4.95 | 12.2 | 3.9 | -- | 0.01 |
| | P9867 (Heat B) | Bal* | 10.3 | 5.3 | 1.44 | 4.9 | 10.2 | 4.0 | -- | 0.004 |
| Alloy 185 | Nominal | Bal* | -- | -- | -- | 6.8 | -- | 6.0 | 14.0 | 0.04 |
| | P9921 | Bal* | -- | -- | 0.001 | 6.82 | -- | 6.10 | 13.85 | 0.04 |

*Balance

Table II

Coating Compositions and Application Processes

| Coating | Type | Composition | Deposition Process |
|---|---|---|---|
| PWA 286 | Overlay | NiCoCrAlY+Si+Hf | Vacuum Plasma Spray |
| PWA 273 | Aluminide (Outward Diffusion) | NiAl | Pack Cementation |

(A)

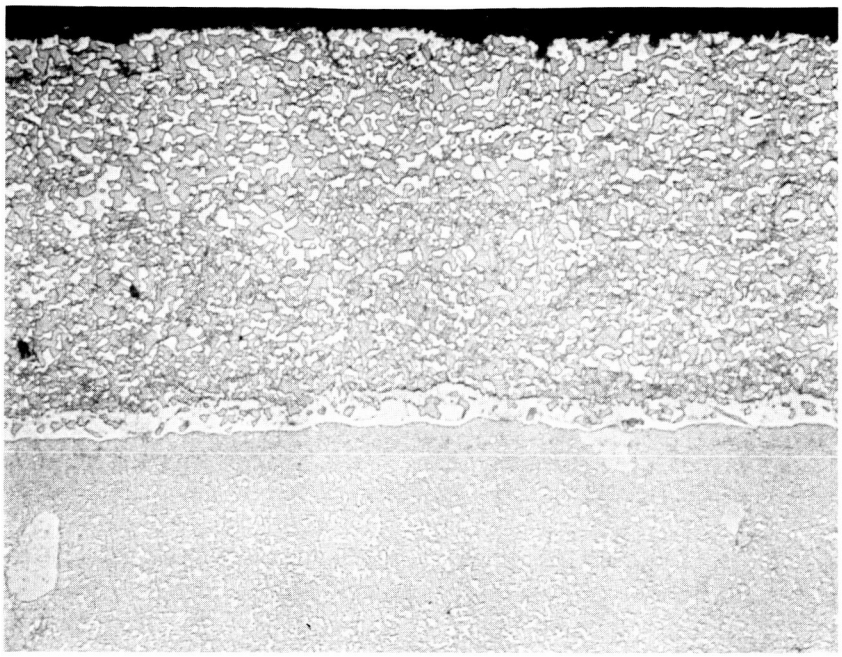



(B)

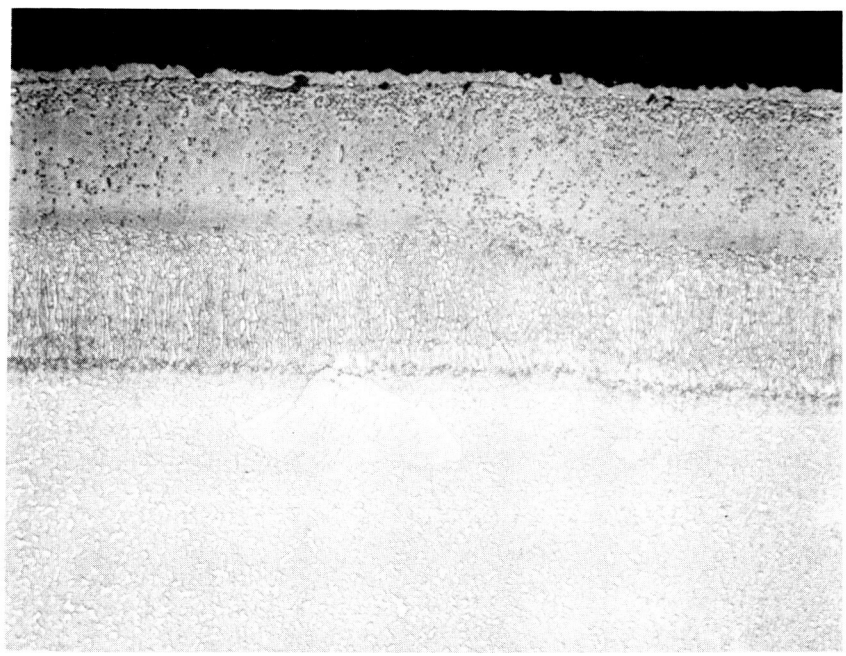

Figure 1 Typical Micrographs of: (A) PWA 286 Overlay Coating, and (B) PWA 273 Diffusion Coating Illustrating the Microstructural Differences Between the Coatings. Note the small interdiffusion zone associated with the overlay coating compared to that of the diffusion coating. The substrate is PWA 1480. (500X Mag., Etchant: Mixed Acids)

## 2.1 PRIMARY ALLOY (PWA 1480) AND COATING SPECIMEN FABRICATION

### 2.1.1 PWA 1480 Material Specimens

Fatigue test specimen geometries were chosen to allow conditions comparable to those found in actual turbine blades to be produced during testing. Figure 2 schematically illustrates the geometries for the hollow tube LCF/TMF (low cycle fatigue/thermomechanical fatigue) specimens. To take full advantage of the MTS external extensometer (see Section 4.3), a ridgeless specimen (Figure 2B) was developed to replace the internally ridged specimen (Figure 2A) previously employed for LCF tests at Pratt & Whitney. Most of Level I fatigue test specimens were fabricated during the previous year. This year, the remainder of Level I and over half of the Level II fatigue test specimens were machined from 2.54 cm (1.0 in) diameter bars. For fatigue testing, the specimens are coated using the standard methods listed in Table II. Complete current status of fatigue specimen fabrication is summarized in Table III.

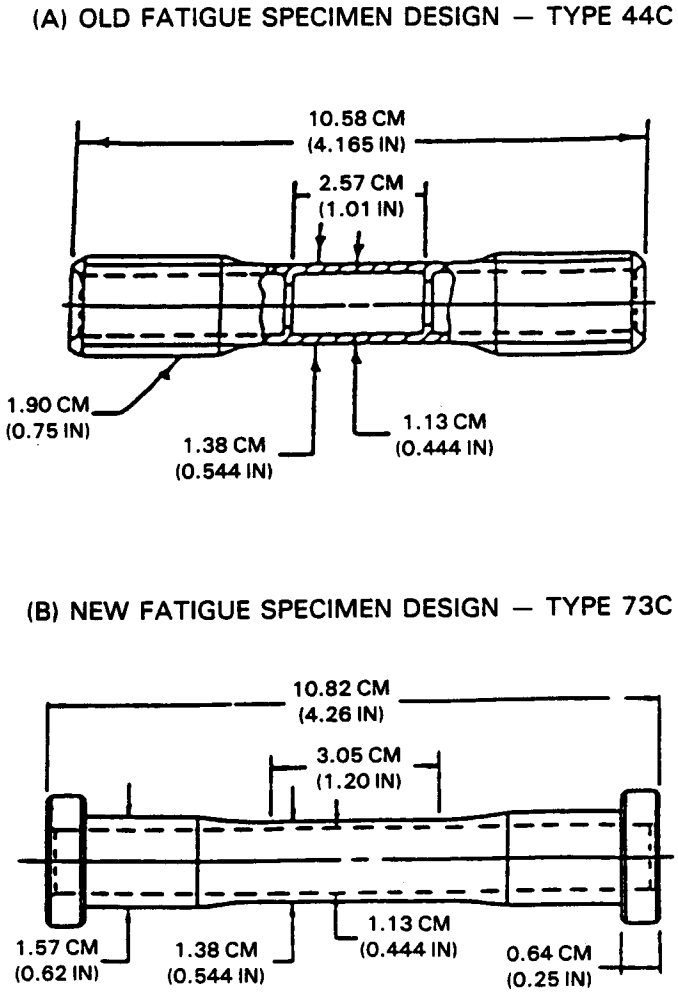


Figure 2 Geometries of Tubular Specimens for Fatigue Testing

Table III

Number of PWA 1480 Fatigue Test Specimens
Fabricated to Date

| Type of Specimen | Coating | Number of Specimens <Orientation> <001> | <111> | <011> | <123> |
|---|---|---|---|---|---|
| Type 44c Fatigue (a) | PWA 286 | 12 | - | - | - |
| | PWA 273 | 12 | - | - | - |
| Type 73c Fatigue (a) | Uncoated* | 12 | 12 | 2 | 2 |
| | PWA 286* | 0 | 0 | 0 | 0 |
| | PWA 273* | 0 | 12 | 0 | 0 |
| | PWA 286** | 30 | 23 | 15 | 15 |
| | PWA 273** | 30 | 12 | 15 | 15 |
| Total Specimens | | 96 | 59 | 32 | 32 |

Notes: * : Ready for test
** : Being coated
(a) : See Figure 2 and Section 4.3

All of the PWA 1480 specimens for physical, thermal, monotonic tensile and creep, and cyclic constitutive testing were fabricated during the previous year (Reference 1).

2.1.2 PWA 286 and PWA 273 Coating Specimens

Test specimens of PWA 286 overlay coating were fabricated to simulate the coating material structure on airfoils (Reference 1). In actual airfoils, the PWA 286 coating is applied by a vacuum plasma spray process followed by shot peening and heat treatment. In order to use bulk specimens of the coating material to determine constitutive properties of actual PWA 286 coating, tensile specimens were fabricated by two processes. In the first process, a billet of coating material was formed from coating powder by hot isostatic pressing (HIP) and then machined into cylindrical specimens (Figure 3A). In the second process, thick layers of coating material were vacuum plasma sprayed onto PWA 1480 flat strips. The PWA 1480 was subsequently removed and a flat overlay specimen machined. Shot peening was not applied since peening would only affect a thin surface layer and leave the bulk of the specimen cross section unaffected. The specimen resulting from the second process is shown in Figure 3B.

(A) TENSILE, RELAXATION, AND STRESS-RUPTURE SPECIMEN
FABRICATED FROM HOT ISOSTATICALLY PRESSED POWDER

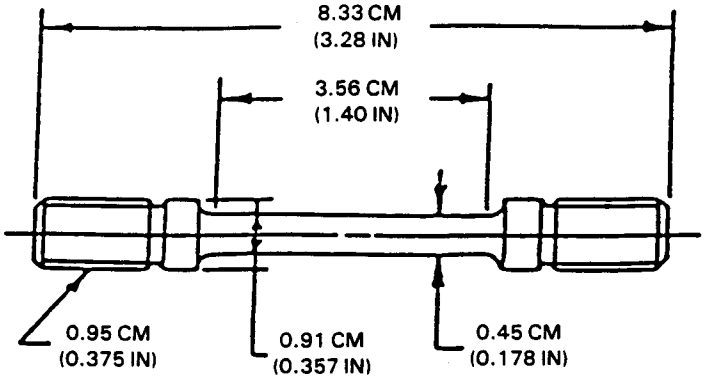


(B) TENSILE, RELAXATION, AND STRESS-RUPTURE SPECIMEN
FABRICATED FROM PLASMA SPRAYED SHEETS

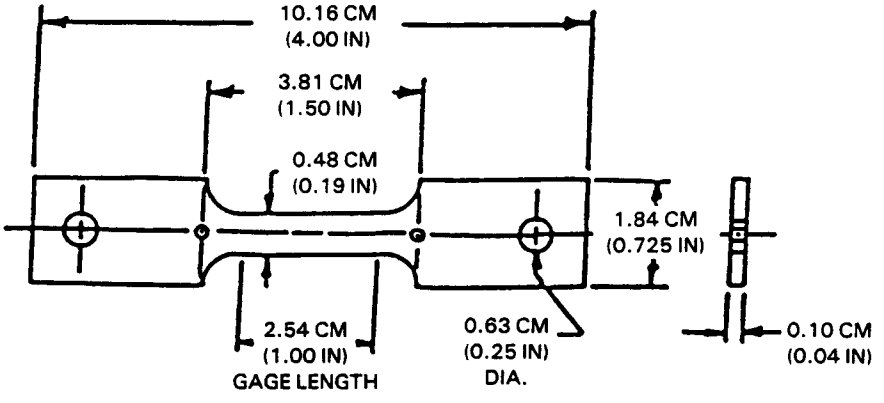


Figure 3 Specimen Designs for Bulk PWA 286 Coating Material Mechanical Property Tests

Photomicrographs of coating structure in both types of specimens are presented in Figure 4. It should be noted that the different porosity levels obtained in the two specimens bracket the porosity of overlay coatings on actual airfoils (Figure 1): the HIP specimen contains virtually no porosity, while the unpeened thick plasma spray specimen contains a high level of porosity (Reference 1).

The structure of diffusion coatings is much more complex than that of overlay coatings. The diffusion coating chemistry and microstructure vary from the coating surface to the substrate (Figure 1) because of interdiffusion between the coating material and the substrate during the coating process, and, as a result, mechanical properties could not be effectively determined using a homogeneous bulk specimen.

Therefore, flat test specimens for PWA 273 coating constitutive tests were fabricated by forming the actual coating on both sides of very thin strips of PWA 1480 substrate material. For this, five specimen strips were machined from each 2.54 cm (1.0 in) diameter PWA 1480 bar used (from master heat P9867). The specimen strips were aligned so that the transverse direction is parallel to a secondary <001> direction. Two different gage thicknesses were used for the substrate strip gage sections: 0.25 mm (0.010 in) and 0.13 mm (0.005 in) as shown in Figure 5. Due to the fragile nature of these specimens, a special support fixture was constructed to hold the specimens during the PWA 273 coating process and subsequent diffusion heat treatment at 1079°C (1975°F) and aging at 871°C (1600°F). The 0.25 mm (0.010 in) thick specimens exhibited sufficient strength when handled in the fixture. Twelve of these specimens were fabricated and are ready for test. However, the 0.13 mm (0.005 in) thick specimens deformed during the diffusion heat treatment even when held in the fixture. Additional specimens are being fabricated.

The microphotographs in Figure 6 show the structure of the completed flat specimens. The 0.25 mm (0.010 in) initial substrate thickness reduces to 0.14 mm (0.0055 in) after coating, while the 0.13 mm (0.005 in) initial thickness reduces to only 0.02 mm (0.0008 in) remaining substrate.

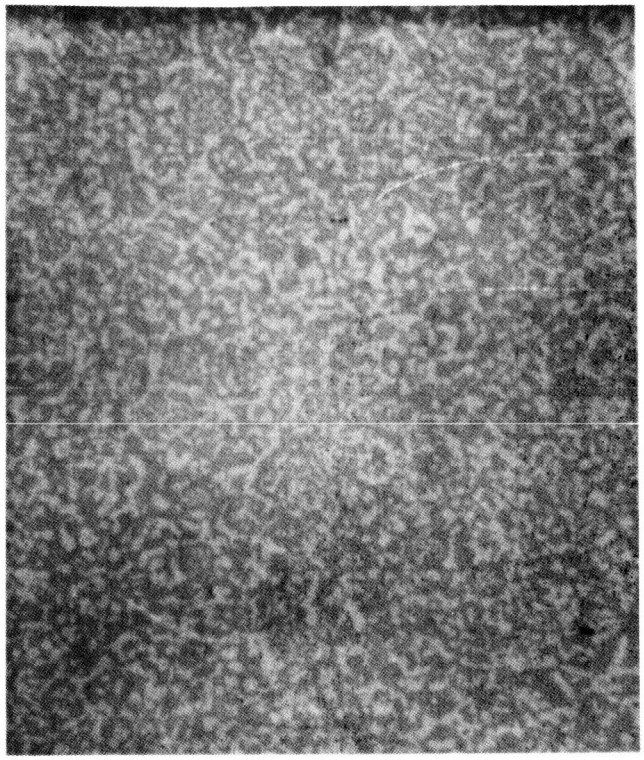

(A) HOT ISOSTATICALLY PRESSED (HIP) SPECIMEN

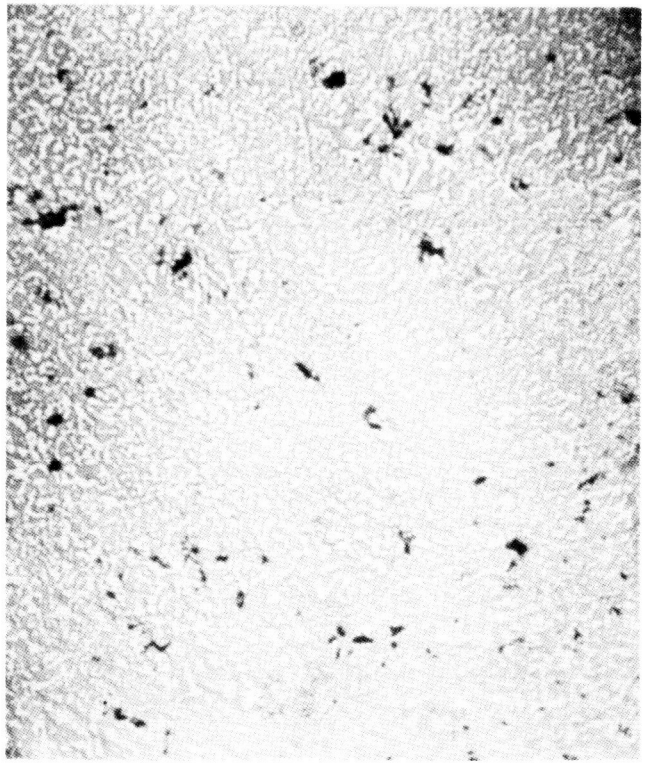

(B) LOW PRESSURE PLASMA SPRAY (LPPS) SPECIMEN

Figure 4 PWA 286 Bulk Specimen Microstructure

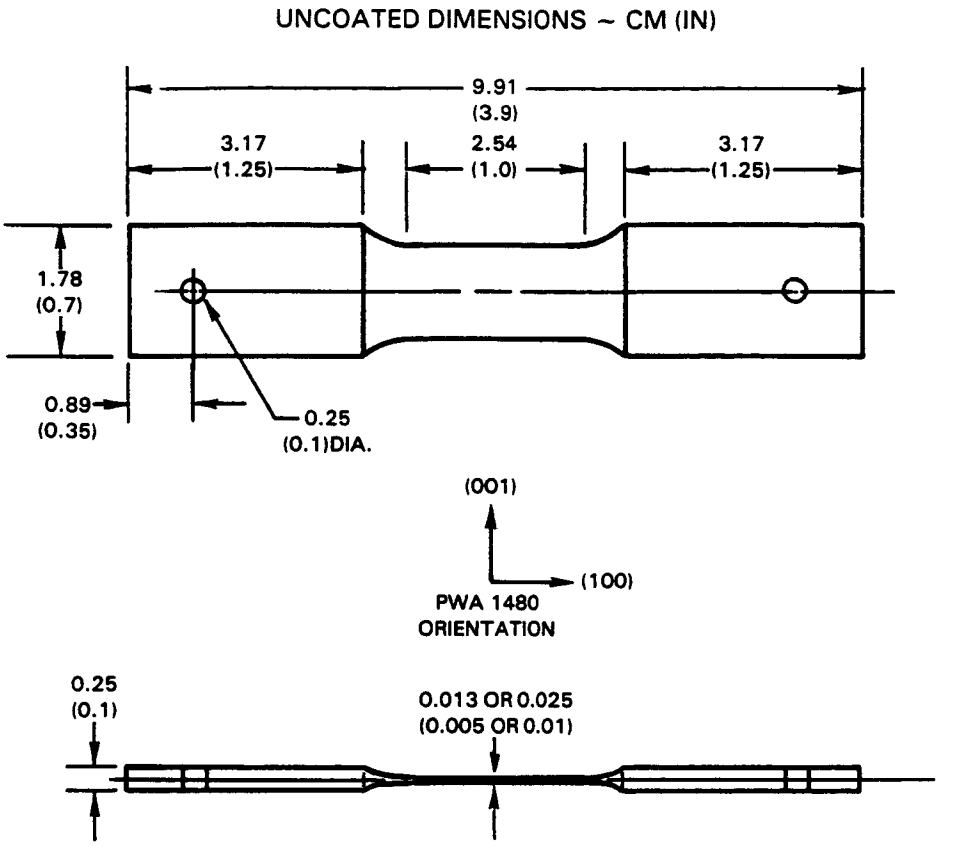


Figure 5 Substrate Design for Diffused Aluminide Coating Mechanical Property Tests

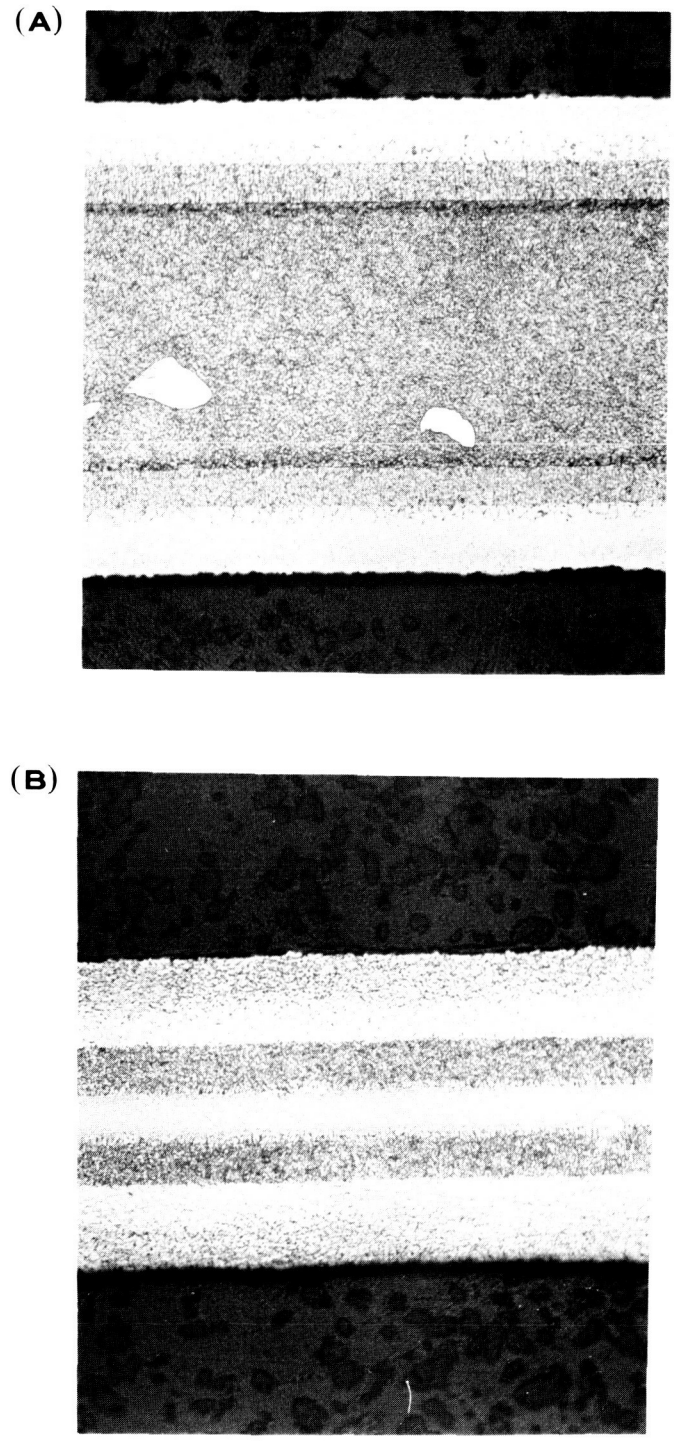


Figure 6 Microstructure of PWA 273 Coated Difference Method Specimens with (A) 0.25 mm (0.010 in) and (B) 0.13 mm (0.005 in) Original PWA 1480 Substrates. The center bands represent the remaining substrate after coating. (250X Mag., Etchant: Mixed Acids)

## 2.2 ALTERNATE SINGLE CRYSTAL MATERIAL (ALLOY 185) SPECIMEN FABRICATION

As with PWA 1480, 2.54 cm (1.0 in) and 1.59 cm (0.625 in) diameter bars of Alloy 185 have been cast using the single crystal directional solidification process. The bars were heat treated at 1316°C (2400°F) followed by a forced gas cool to refine and homogenize the gamma prime hardener without the onset of incipient melting. The same inspection procedure as used for PWA 1480 cast bars was employed to ensure the quality of the Alloy 185 castings used for specimen fabrication. Table IV lists the acceptable Alloy 185 bars cast to date.

Table IV

Number of Acceptable Alloy 185 Cast Bars

| Orientation | <001> | <111> | <011> | <123> |
|---|---|---|---|---|
| 2.54 cm (1.0 in) diameter bars | 16 | 7 | 14 | 0 |
| 1.59 cm (0.625 in) diameter bars | 19 | 2 | 17 | 15 |

## 2.3 PHYSICAL, THERMAL AND MONOTONIC MECHANICAL PROPERTIES

Thermal-physical and monotonic mechanical property tests of PWA 1480 single crystal material and the two selected coatings (PWA 273 diffused aluminide and PWA 286 overlay) have been completed. Additional testing is planned to determine three-dimensional elastic constants for PWA 1480.

### 2.3.1 Thermal-Physical Properties

The thermal-physical properties of PWA 1480 single crystal material, unlike mechanical properties, are isotropic. Therefore, measurements are required only for a single orientation.

Thermal-physical property tests for <001> oriented PWA 1480, PWA 273 and PWA 286 were conducted at Southern Research Institute. Thermal conductivity, thermal expansion, specific heat and density property data were obtained and are included in Appendices A and B. Property curves based on the data are presented in Figures 7 through 9, respectively.

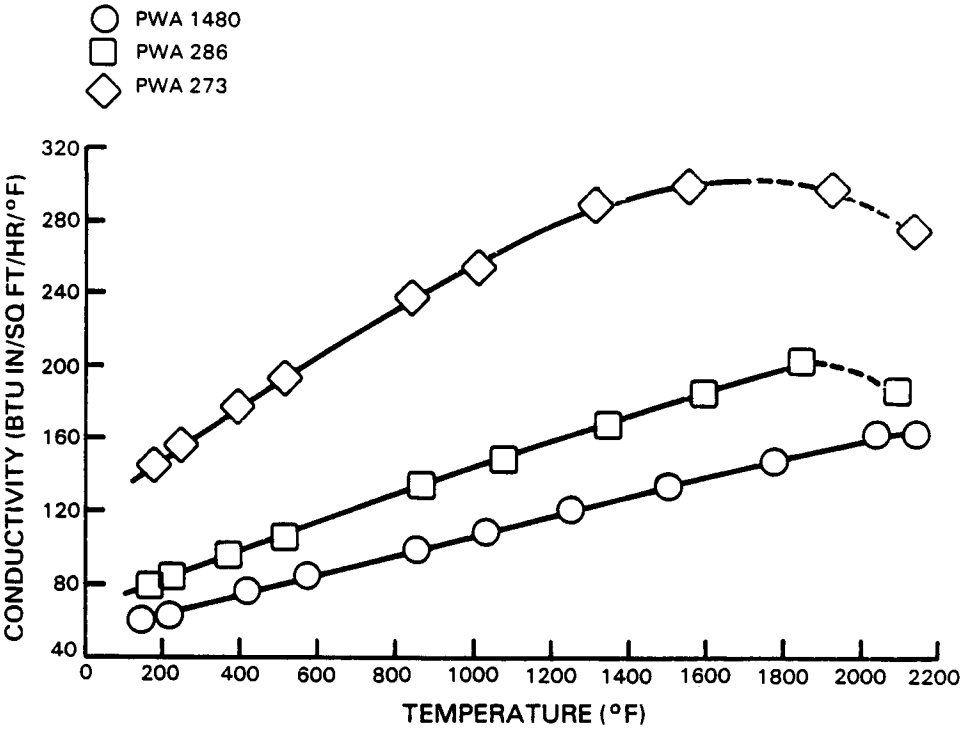


Figure 7 Measured Thermal Conductivity of PWA 273, PWA 286 and PWA 1480

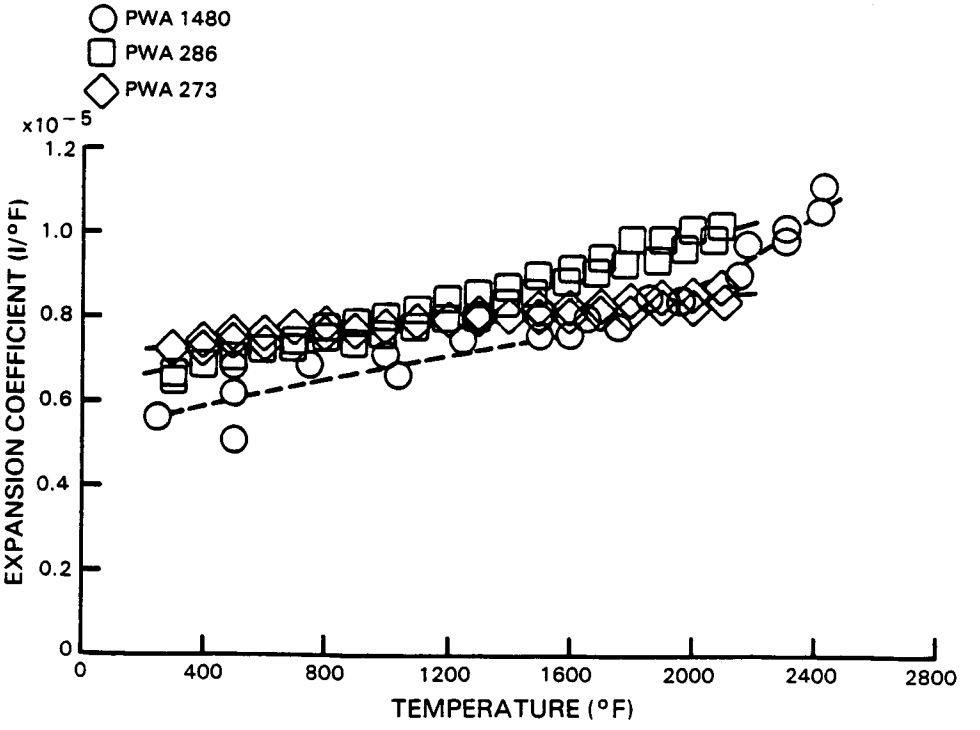


Figure 8 Mean Coefficient of Linear Thermal Expansion for PWA 273, PWA 286 and PWA 1480

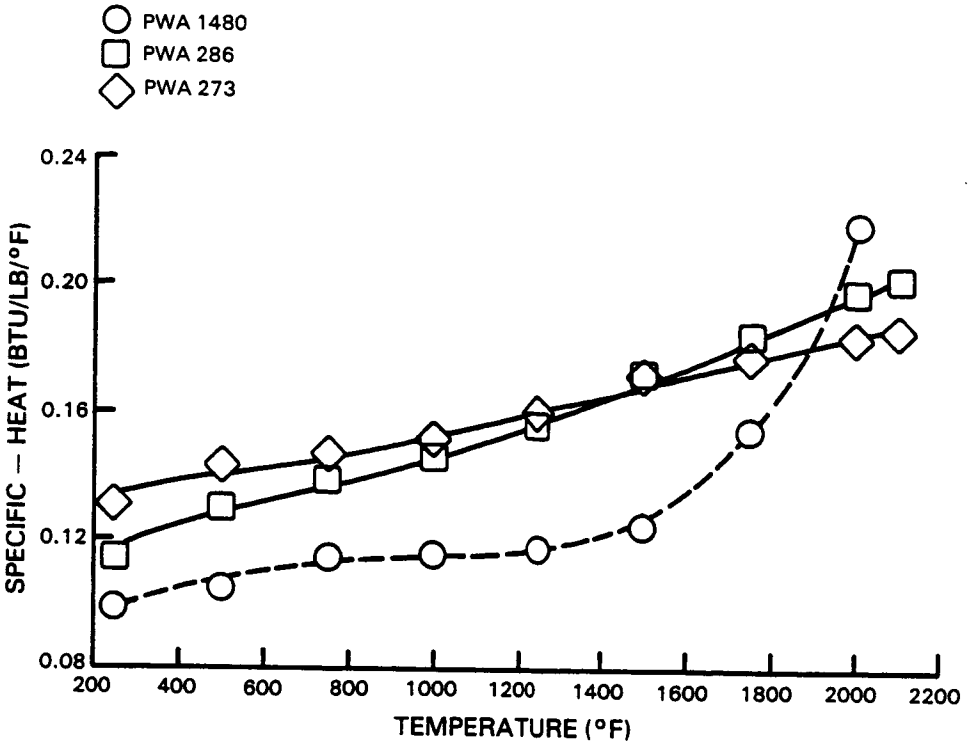


Figure 9 Measured Specific Heat of PWA 273, PWA 286 and PWA 1480

2.3.2 Tensile Properties

A total of 40 monotonic tensile tests were conducted on PWA 1480 single crystal specimens with orientations of <100>, <110>, <111> and <123>. All tests were run at the American Society for Testing Materials (ASTM) standard strain rate of 0.005 $min^{-1}$. Tests included uncoated and aluminide diffusion and NiCoCrAlY overlay coated <100> and <111> oriented specimens. A summary of all test conditions and observed material properties is presented in Reference 1.

2.3.3 Creep Properties

2.3.3.1 Creep Properties of PWA 1480 Single Crystal

A total of 40 monotonic creep tests were conducted on PWA 1480 single crystal specimens with orientations of <100>, <110>, <111> and <123>. Tests were run at constant temperature and load conditions, and included uncoated and aluminide diffusion and NiCoCrAlY overlay coated specimens. The test results are summarized in Table V.

2.3.3.2 Creep Properties of PWA 286 Overlay Coating

Monotonic creep tests of the overlay coating were previously conducted, and the test results are presented in Reference 1.

# Table V

## PWA 1480 Monotonic Creep Data

| Temperature °C (°F) | Spec. ID | Orient. | Coat Type | Stress MPa | (ksi) | % of 0.2% Yield | Life (hours) | Creep Rate (minutes)$^{-1}$ | Elong. (%) | RA (%) |
|---|---|---|---|---|---|---|---|---|---|---|
| 871 (1600) | JA-40 | <001> | -- | 413.7 | (60) | 57.8 | 462.9 | 8.84E-07 | 12.0 | 20.1 |
| | JA-41 | | -- | 517.1 | (75) | 72.3 | 79.0 | 8.82E-06 | 15.3 | 28.9 |
| | KA-10 | <011> | -- | 413.7 | (60) | 52.6 | 330.7 | 7.33E-07 | 3.2 | 1.6 |
| | KA-11 | | -- | 482.6 | (70) | 61.4 | 83.5 | 3.79E-06 | 3.2 | 4.6 |
| | MA-10 | <123> | -- | 413.7 | (60) | 66.0 | 167.1 | 4.66E-06 | 7.5 | 9.7 |
| | MA-11 | | -- | 482.6 | (70) | 77.1 | 42.6 | 3.22E-05 | 15.5 | 19.1 |
| | LA-56 | <111> | -- | 413.7 | (60) | 59.4 | 373.7 | 4.18E-07 | 13.0 | 16.7 |
| | LA-57 | | -- | 482.6 | (70) | 69.3 | 67.1 | 2.90E-05 | 14.9 | 22.8 |
| 982 (1800) | JA-42 | <001> | -- | 220.6 | (32) | 48.8 | Stopped at 5.4 hours for TEM[1] | | | |
| | JA-27 | | 273[2,3] | 231.7 | (33.6) | 53.0 | 89.1 | 3.94E-06 | 25.2 | 44.2 |
| | JA-15 | | 286[2,4] | 237.9 | (34.5) | 55.5 | 105.5 | 3.65E-06 | 20.0 | 42.3 |
| | JA-45 | | -- | 248.2 | (36) | 54.9 | 80.5 | 4.74E-06 | 20.7 | 41.4 |
| | JA-28 | | 273[2,3] | 260.6 | (37.8) | 59.6 | 53.3 | 8.74E-06 | 24.3 | 40.6 |
| | JA-17 | | 286[2,4] | 268.2 | (38.9) | 62.5 | 51.7 | 8.48E-06 | 20.7 | 36.3 |
| | KA-14 | <011> | -- | 248.2 | (36) | 47.7 | 75.4 | 1.79E-06 | Failed outside gage | |
| | KA-13 | | -- | 248.2 | (36) | 47.7 | 88.7 | 1.31E-06 | 8.6 | 39.8 |
| | MA-12 | <123> | -- | 206.9 | (30) | 63.8 | 277.1 | 5.87E-07 | 23.5 | 57.4 |
| | MA-13 | | -- | 248.2 | (36) | 76.6 | 76.6 | 3.12E-06 | 23.5 | 33.1 |
| | LA-58 | <111> | -- | 220.6 | (32) | 51.6 | 678.6 | 9.37E-07 | 17.1 | 19.9 |
| | LA-30 | | 273[2,3] | 230.5 | (33.4) | 53.9 | Stopped at 17.3 hours for TEM[1] | | | |
| | LA-20 | | 286[2,4] | 239.7 | (34.8) | 56.2 | 274.6 | 3.61E-06 | 17.5 | 24.1 |
| | LA-59 | | -- | 248.2 | (36) | 58.1 | 258.1 | 3.58E-06 | 12.9 | 17.2 |
| | LA-31 | | 273[2,3] | 259.6 | (37.6) | 60.7 | 156.3 | 9.06E-06 | 19.6 | 22.4 |
| | LA-21 | | 286[2,4] | 266.0 | (38.6) | 62.3 | Stopped at 44.8 hours for TEM[1] | | | |
| 1093 (2000) | JA-46 | <001> | -- | 117.2 | (17) | 42.6 | 132.2 | 9.24E-07 | 13.2 | 49.5 |
| | JA-48 | | -- | 117.2 | (17) | 42.6 | 137.1 | 9.03E-07 | 16.1 | 50.9 |
| | JA-29 | | 273[2,3] | 108.5 | (15.7) | 39.4 | Stopped at 29.8 hours for TEM[1] | | | |
| | JA-18 | | 286[2,4] | 112.9 | (16.4) | 41.1 | 223.9 | 5.73E-07 | 13.5 | 48.2 |
| | JA-30 | | 273[2,3] | 123.1 | (17.8) | 44.7 | 76.4 | 2.97E-06 | 20.6 | 58.1 |
| | JA-19 | | 286[2,4] | 297.4 | (43.1) | 108.1 | Stopped at 0.4 hour for TEM[1] | | | |
| | KA-15 | <011> | -- | 89.6 | (13) | 28.4 | 197.6 | 7.70E-08 | 2.7 | 4.9 |
| | KA-16 | | -- | 103.4 | (15) | 32.8 | 138.7 | 3.02E-07 | 6.0 | 30.3 |
| | MA-14 | <123> | -- | 89.6 | (13) | 32.9 | 251.2 | 3.29E-07 | 11.9 | 37.1 |
| | MA-17 | | -- | 103.4 | (15) | 37.9 | 130.7 | 6.59E-07 | 14.0 | 19.8 |
| | LA-60 | <111> | -- | 89.6 | (13) | 34.5 | 825.7 | 2.38E-07 | 13.0 | 17.0 |
| | LA-32 | | 273[2,3] | 144.6 | (21) | 55.7 | 83.2 | Not available | 12.0 | 17.1 |
| | LA-22 | | 286[2,4] | 111.0 | (16.1) | 42.7 | Stopped at 132.3 hours for TEM[1] | | | |
| | LA-61 | | -- | 103.4 | (15) | 39.8 | 372.4 | 1.81E-07 | Failed outside gage | |
| | LA-34 | | 273[2,3] | 180.8 | (26.2) | 69.5 | 14.6 | 4.05E-05 | 18.5 | 22.3 |
| | LA-23 | | 286[2,4] | 111.5 | (16.2) | 43.0 | 322.4 | 8.37E-07 | 9.6 | 19.7 |

Notes:

1. Transmission electron microscopy (TEM)
2. Cross sectional area used to calculate stresses excludes coating area
3. Aluminide diffusion
4. NiCoCrAlY overlay

# SECTION 3.0

# TASK II - SELECTION OF CANDIDATE LIFE PREDICTION AND CONSTITUTIVE MODELS

## 3.1 SELECTION OF CONSTITUTIVE MODELS FOR COATINGS AND SINGLE CRYSTAL MATERIALS

Basic to life prediction for any structural component is the description of local stress-strain histories which requires availability of good constitutive models. This is particularly true when predicting lives within the hot section of a gas turbine engine. As a gas turbine part is cycled through a wide range of stresses, strains and temperatures, deformation and damage accumulate by a variety of mechanisms both in the single crystal alloy base material and the coating, all of which could play an important role in the part's ultimate failure. It is the goal of constitutive modeling to predict this stress-strain history and, possibly, the damage history, so that the conditions at fatigue initiation are accurately known.

During the previous year, candidate constitutive models for the single crystal material and the overlay coating were selected for further evaluation (Reference 1). The selected models included:

1. Coatings

   a. Classical model (uncoupled plasticity and creep)
   b. Walker's model (unified viscoplastic behavior)
   c. Simplified Walker's model (no back stress term)
   d. Moreno's approach (hybrid model for Hastelloy X)
   e. Stowell equation (based on diffusion mechanism)

2. Single Crystal Material

   a. Classical Hill model (based on Von Mises yield function)
   b. Lee and Zaverl model (macroscopic viscoplastic model)
   c. Micromechanical Viscoplastic Formulation (extension of Walker's model to crystallographic deformation).

Detailed descriptions of these models and discussion of their selection are presented in Reference 1. The selection of candidate life prediction models is discussed in the following sections.

## 3.2 SELECTION OF LIFE PREDICTION MODELS

### 3.2.1 Literature Survey

In order to identify life prediction models which are applicable to coated anisotropic materials of gas turbine airfoils, a literature survey was conducted as part of the work reported in Reference 1. The survey resulted in an extensive listing of model concepts that have been used to match available data and meet the specific needs of individual investigators.

Three broad classes of life models are available: phenomenological, cumulative damage, and crack growth.

In general, all of the phenomenological models have the advantage of simplicity and a rather direct relationship to data bases. A drawback, however, is that they are not very amenable to accounting for significant interaction effects when different damage mechanisms (e.g., cyclic creep, fatigue) operate either simultaneously or sequentially as a result of complex high temperature loading patterns. The two most widely used methods in this group are the Coffin-Manson and Hysteretic Energy models.

The cumulative damage approaches assume that the plastic and creep components of inelastic strain cause damage which can be explicitly predicted and which define the state of the material. Damage is considered to be zero in the initial undamaged state and failure occurs when a critical level is reached due to plastic, cyclic creep or monotonic creep deformations. A number of different definitions of damage and approaches for counting damage are used. Nearly all of these require use of a constitutive model to determine the portion of damage caused by a particular load condition. Life prediction models which use this approach are: Linear Time and Cycle Fraction, Ductility Exhaustion, Continuous Damage, Strain Range Partitioning, and Cyclic Damage Accumulation.

A particularly attractive cumulative damage concept is that of Continuous Damage, one of several Damage Mechanics models, which considers damage as a material state variable defined on a differential increment basis. A major advantage of this method is the ability to integrate damage for arbitrary loading sequences including compression-tension differences, but a disadvantage is the complexity of defining damage properties for the materials. Similar advantages and disadvantages are also present for the crack growth models. However, the crack growth models clearly are better suited for predicting times to propagate previously initiated cracks to failure than for modeling crack initiation life in single crystal turbine airfoil materials.

Fatigue crack initiation in turbine airfoil materials almost always has been associated with different types of discontinuities in the microstructure. In conventional polycrystalline materials, the discontinuities could be brittle phases, grain boundaries, porosity or surface oxidation. In advanced anisotropic materials, the internal discontinuities are reduced or eliminated, and cracking tends to be increasingly surface initiated (Reference 1). It is widely recognized that crack initiation and propagation are different. However, the surveyed models are based on total life to failure or impending failure indicated by measured load drop; therefore, including both initiation and propagation portions of life.

Several of the existing models have successfully correlated limited data for coated and anisotropic materials tested under selected load cycles. The coatings are found to substantially affect cracking life, generally increasing lives at high temperatures but decreasing them at low temperatures.

A detailed discussion of the survey findings and individual model descriptions are presented in Appendix C of Reference 1.

### 3.2.2 Life Prediction Model Approach

As a result of the literature survey (Reference 1) and previous Pratt & Whitney experience and specimen tests conducted under this program (see Section 4.3.3), it has been concluded that coatings have a role equally important with that of the base material in turbine airfoil cracking.

Coatings, applied to the airfoil surfaces in order to provide high temperature oxidation protection, are found to serve as primary crack initiation sites at turbine operating conditions and are, therefore, a major determinant of cracking location and life. Although understanding of the structural behavior of coatings still is in the very early stages, coating cracking appears related to cyclic loading and inelastic deformations, similar to that of structural materials. The coatings can undergo substantial inelastic deformations even at moderately low strain levels, while the base materials remain nominally elastic. Base material cracks can subsequently develop from the coating crack and propagate to failure. Base material cracks are not initiated at these conditions without the presence of coating cracks or sufficiently large defects.

Base material cracking without coating cracks or defects can be experienced on coated single crystal specimens under very high cyclic stresses, sometimes employed to reduce testing times and lower costs of test programs. At sufficiently high stresses, macroscopic inelasticity is caused throughout the test specimen cross section, occasionally exhibiting visible slip bands on the specimen surface. This results in fatigue crack initiation along a specimen's crystallographic planes and early fracture. Examples of this type of cracking were observed in the present program in some strain controlled tests of <111> oriented specimens (see Section 4.3.3) incurring stress levels which approached the yield strength and were significantly higher than those normally present in turbine blades.

When sufficiently high strains are applied to specimens having limited ductility coatings (diffusion coatings at low temperatures), coating cracking similar to brittle fracture can occur. This type of failure also is usually not found in turbine blades.

The large variety of cracking modes that have been experienced on coated anisotropic material test specimens and component parts suggests that a complex life prediction approach is required to determine when such materials will fail due to fatigue. For coated surfaces, the approach must include the capability to account for coating cracking, coating affected cracking of the base alloy and crack propagation in the base alloy. Base material crack initiation is a competing failure mode to coating cracking and requires additional predictive capabilities. These include predicting crack initiation from three sources: macroscopic inelasticity, uncoated surface interaction with the environment, and microscopic defects.

The following overall life prediction approach is proposed:

$$N_f = N_C + N_{SC} + N_{SP} \quad (3\text{-}1)$$

or

$$= N_{SI} + N_{SP} \text{ (whichever is smaller)} \quad (3\text{-}2)$$

where $N_f$ = Total cycles to fail specimen or component

$N_C$ = Cycles to crack Coating, determined by coating properties and load history

$N_{SC}$ = Cycles to initiate Substrate (base alloy) crack at Coating crack

$N_{SI}$ = Cycles to Initiate Substrate (base alloy) crack due to macroscopic slip, oxidation effects or defects

$N_{SP}$ = Cycles to Propagate Substrate (base alloy) crack to failure.

In this program, cracking of coated single crystal materials operating at relevant turbine airfoil conditions is addressed.

### 3.2.3 Candidate Life Prediction Models

Coatings and single crystal materials differ not only in crystal structure (coatings are polycrystalline) but also in physical and mechanical properties. Accordingly, different candidate models have been selected for predicting the coating and base material portions of coated single crystal material cracking life.

Coatings:

Two candidate models for coating cracking life prediction have been selected for further evaluation. Since coatings are subject to significant inelastic strains during normal operating conditions, but remain sufficiently ductile to endure these strains, inelastic strain is considered to be a primary correlating parameter. Therefore, two of the selected models belong to the simple phenomenological model group. These are the Coffin-Manson model which relates life to inelastic strain and a Hysteretic Energy model, both assuming logarithmic relationships between life and a load parameter (Reference 1), as described below. An important requirement for these models is the ability to account for environmental degradation in the coatings.

Coffin-Manson:

$$\Delta e_{inel} \cdot N^B = C \quad (3\text{-}3)$$

Hysteretic Energy:

$$\Delta W_T \cdot N^P = C_1 \quad (3\text{-}4)$$

where $\Delta e_{inel}$ = inelastic strain range

$\Delta W_T$ = tensile hysteretic energy

N = cracking life, including cycle frequency correction for environmental exposure

B, P, C, $C_1$ = material constants.

Simple models are particularly appropriate for coating life prediction because structural modeling and experimental capabilities for coatings substantially lag those for structural materials. However, simple models have not always successfully predicted fatigue cracking under complex load cycles in past applications. This has been especially true for isotropic (polycrystalline) materials in high temperature fatigue for which Strain Range Partitioning (SRP) was developed (Reference 3). Because coatings in essence also are polycrystalline materials, SRP capabilities or similar capabilities of damage mechanics models must be considered if the simple phenomenological models are proven to be inadequate for correlating coating cracking data.

The increased modeling capabilities of complex life prediction models require obtaining specialized material property data. However, experimental capabilities for obtaining this data using free standing coating specimens have not yet been successfully demonstrated. The difficulties are: (1) fabricability of the coating specimens, and (2) compressive testing severely limited by buckling at elevated temperatures. Consequently, coating life properties must be determined using coated base alloy composite specimens, but this causes specimen deformations to be base alloy controlled and results in complex hysteresis loops for the coating. As a result, the required life relationships would have to be extracted from complex cycle results using regression analysis.

Single Crystal Materials:

In order to extend previously developed life prediction models of isotropic materials to anisotropic materials such as single crystals, a method to account for material orientation effects is required. Similar to the methods for single crystal constitutive modeling, both macroscopic and micromechanics approaches are possible. The macroscopic approach describes anisotropy effects in terms of bulk material properties which can be related to the applied load direction relative to crystallographic orientation. Use of this approach generally assumes that the initiating crack orientation is known, usually normal to the applied load direction, as indicated by previous Pratt & Whitney experience and data already obtained in this program. The micromechanics model utilizes material deformations at the slip level. The strains applied to the specimen are resolved into components along the individual slip directions which depend on the material orientation. Fatigue life can then be related to the resulting slip plane stresses and strains. In concept, this model could be used to predict cracking life as well as crack orientation.

A simplified form of the micromechanics approach was previously used by A. E. Gemma to correlate crack propagation lives for different orientations of PWA 1480 under thermomechanical loading. In these tests also, the cracks were propagating normal to the applied loads which were cycled out-of-phase with the temperature. It was assumed that, for each orientation, slip is equally distributed among the available octahedral slip directions of the face centered cubic crystal structure characteristic of nickel-base alloys (Reference 4).

A relatively simple life prediction method worthy of further evaluation is a modified Hysteretic Energy model, which has been previously used to correlate fatigue life data for PWA 1480 under limited load cycles and includes orientation accountability (Reference 5). Using a hysteretic energy term modified by macroscopic material properties and resolved octahedral normal stress, the model collapsed isothermal low cycle fatigue lives of <001> and <111> oriented specimens in the 427°C to 982°C (800°F to 1800°F) temperature range. The model is described as follows:

$$N = A \cdot \Delta W_n{}^{B} \tag{3-5}$$

where $\Delta W_n = \Delta W_T \cdot \sigma_{oct}/E_{load}$ (3-6)

$\Delta W_T$ = tensile hysteretic energy

$\sigma_{oct}$ = resolved stress normal to octahedral plane

$E_{load}$ = loading direction modulus

A, B = material constants.

A major limitation of the Hysteretic Energy model for elevated temperature fatigue life prediction of isotropic materials was its inability to distinguish between the different effects of creep and plastic deformations on failure mode and life. In the isotropic (polycrystalline) materials, the grain boundaries substantially limit life at high temperatures and slow strain rates (creep conditions), while transgranular failures generally occurred at low temperatures or fast strain rates (plasticity conditions). Single crystal materials have no grain boundaries, but creep-plasticity differences must continue to be considered.

Another candidate life prediction concept under consideration is that of Damage Mechanics, which includes the Continuous Damage model (References 1 and 6). A characteristic feature of this concept is the definition of damage growth in differential form for both creep and fatigue components, which can be integrated over a given load history to predict life. This feature allows accountability for creep and plasticity difference, if any, similar to SRP and is considered to be particularly attractive for complex loading cycles experienced on turbine airfoils. The general form of the differential damage equation is as follows:

$$dD = f(\sigma, D, T)\, dt + g(\sigma_M, \bar{\sigma}, D, T) \qquad (3\text{-}7)$$

where $D$ = damage parameter
$f$ = creep damage rate
$g$ = cyclic damage rate
$T$ = temperature
$\sigma$ = instantaneous stress
$\sigma_M$ = maximum stress
$\bar{\sigma}$ = mean stress.

When the two damage rate terms, selected to define the failure behavior of a material, and the loads are simply formulated, this expression can be integrated between suitable bounds and an analytical solution obtained. However, numerical solutions will be required when simple formulations are not possible. Cyclic Damage Accumulation (CDA), a recently defined life prediction model (Reference 7), also is based on Damage Mechanics principles. However, CDA differs from Continuous Damage in the definition of damage level at which failure occurs. Continuous Damage assumes that total damage at failure always is unity, regardless of how it is accumulated. In contrast, CDA postulates that damage level for failure can vary with loading conditions. Development of CDA is still continuing under a separate program for polycrystalline materials, and its results will continue to be considered for this program.

Application of Damage Mechanics is new to anisotropic materials, and a model for describing material orientation effects on life currently is not available. However, both the micromechanics and simplified micromechanics approaches are viable candidates.

SECTION 4.0

TASK III - LEVEL I EXPERIMENTS

## 4.1 COATING CONSTITUTIVE TESTS

Cyclic stress relaxation tests of coatings included in this program are used to determine viscoplastic behavior of the coating materials for constitutive modeling. Testing of PWA 286 overlay coating was previously started (Reference 1) and completed this year. Testing of PWA 273 diffused aluminide required test specimen fabrication and testing technique development which were conducted this year.

### 4.1.1 PWA 286 Overlay Coating

Cyclic stress relaxation tests of the sort presented in Figure 10 were used to obtain overlay coating properties at various temperatures. Several specimens were exposed 100 hours at 1093°C (2000°F) prior to testing to simulate long-term bulk environmental effects.

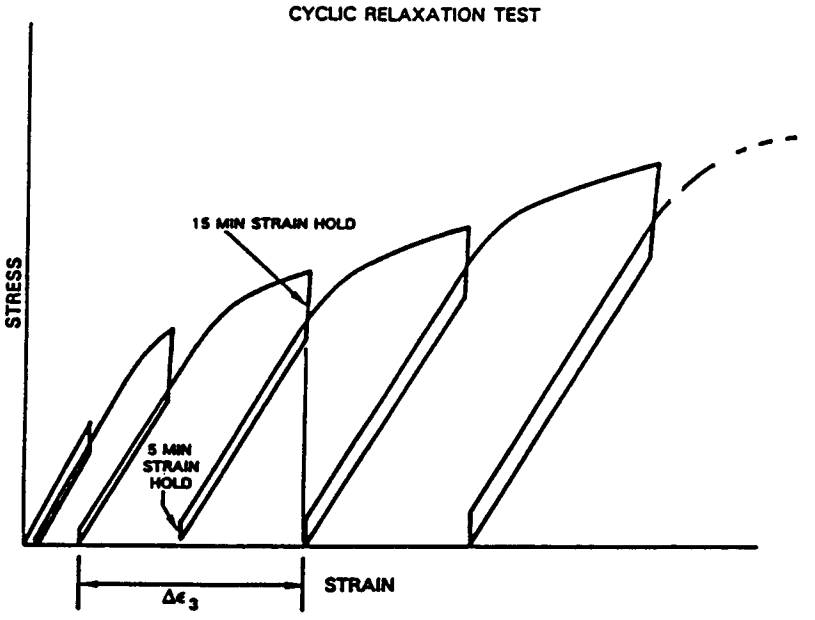


RECORD STRESS, STRAIN, TIME

| CYCLE | STRAIN INCREMENT |
|---|---|
| 1 | .1% |
| 2 | .2 |
| 3 | .3 |
| 4 | .4 |
| 5 | .6 |
| 6 | .8 |
| 7 | 1.0 |

Figure 10 Representative Stress Relaxation Test Used to Obtain Coating Behavior

Baseline isothermal PWA 286 stress relaxation tests were conducted in two separate test series. The first series of tests was conducted using a capacitance type extensometer which measured specimen deflection between dimples located just outside the constant cross section gage region. Later, it was determined that the dimple-to-dimple deflection measurements obtained were an inaccurate means for representing specimen gage section deflection without some calibration for the additional specimen length between the gage section and dimple locations. Subsequently, the second isothermal baseline test series was conducted using MTS extensometry which monitored a 2.54 cm (1.0 in) portion of the gage section.

The test facility used for the first series of isothermal baseline tests included a servo-controlled, closed loop screw driven testing machine with set point controllers, an electrical resistance clamshell furnace, and a thermocouple for temperature monitoring. Axial deflection measurement was accomplished with a capacitance type extensometer. The extensometer specimen contact arms were placed into small dimples located just outside the constant cross-section gage region. In the second test series, a servo-controlled, closed loop hydraulic testing machine with MTS controllers was used. Special software developed for computer control of the aluminide coating tests (see Section 4.1.2) was used which included a strain hold at zero stress to allow positive relaxation to occur. Axial deflection measurement was accomplished with an MTS extensometer.

The baseline isothermal stress relaxation tests included eight temperature conditions spanning the temperature range of 427°C to 1093°C (800°F to 2000°F). The second test series was specifically designed not only to allow calibration of the initial tests, but also to capture positive stress relaxation relevant to obtaining Walker unified model constants. The positive relaxation was accomplished by incorporating a strain hold at the end of each cycle unloading such as is depicted in Figure 10.

The observed relaxation response between HIP, vacuum plasma spray, and exposed HIP PWA 286 specimens is similar in shape (Figure 11). Thus, any constitutive model formulation which predicts the response of any one specimen type (i.e., HIP, vacuum plasma spray, or exposed HIP) should be equally applicable to the other specimen types. Therefore, only a single specimen type needs to be considered during the model evaluation/selection process. Based on specimen and data availability, the unexposed HIP PWA 286 specimen design was chosen for that purpose.

Three thermomechanical fatigue (TMF) constitutive tests were conducted to supply complex verification information for the PWA 286 constitutive models developed from isothermal data. The TMF tests also utilized MTS extensometry for monitoring gage section deflection.

A summary of constitutive test conditions is presented in Table VI. Constitutive test data from the first baseline test series are presented in Reference 1. Constitutive test data from the second series are provided in Appendix C. The TMF test used for initial constitutive model verification is presented in Appendix D.

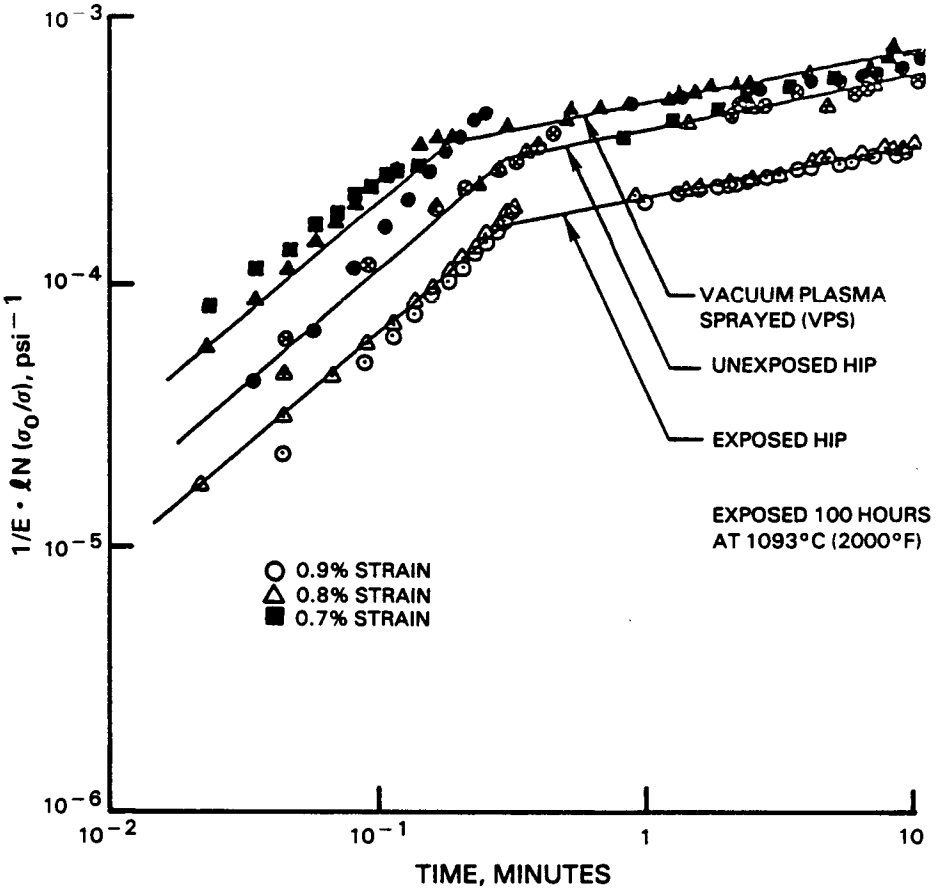


Figure 11 Short Time Creep Behavior of PWA 286 at 871°C (1800°F)

Table VI

Summary of PWA 286 Coating Constitutive Tests

Exposed = 100 hours at 1093°C (2000°F)

| Test Condition °C (°F) | Test Type | Virgin (V) or Exposed (E) | Number of HIP PWA 286 | Number of Vacuum Sprayed PWA 286 |
|---|---|---|---|---|
| 427 (800) | iso | V | 2 | |
| 538 (1000) | iso | V | 2 | |
| 649 (1200) | iso | V | 2 | |
| 760 (1400) | iso | V | 2 | |
| | | E | 1 | |
| 871 (1600) | iso | V | 2 | 2 |
| | | E | 1 | 1 |
| 982 (1800) | iso | V | 1 | 1 |
| | | E | 1 | 1 |
| 1038 (1900) | iso | V | 1 | |
| | | E | | 1 |
| 1093 (2000) | iso | V | 2 | |
| 427-871 (800-1600) out-of-phase 0->137.9 MPa 0->20.0 ksi | TMF | V | 2 | |
| 427-871 (800-1600) in-phase 0->62.1 MPa 0->9.0 ksi | TMF | V | 1 | |
| 427-871 (800-1600) out-of-phase ±0.4% | TMF | V | 2 | |

Notes:

iso = isothermal stress relaxation
TMF = thermomechanical fatigue

4.1.2 PWA 273 Aluminide Diffusion Coating

Testing of PWA 273 coating to determine constitutive properties has begun. Specimens currently being tested are 0.25 mm (0.010 in) thick PWA 1480 strips coated on both sides with PWA 273 coating (Figure 5). Specimens of other thicknesses will be tested in the future. Constitutive models will be determined for each thickness, and properties of the coating will be estimated by extrapolating model constants to zero substrate thickness.

A cyclic relaxation test, similar to that shown in Figure 10, is being used to determine specimen properties at various temperatures. Tests have been completed at 427°C, 593°C and 760°C (800°F, 1100°F and 1400°F). The data from the 760°C (1400°F) test are presented in Figure 12. Significant stress relaxation occurs during the 15 minute strain holds. Thus, the properties of the 0.25 mm (0.010 in) thick specimen are believed to be significantly influenced by the coating. This indicates that 0.25 mm (0.010 in) specimen data will be useful in the extrapolation scheme described above.

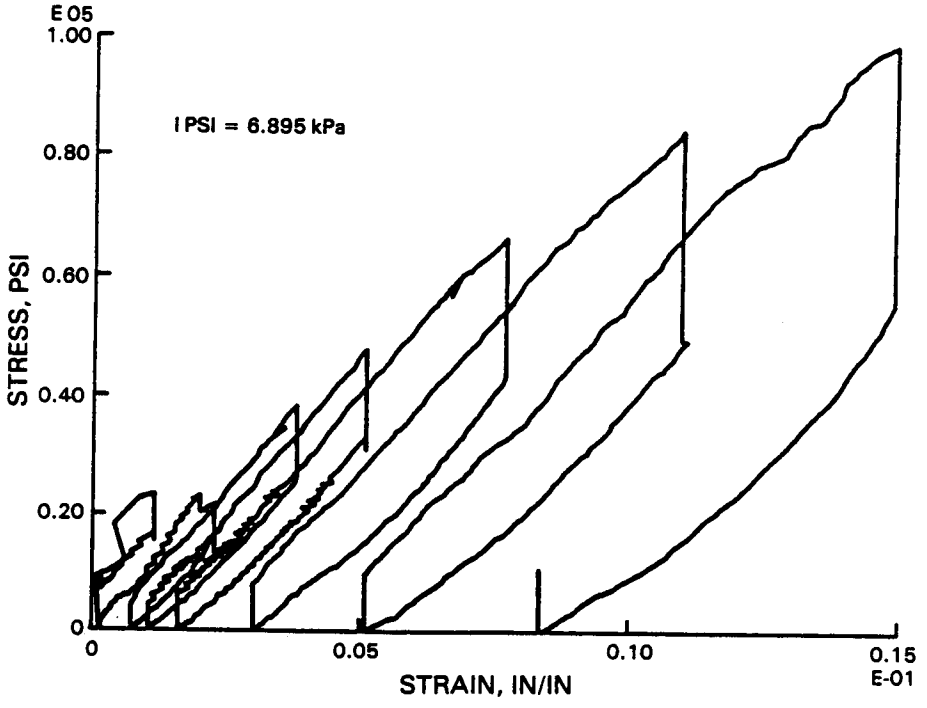


Figure 12 PWA 273 Aluminide Coated 0.25 mm (0.010 in) <001> PWA 1480 Strip; Stress Relaxation Test Conducted at 760°C (1400°F)

In order to obtain these data, significant development of testing techniques has been required, including rig control improvements and extensometry development. One difficulty with coating material stress relaxation tests was that operator control during load application was not sufficiently sensitive to maintain constant strain rates. Also, maintaining constant strain hold after stress relaxed was difficult. For this reason, computer controls were installed, making use of a test software package developed in a separate Pratt & Whitney program. Specimen supported extensometer hardware subsequently proved to be too heavy for the specimens used. A counter balanced lever type extensometer was then developed and fabricated also in a Pratt & Whitney program, so that minimum load is applied to the specimen. This extensometer is schematically shown in Figure 13.

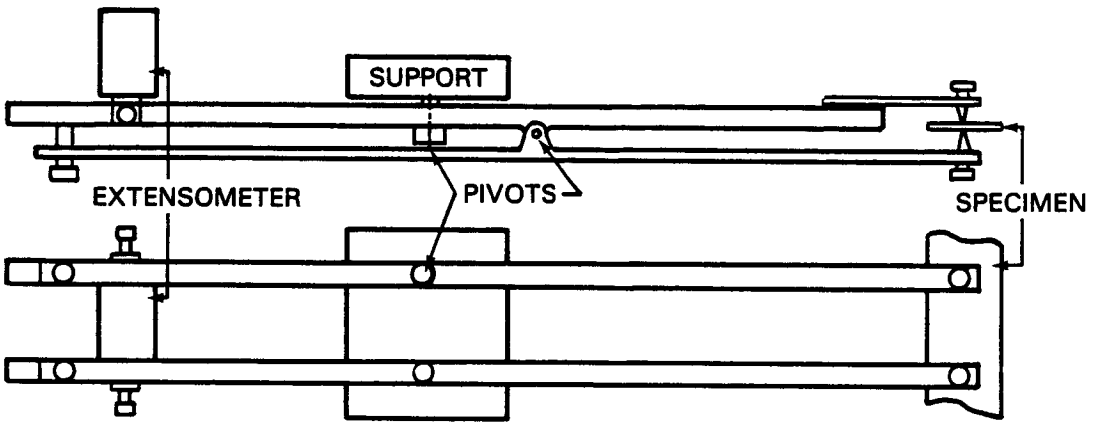


Figure 13 Schematic of Extensometer Arrangement for PWA 273 Coated Thin Specimen Tests

Testing of 0.25 mm (0.010 in) thick specimens at other temperatures will continue. In addition, coating trials on 0.13 mm (0.005 in) thick specimens are in process.

Further improvement of testing technique will be necessary to achieve required test accuracies at high temperatures. A new lever type extensometer using silica rods for low thermal expansion distortion, ball bushings for better alignment, and a linear variable differential transformer (LVDT) extensometer for increased measurement sensitivity is planned.

## 4.2 SINGLE CRYSTAL CONSTITUTIVE TESTS

The cyclic constitutive tests on uncoated primary single crystal material (PWA 1480) have been nearly completed. A total of 33 tests were conducted, as summarized in Table VII. Tests were conducted over the full range of temperatures applicable to the turbine blade using specimens oriented in four crystallographic directions: <100>, <110>, <123> and <111>. The specimen shown in Figure 14 was used for all but one of the tests; specimen number JB44 which was the tubular specimen.

Table VII

Summary of Cyclic Constitutive Tests

| | Temperature | | | | | | | | |
|---|---|---|---|---|---|---|---|---|---|
| Orientation | 21°C | 427°C | 649°C | 760°C | 872°C | 982°C | 1038°C | 1079°C | 1149°C |
| <100> | | JA61 | JA64 | JA44 | JA63<br>JA67 | JA58<br>JA66<br>JA68 | JA69 | JB44 | JA65 |
| <100> | | KA27 | KA31 | KA26 | KA23<br>KA63 | KA22 | | | |
| <111> | | LA66 | LA71 | LA63<br>LA67 | LA68<br>LA65 | LA64<br>LA69 | LA62 | | |
| <123> | MA27 | MA26<br>MA28<br>MA30 | | MA25 | MA35 | MA23<br>MA30 | | | |

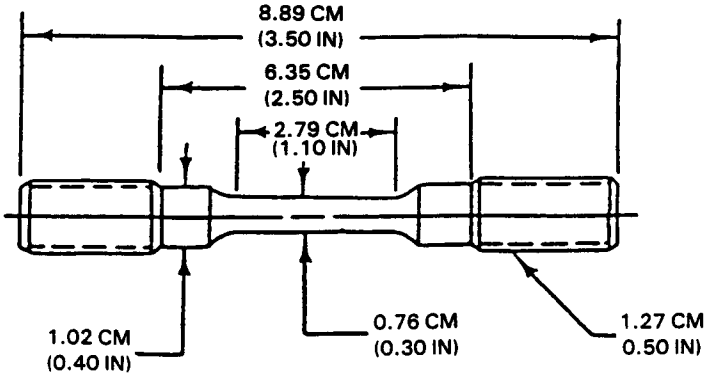


Figure 14 Cyclic Constitutive Test Specimen

Three basic types of data were obtained:

1. Stablized hysteresis loops at several different strain ranges
2. Strain rate sensitivity data
3. Creep and relaxation behavior at various points on a given hysteresis loop.

The test conditions for each specimen are included in Appendix E. At the higher temperatures, it was possible to obtain a large amount of data from a single specimen. However, at temperatures below approximately 760°C (1400°F), the deformation was dominated by discrete slip bands which appeared precipitously at octahedral slip system stresses of approximately 400 MPa (60 ksi). The first appearance of slip bands was invariably concentrated in a portion of the gage section rather than being dispersed uniformly. As cycling proceeded at an imposed strain range, the intensity (i.e., the number of lines) in a slip band increased, but the slip band remained confined to the original region of the gage section. The resulting structural response of the specimen gave the appearance of cyclic hardening (Figure 15). However, the response shown in Figure 15 is the structural response of the specimen rather than a true material stress-strain response. This was illustrated by a test conducted on specimen MA27. Two extensometers, one with a 2.54 cm (1.0 in) gage length and the other with a 1.27 cm (0.5 in) gage length, were attached to the same specimen and the specimen was cycled between fixed strain limits.

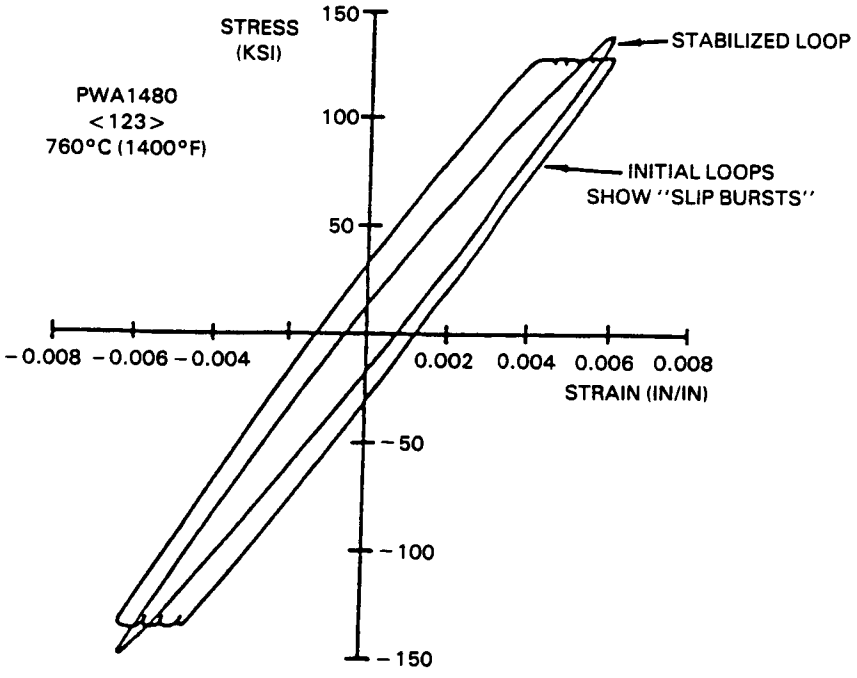


Figure 15 Apparent Cyclic Hardening During Cyclic Constitutive Test at 760°C (1400°F)

Slip bands were observed to appear within the one 2.54 cm (1.0 in) gage length but extended only a small distance into the 1.27 cm (0.5 in) gage section. As shown in Figure 16, different apparent "stress-strain" responses were measured. Due to this discrete deformation, the amount of data that can be obtained from a single specimen is limited and no additional cyclic constitutive tests below 760°C are planned in the Base Program. Material behavior at these lower temperatures will be investigated more completely in the Option 1 Program.

At temperatures above approximately 760°C (1400°F), it was possible to obtain a large amount of constitutive data from a single specimen as shown by the number and variety of test conditions listed in Appendix E. This has reduced the need for duplicate tests. The high temperature testing is nearly complete. At least one additional test at 1149°C (2100°F) will be conducted to complete the test matrix.

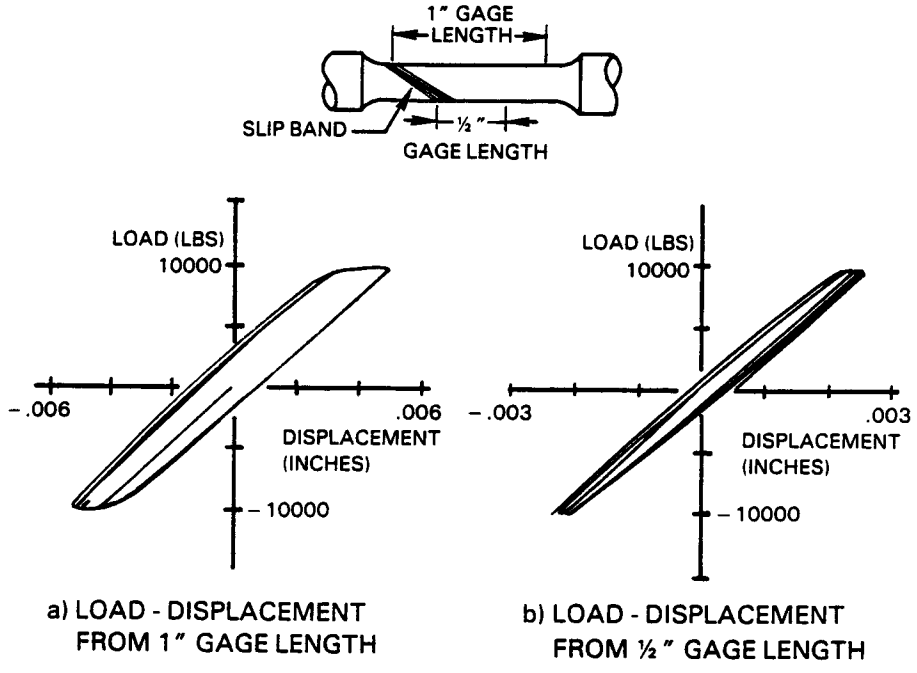


Figure 16 Load-Displacement Behavior as Monitored by Two Extensometers

## 4.3 SINGLE CRYSTAL FATIGUE TESTS

### 4.3.1 Test Facility

The test facility used for isothermal and thermomechanical fatigue (TMF) tests consists of a servo-controlled, closed loop hydraulic testing machine with MTS controllers, a low frequency (10 kHz) 20kW TOCCO induction heater, and an Ircon model 7000 radiation pyrometer, calibrated over a temperature range of 260°C to 1371°C (500°F to 2500°F), for temperature measurement. Induction heating was selected to accommodate MTS external extensometry and specimen inspection and to provide adequate heating rates. The quartz rods of the MTS extensometer, which define a 2.54 cm (1.0 in) gage section, are spring loaded against the specimen and did not show any signs of slippage during testing. A typical test setup is illustrated in Figures 17 and 18.

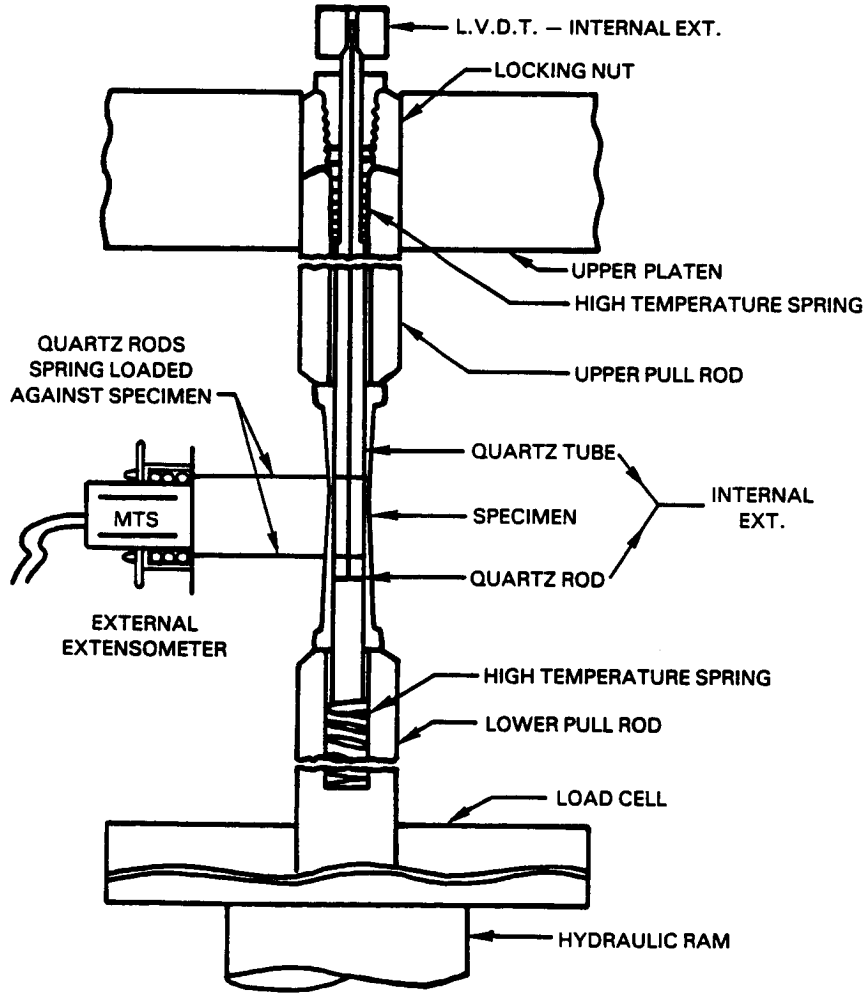


Figure 17 Extensometry Setup for Fatigue Testing


Figure 18 Thermomechanical Fatigue Test Rig

4.3.2 Deflection Measurement

At Pratt & Whitney, two methods of measuring hollow specimen uniaxial deflection are available. One method, which was developed in-house in the late 1960s, uses quartz tubes spring loaded against specimen ID circumferential ridges and which protrude out the ends of the specimen. Deflection measurement is obtained by connecting the quartz rod protrusions to a linear variable differential transformer (LVDT). The other deflection measurement device is an MTS externally mounted extensometer which uses quartz rods laterally spring loaded against the OD surface of the specimen.

An in-depth comparison of the two extensometers was conducted in order to select the best method for this program. A "piggy-back" setup, presented in Figure 17, was used to obtain simultaneous deflection measurements with both systems in room temperature tests of uncoated <001> PWA 1480 single crystal and PWA 1455 (B1900 + Hf) polycrystal specimens. The measured deflections were compared with strain gage measurements and interpreted using finite element analysis.

The evaluation results are summarized in Table VIII. It is shown that the MTS extensometer consistently produced lower mechanical strain readings than the internal ridge supported extensometer. The MTS extensometer readings were in close agreement with the strain gage readings. Subsequent finite element analysis indicated that the internal ridge deflection measurements are amplified by specimen distortion at the ridge, which could be corrected using an effective gage length (Table VIII). A similar correction was also found to be necessary to internal ridge deflection measurements in TMF tests (Table IX).

Although reliable results could be obtained with either extensometer, the MTS externally mounted system was chosen to be used in this program. Consequently, the hollow fatigue specimen was redesigned as shown in Figure 19. All future specimens will be machined to the new configuration.

Table VIII

Extensometer Comparison at Room Temperature
on Uncoated PWA 1480 <001> and PWA 1455 (B1900+Hf)

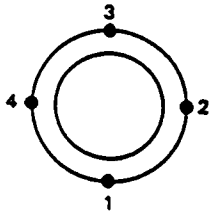


Specimen cross-section
showing strain gage locations

| Material | Rig Number | MTS Extensometer Location | Strain Range (%) Uncorrected Internal Extensometer | Corrected Internal Extensometer[3] | MTS External Extensometer | Average of Strain Gages |
|---|---|---|---|---|---|---|
| PWA 1480 <001>[1] | 1 | 2 | 0.324 | 0.309 | 0.300 | 0.298 |
| PWA 1480 <001>[1] | 1 | 1 | 0.324 | 0.309 | 0.293 | 0.296 |
| PWA 1480 <001> | 2 | 1 | 0.330 | 0.315 | 0.300 | 0.302 |
| PWA 1455 | 2 | 1 | 0.188 | 0.177 | 0.172 | 0.178 |
| PWA 1455 | 2 | 4 | 0.188 | 0.177 | 0.178 | 0.178 |
| PWA 1455[1] | 2 | 1 | 0.188 | 0.177 | 0.164 | 0.178 |
| PWA 1455[2] | 2 | 2 | 0.188 | 0.177 | 0.174 | 0.178 |
| PWA 1455 | 2 | 2 | 0.188 | 0.177 | 0.172 | 0.178 |
| PWA 1455[2] | 2 | 4 | 0.188 | 0.177 | 0.178 | 0.178 |
| PWA 1455[2] | 2 | 3 | 0.188 | 0.177 | 0.177 | 0.178 |
| PWA 1455 | 2 | 3 | 0.188 | 0.177 | 0.178 | 0.178 |

1 - Multiple readings (2 or more) are identical

2 - Alternate MTS extensometer

3 - Corrected by 2D finite element analysis

Table IX

Extensometer Comparison on Uncoated PWA 1480 <001>
During Thermomechanical Cycling

| Test Condition | Measured Total Strain (%) Range HTS | Measured Total Strain (%) Range Internal | Measured Thermal Strain (%) Range HTS | Measured Thermal Strain (%) Range Internal | Calculated Mechanical Strain (%) Range HTS | Calculated Mechanical Strain (%) Range Internal |
|---|---|---|---|---|---|---|
| 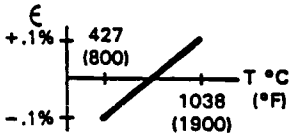  | 1.174 | 1.174 | 0.990 | 0.974 | 0.184 | 0.200 |
| 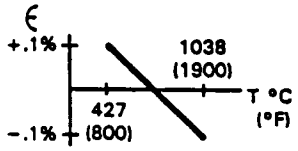  | 0.823 | 0.776 | 0.990 | 0.960 | 0.167 | 0.104 |

(A) OLD FATIGUE SPECIMEN DESIGN

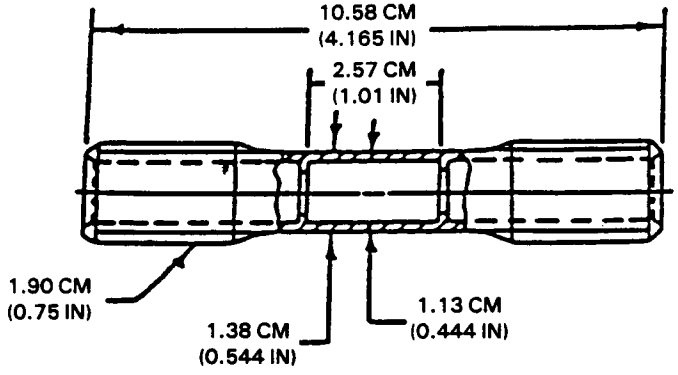


(B) NEW FATIGUE SPECIMEN DESIGN

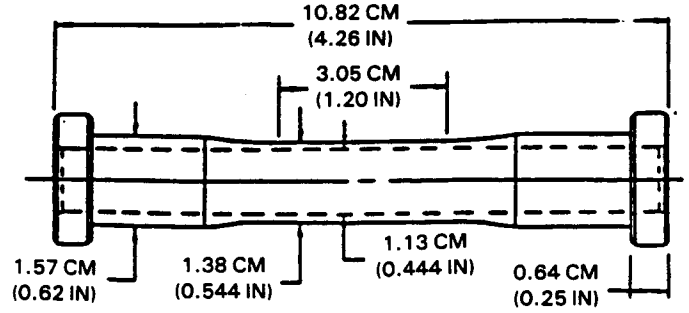


Figure 19 LCF/TMF Specimen Design Comparison

### 4.3.3 Fatigue Tests

Isothermal and TMF tests were conducted to define crack initiation life of coated PWA 1480 single crystal material and provide data for life prediction model evaluations. All fatigue tests used the specimen geometry shown in Figures 19(A) or 19(B). The latter design (denoted as 73C) relies on an MTS extensometer for deflection measurement. Where necessary, the recorded deflections obtained from the internal extensometer in the 44C design were corrected by 2-D finite element analysis to be consistent with the MTS extensometry. During testing, argon gas is slowly bubbled into the ID cavity of the specimen in order to purge atmospheric air and help retard oxide formation on the uncoated internal surface.

Level I tests were limited to key variables considered relevant to creep-fatigue life prediction. The variables include crystallographic orientation, coating, strain range, mean strain, strain rate, strain hold periods and temperature. Tests were conducted under strain load conditions. Specimen life trends indicate that each of the above factors are important with two possible exceptions. First, the 1038°C (1900°F) hold time tests (PC and CP types) produced the same average life debit relative to the rapid cycle (PP type) tests. Second, compressive mean strain during out-of-phase TMF did not signficantly alter life. A summary of fatigue tests through this reporting period is presented in Tables X and XI.

Fatigue life data for the coatings as well as the PWA 1480 substrate have been obtained from the coated specimen tests. Using a series of acetate replicas from each specimen's surface, onset of coating cracking and crack progression on the surface were determined. Representative replica results are presented in Figure 20. Metallographic inspection of the tested specimens was performed at the conclusion of each test in order to interpret replica findings, characterize cracking patterns and positively identify failure initiation sites. Specimen load, strain and temperature histories were monitored during the course of testing to provide model information.

Both the PWA 286 overlay and PWA 273 diffusion coated specimens generally were found to develop coating cracks substantially before specimen failure (Tables X and XI). Subsequent metallographic inspections of failed specimens indicated that, in many specimens, the coating cracks had progressed into the PWA 1480 substrate and directly caused failure. However, in some specimens, the coating cracks did not extend into the substrate, and the failure resulted from a competing crack initiated at the specimen ID which was uncoated. The coating cracks penetrated into the substrate in both out-of-phase TMF and isothermal LCF tests of specimens with PWA 273 diffusion coating, but only in the out-of-phase TMF tests with PWA 286 overlay coating. In these tests, the coating initiated cracking constituted the dominant failure mode and valid data for both coating cracking and specimen failure were obtained. However, initiated coating cracks did not penetrate into the substrate in 1038°C (1900°F) isothermal LCF tests of PWA 286 coated specimens, and eventual failure of these specimens was caused by the specimen ID cracks. Coating cracking lives in these tests were much shorter than specimen lives and, therefore, are considered to be insignificantly affected by the ID cracking. It is felt that, although coating cracks are generated during high temperature fatigue, lower temperature fatigue may be necessary to grow the PWA 286 coating cracks into the PWA 1480 substrate. Representative coating crack photomicrographs for 1038°C (1900°F) isothermal LCF and 427°C to 1038°C (800°F to 1900°F) out-of-phase TMF tests are presented in Figure 21.

# Table X

## Summary of Level I PWA 1480 Isothermal Fatigue Tests

| Spec. ID | Nominal Orient. | Coat[1] Type | Spec[2] Type | Temperature °C (°F) | Cycle[3] Type | $\Delta\epsilon_t$ % | $R_\epsilon$ | Freq cpm | $\Delta\sigma_0$ MPa (ksi) | $\Delta\sigma_{1/2}$ MPa (ksi) | $\sigma_{M_0}$ MPa (ksi) | $\sigma_{M_{1/2}}$ MPa (ksi) | $N_c$ cycles | 5% cycles | 10% cycles | SEPR cycles |
|---|---|---|---|---|---|---|---|---|---|---|---|---|---|---|---|---|
| JB-31 | <001> | 273 | 44C | 927 (1700) | PP | 0.8 | 0 | 6.0 | 747.4 (108.4) | 710.2 (103.0) | 6.9 (1.0) | 26.9 (3.9) | 400 | 6000 | 6070 | 6474 |
| JB-2 | <001> | 286 | 44C | 927 (1700) | PP | 0.8 | 0 | 1.0 | 712.9 (103.4) | 668.8 (97.0) | 0.0 (0.0) | -13.8 (-2.0) | 2000 | 6800 | 7010 | 7167 |
| JB-33 | <001> | 273 | 44C | 1038 (1900) | PP | 0.8 | 0 | 1.0 | 482.6 (70.0) | 396.5 (57.5) | 0.0 (0.0) | 3.4 (0.5) | 700 | 580 | 950 | 3742 |
| JB-35 | <001> | 273 | 44C | 1038 (1900) | CP | 0.8 | 0 | 0.91 | 568.8 (82.5) | 470.9 (68.3) | 0.0 (0.0) | -83.4 (-12.1) | 120 | 680 | 1450 | 3750 |
| JB-36 | <001> | 273 | 44C | 1038 (1900) | PC | 0.8 | 0 | 0.91 | 541.3 (78.5) | 539.2 (78.2) | 8.3 (1.2) | 68.9 (10.0) | 150 | 680 | 720 | 745 |
| JB-39 | <001> | 273 | 44C* | 1038 (1900) | PP | 0.8 | 0 | 6.0 | 580.6 (84.2) | 484.0 (70.2) | -6.2 (-0.9) | 1.4 (0.2) | 1100 | 580 | 860 | 5325 |
| JB-5 | <001> | 286 | 44C | 1038 (1900) | PP | 0.8 | 0 | 1.0 | 538.5 (78.1) | 437.8 (63.5) | -0.7 (-0.1) | 1.4 (0.2) | 550 | 600 | 800 | 2595 |
| JB-6 | <001> | 286 | 44C | 1038 (1900) | PC | 0.8 | 0 | 0.91 | 587.5 (85.2) | 532.3 (77.2) | 28.9 (4.2) | 75.8 (11.0) | 610 | 250 | 960 | 1100 |
| JB-20 | <001> | 286 | 44C* | 1038 (1900) | PC | 0.8 | 0 | 0.91 | 568.8 (82.5) | 569.3 (73.0) | 4.8 (0.7) | 77.2 (11.2) | 1150 | 200 | 1450 | 2192 |
| JB-71 | <001> | 286 | 44C* | 1038 (1900) | CP | 0.8 | 0 | 0.91 | 517.1 (75.0) | 472.3 (68.5) | -3.4 (-0.5) | -68.9 (-10.0) | 850 | 500 | 1250 | 1514 |
| JB-25 | <001> | 286 | 44C* | 1038 (1900) | PP | 0.8 | 0 | 6.0 | 562.6 (81.6) | 493.7 (71.6) | 11.7 (1.7) | 5.5 (0.8) | >1750 | 1000 | 1800 | 4285 |
| JB-78 | <001> | 286 | 44C* | 1038 (1900) | PP | 1.04 | 0 | 4.6 | 660.5 (95.8) | 546.1 (79.2) | -9.7 (-1.4) | 7.6 (1.1) | 1000 | 170 | 410 | 1929 |
| JB-79 | <001> | 273 | 44C* | 1038 (1900) | PP | 1.04 | 0 | 4.6 | 666.7 (96.7) | 613.7 (89.0) | 7.6 (1.1) | 5.5 (0.8) | 575 | 250 | 1200 | 1856 |
| JB-42 | <001> | -- | 73C | 1038 (1900) | PC | 0.8 | 0 | 0.91 | 548.2 (79.5) | 510.2 (74.0) | 31.0 (4.5) | 79.3 (11.5) | -- | 700 | 1700 | 1900 |
| LB-19 | <111> | 273 | 73C | 760 (1400) | PP[4] | 0.6 | 0 | 8.0 | 1508.5 (218.2) | 1511.4 (219.2) | 0.0 (0.0) | 27.6 (4.0) | 1370 | 1900 | 1920 | 1953 |
| LB-25 | <111> | 273 | 73C | 760 (1400) | PP | 0.6 | 0 | 8.0 | 1586.5 (230.1) | 1552.8 (225.2) | 0.0 (0.0) | 26.9 (3.9) | 925 | 1720 | X | 1724 |
| LB-36 | <111> | -- | 73C | 760 (1400) | PP[4] | 0.6 | 0 | 8.0 | 1511.4 (219.2) | 1525.2 (221.2) | 0.0 (0.0) | 1.4 (0.2) | -- | 2300 | X | 2331 |
| LB-59 | <111> | -- | 73C | 760 (1400) | PP | 0.6 | 0 | 8.0 | 1602.4 (232.4) | 1615.5 (234.3) | 0.0 (0.0) | 58.6 (8.5) | -- | X | X | 1445 |
| LB-120 | <111> | 273 | 73C | 760 (1400) | PP | 0.6 | 0 | 0.5 | 1547.9 (224.5) | 1509.3 (218.9) | -32.4 (-4.7) | 13.1 (1.9) | 975 | 1200 | X | 1202 |
| LB-121 | <111> | 273 | 73C | 760 (1400) | PP | 0.6 | 0 | 0.5 | 1606.5 (233.0) | 1599.6 (232.0) | -39.3 (-5.7) | 13.1 (1.9) | 300 | 420 | 480 | >565 |
| LB-124 | <111> | 273 | 73C | 760 (1400) | PP | 0.6 | 0 | 0.5 | 1571.4 (227.9) | 1531.4 (222.1) | 0.0 (0.0) | 0.0 (0.0) | 1110 | 1350 | X | >1362 |

Notes:

1. 273 = NiAl diffusion
   286 = NiCoCrAlY overlay
   -- = uncoated

2. 44C = internal ridge tube fatigue specimen
   44C* = same as 44C but ridges were machined off
   73C = smooth bore tube fatigue specimen

3. PP = continuous cycling
   PC = 60 second hold at min. strain
   CP = 60 second hold at max. strain

4. Strain cycle was a sine wave

## Table XI

## Summary of Level I PWA 1480 Thermomechanical Fatigue Tests, 427°C to 1038°C (800°F to 1900°F)

| Spec. ID | Nominal Orient. | Coat[1] Type | Spec[2] Type | Cycle[3] Type | $\Delta\epsilon_t$ % | $V_\epsilon$ | Freq cpm | $\Delta\sigma_0$ MPa (ksi) | $\Delta\sigma_{1/2}$ MPa (ksi) | $\sigma_{M_0}$ MPa (ksi) | $\sigma_{M_{1/2}}$ MPa (ksi) | $N_c$ cycles | 5% cycles | 10% cycles | SEPR cycles |
|---|---|---|---|---|---|---|---|---|---|---|---|---|---|---|---|
| JB-46 | <001> | -- | 73C | I | 0.8 | 0 | 1.0 | 774.3 (112.3) | 765.3 (111.0) | 160.0 (23.2) | 248.2 (36.0) | --- | 2500 | X | 2589 |
| JB-51 | <001> | -- | 73C | I | 0.55 | 0 | 1.0 | 563.3 ( 81.7) | 610.2 ( 88.5) | 115.9 (16.8) | 203.4 (29.5) | --- | 11500 | 11700 | 11806 |
| JB-19 | <001> | 273 | 44C | I | 0.83 | 0 | 1.0 | 689.5 (100.0) | 774.3 (112.3) | 107.6 (15.6) | 220.6 (32.0) | <12 | X | X | 580 |
| JB-22 | <001> | 273 | 44C | I | 0.52 | 0 | 1.0 | 513.0 ( 74.4) | 536.4 ( 77.8) | 66.2 ( 9.6) | 138.6 (20.1) | 150 | 3600 | 3650 | 3772 |
| JB-38 | <001> | 273 | 44C | Z | 0.76[4] | 0 | 0.5 | 818.4 (118.7) | 824.6 (119.6) | 144.1 (20.9) | 257.2 (37.3) | 650 | 1505 | X | 1505 |
| JB-72 | <001> | 273 | 44C* | Z | 0.8 | 0 | 0.5 | 803.3 (116.5) | 828.8 (120.2) | 117.2 (17.0) | 243.4 (35.3) | <50 | X | X | 876 |
| JB-81 | <001> | 273 | 44C* | I | 0.8 | -1 | 1.0 | 963.2 (139.7) | 824.6 (119.6) | -56.5 (-8.2) | 259.3 (37.6) | <20 | 520 | 535 | 541 |
| JB-9 | <001> | 286 | 44C | I | 0.76[4] | 0 | 1.0 | 772.9 (112.1) | 823.9 (119.5) | 120.7 (17.5) | 244.1 (35.4) | 350 | 1820 | 1875 | 1878 |
| JB-10 | <001> | 286 | 44C | I | 0.50 | 0 | 1.0 | 576.4 ( 83.6) | 611.6 ( 88.7) | 100.7 (14.6) | 178.6 (25.9) | 425 | 3100 | 4010 | 4105 |
| JB-21 | <001> | 286 | 44C* | Z | 0.8 | 0 | 0.5 | 888.1 (128.8) | 888.1 (128.8) | 147.6 (21.4) | 253.7 (36.8) | 820 | X | X | 1847 |
| JB-80 | <001> | 286 | 44C* | I | 0.8 | -1 | 1.0 | 1002.5 (145.4) | 902.6 (130.9) | -24.8 (-3.6) | 376.5 (54.6) | 230 | 1472 | X | 1472 |
| JB-47 | <001> | -- | 73C | II | 0.8 | 0 | 1.0 | 887.4 (128.7) | 857.0 (124.3) | -96.5 (-14.0) | -263.4 (-38.2) | --- | 4100 | 5100 | 6075 |
| JB-29 | <001> | 273 | 44C | II | 0.75 | 0 | 1.0 | 787.4 (114.2) | 760.5 (110.3) | -116.5 (-16.9) | -315.8 (-45.8) | 770 | X | X | 710339 |
| JB-11 | <001> | 286 | 44C | II | 0.79 | 0 | 1.0 | 844.6 (122.5) | 862.6 (125.1) | -122.7 (-17.8) | -291.7 (-42.3) | >10000 | 10100 | 10300 | 10535 |
| LB-20 | <111> | 273 | 73C | I | 0.3 | 0 | 1.0 | 766.7 (111.2) | 744.7 (108.0) | 173.8 (25.2) | 291.0 (42.2) | 130 | 1400 | X | 1408 |
| LB-23 | <111> | 273 | 73C | I | 0.25 | 0 | 1.0 | 689.5 (100.0) | 634.3 ( 92.0) | 122.0 (17.7) | 195.1 (28.3) | >6900 | X | X | 8211 |
| LB-33 | <111> | -- | 73C | I | 0.8 | 0 | 1.0 | 1659.6 (240.7) | 1644.5 (238.5) | 173.8 (25.2) | 291.0 (42.2) | --- | 140 | 155 | 162 |
| LB-34 | <111> | -- | 73C | I | 0.55 | 0 | 1.0 | 1246.6 (180.8) | 1305.9 (189.4) | 265.5 (38.5) | 311.7 (45.2) | --- | 140 | X | 151 |
| LB-35 | <111> | -- | 73C | I | 0.4 | 0 | 1.0 | 986.7 (143.1) | 1104.6 (160.2) | 335.1 (48.6) | 325.4 (47.2) | --- | 530 | X | 537 |
| LB-56 | <111> | -- | 73C | I | 0.3 | 0 | 1.0 | 788.1 (114.3) | 837.1 (121.4) | 216.5 (31.4) | 359.9 (52.2) | --- | 1400 | 1600 | 2067 |

Notes:

1. 273 = NiAl diffusion
   286 = NiCoCrAlY overlay
   -- = uncoated

2. 44C = internal ridge tube fatigue specimen
   44C* = same as 44C but ridges were machined off
   73C = smooth bore tube fatigue specimen

3. See figures at right

4. Strains controlled by internal extensometer; $\Delta\epsilon_t$ corrected by 2D finite element analysis

$V_\epsilon$ = $(\epsilon_{max} + \epsilon_{min}) / (\epsilon_{max} - \epsilon_{min})$

$\Delta\sigma_0$ = initial stress range

$\Delta\sigma_{1/2}$ = one-half life stress range

$\sigma_{m_0}$ = initial mean stress

$\sigma_{m_{1/2}}$ = one-half life mean stress

$Nc_i$ = coating cracking life

5% = 5% stress range drop life

10% = 10% stress range drop life

SEPR = failure life

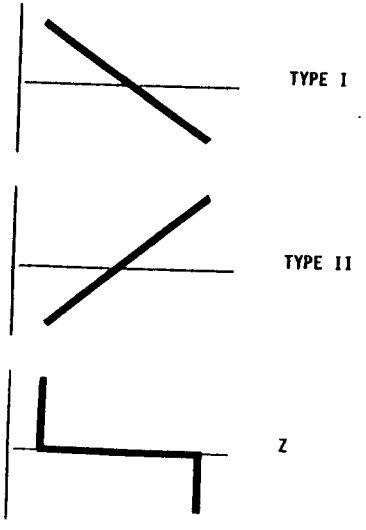

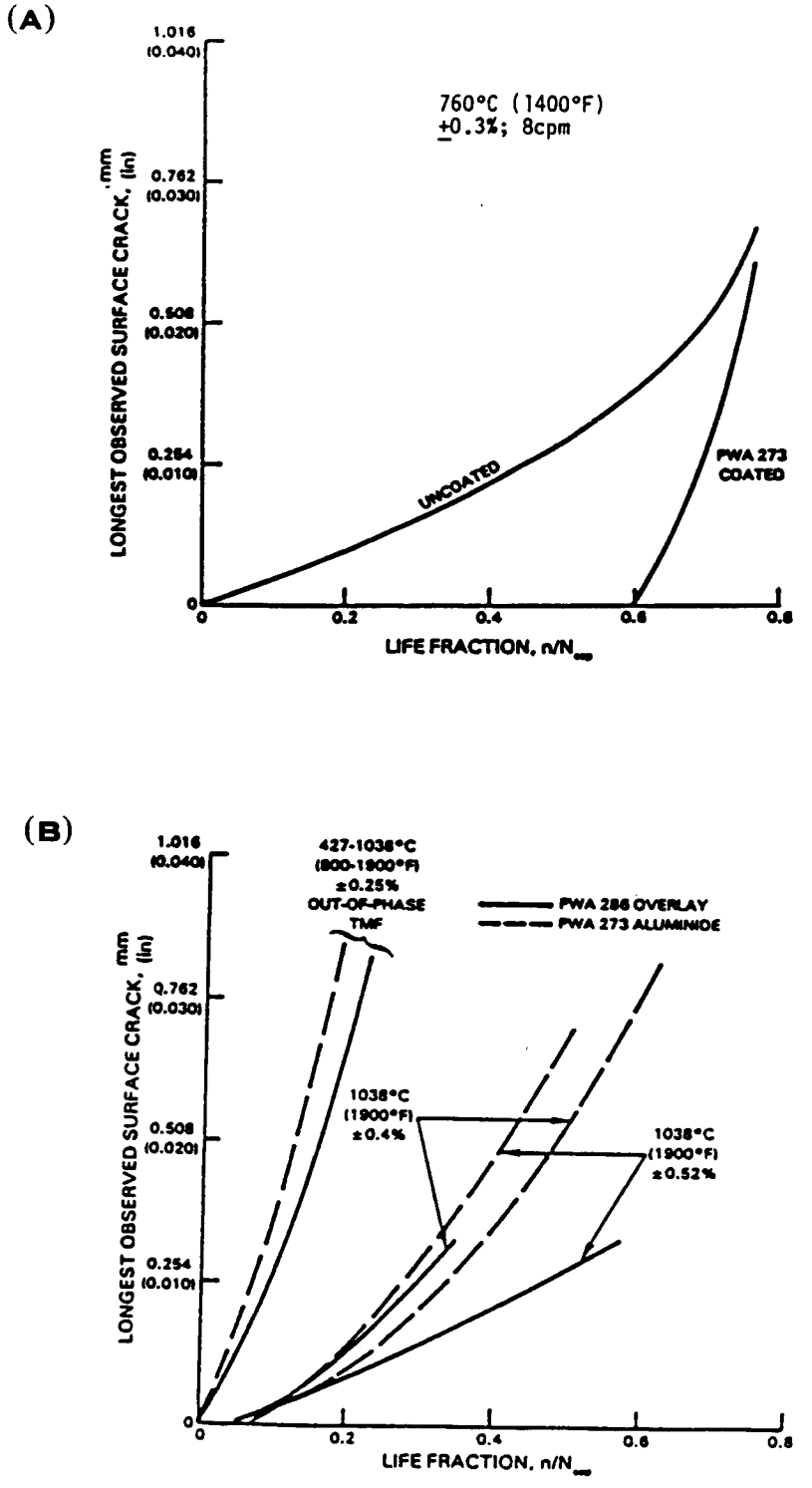


Figure 20 Representative Replica Data from Fatigue Tests: (A) 760°C (1400°F) Isothermal Tests of PWA 1480 <111> Specimens, and (B) 1038°C (1900°F) Isothermal and 427°C to 1038°C (800°F to 1900°F) Out-Of-Phase TMF Tests of PWA 1480 <100> Specimens

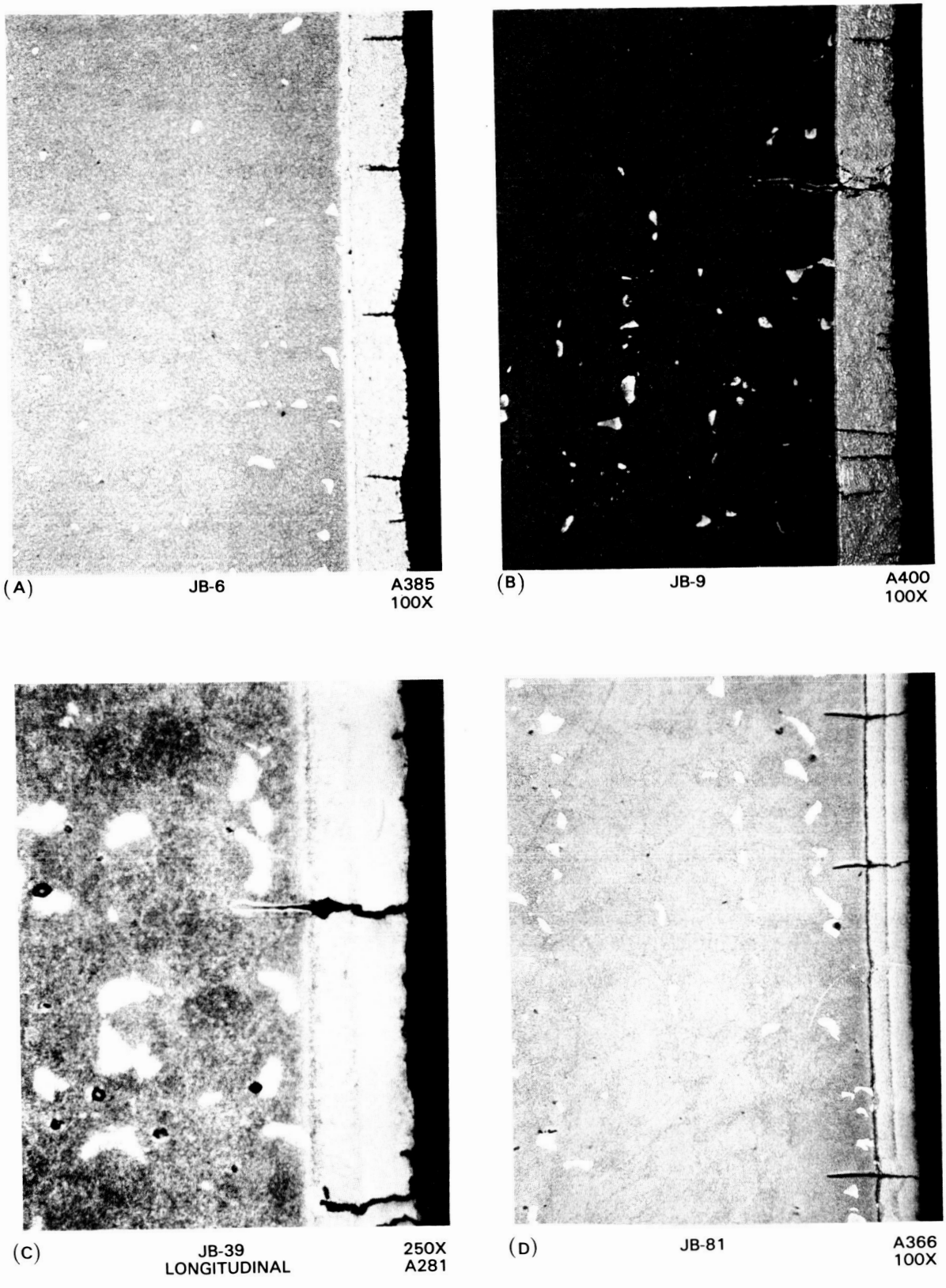


Figure 21 Representative Coating Cracks: (A) PWA 286, 1038°C (1900°F) LCF; (B) PWA 286, 427°C to 1038°C (800°F to 1900°F) Out-Of-Phase TMF; (C) PWA 273, 1038°C (1900°F) LCF; and (D) PWA 273, 427°C to 1038°C (800°F to 1900°F) TMF

Representative hysteresis loops from isothermal and TMF tests are presented in Figures 22 through 26. A review of 1038°C (1900°F) isothermal LCF specimen tests indicates that the <001> oriented PWA 1480 cyclicly softened. The <111> PWA 1480 substrate tests conducted at 760°C (1400°F) were virtually unaffected by cycling, neither signficantly softening nor hardening. By contrast, cyclic hardening was observed in the <001> PWA 1480 TMF tests, while the <111> PWA 1480 TMF tests did not harden or soften. At lower strain ranges, less hardening of the <001> PWA 1480 is anticipated.

Four TMF specimens were examined using Transmission Electron Microscopy (TEM) to determine the effects of coatings, strain range, and cycle path on the PWA 1480 substrate microstructure. A summary of those investigations is presented in Table XII. TEM thin foils were prepared by sectioning the hollow specimen walls parallel to the specimen axis, grinding on both sides down to a thickness of 0.203 mm (0.008 in), and then punching out disks directly below the fracture origin. The disks were then thinned by electropolishing and ion milling.

Specimens JB-9 and JB-19 were both tested at approximately the same conditions; however, JB-9 was coated with PWA 286 overlay coating while JB-19 was coated with PWA 273 aluminide. The fracture surfaces of these two specimens, which are presented in Figures 27 and 28, are different in nature as discussed in Reference 1. As shown in Figures 29 and 30, both specimens contain fine pinpoint-like precipitates in the $\gamma$ matrix. The more intense dislocation activity and the greater amount of $\gamma'$ agglomeration observed in JB-9 as compared to JB-19 is a reflection of the greater number of test cycles which JB-9 experienced. Because both specimens had similar hysteresis loops, the lower separation life of JB-19 is primarily attributed to the short cracking life of the PWA 273 aluminide coating.

Specimen JB-22 had the same coating as JB-19 (i.e., PWA 273 aluminide) and was also subjected to identical test conditions, except that the mechanical strain was lowered to $\pm$0.26%. As would be expected, the separation life of JB-22 is considerably longer than that of JB-19 (3,772 cycles versus 580 cycles). Examination of Figures 29 through 32 reveals that JB-22 and JB-19 have similar fracture surfaces and dislocation structures. Again, the greater $\gamma'$ agglomeration in JB-22 is a result of the greater number of test cycles JB-22 experienced.

Specimen JB-11 was tested using the same coating and mechanical strain range as JB-9, but used an in-phase temperature cycle instead of an out-of-phase cycle. As shown in Figures 33 and 34, the fracture surface of JB-11 was heavily oxidized and there was more agglomeration of $\gamma'$ compared to JB-9 (Figures 27 and 29); both features indicative of longer exposure. It is thought that the longer life of JB-11 compared to JB-9 (10,535 cycles versus 1,878 cycles) could be related to the stress relaxation characteristics associated with the test cycles, which are depicted by the respective hysteresis loops and can be measured by cycle mean stresses (Table X). In-phase TMF cycling biases the hysteresis loop toward compression (compressive mean stress), while out-of-phase cyclic relaxation biases the loop toward tension (tensile mean stress).

Examination of isothermal test specimen fracture and dislocation structures and stress trends is planned so that comparisons can be made between isothermal and TMF structures.

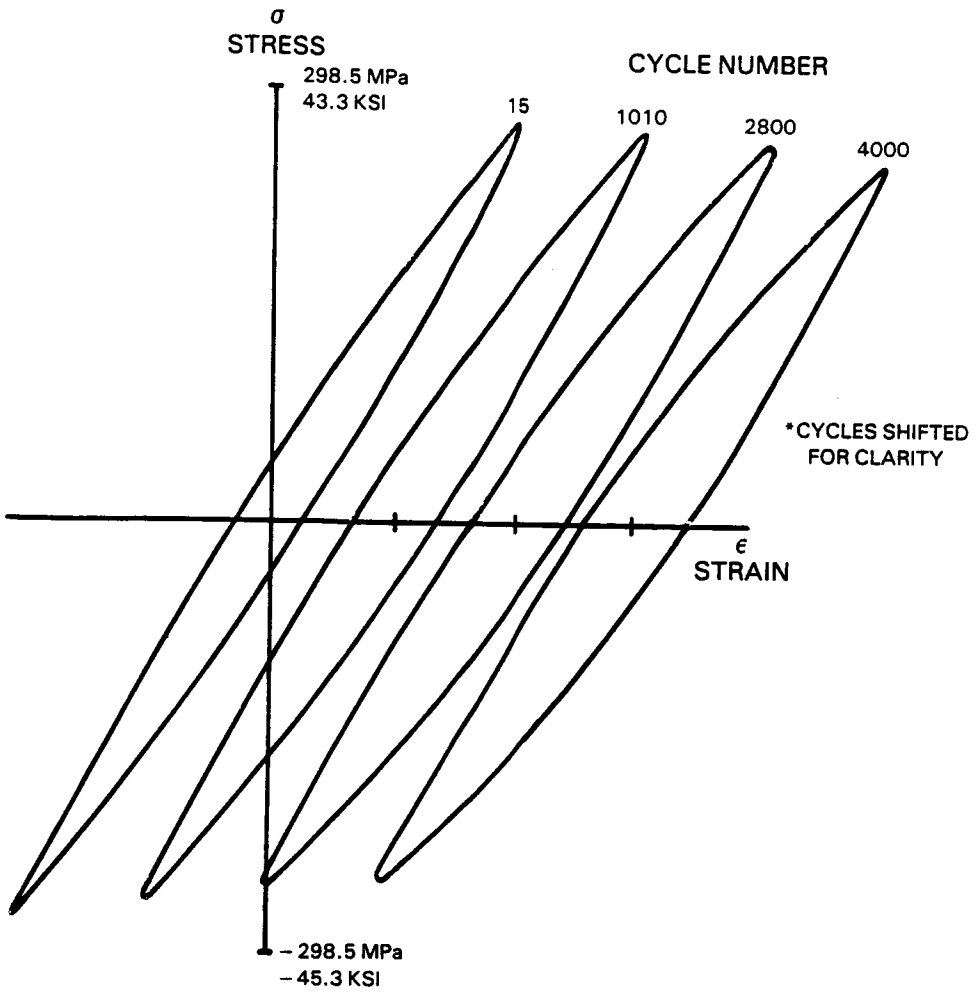


Figure 22 Cyclic Response of 1038°C (1900°F) Fatigue Test with $\Delta\epsilon = \pm 0.4\%$, 6 cpm <001> PWA 1480

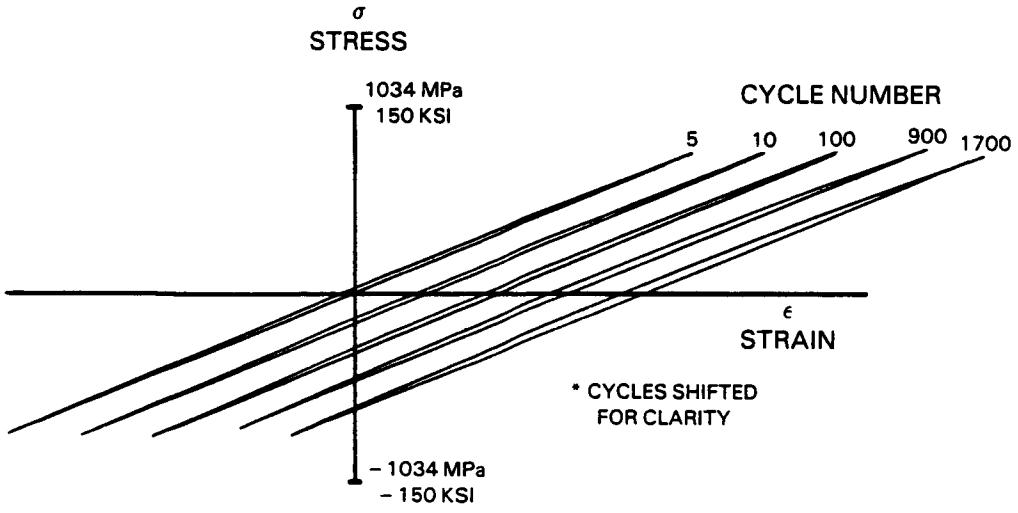


Figure 23 Cyclic Response of 760°C (1400°F) Fatigue Test with $\Delta\epsilon = \pm 0.3\%$, 8 cpm <111> PWA 1480

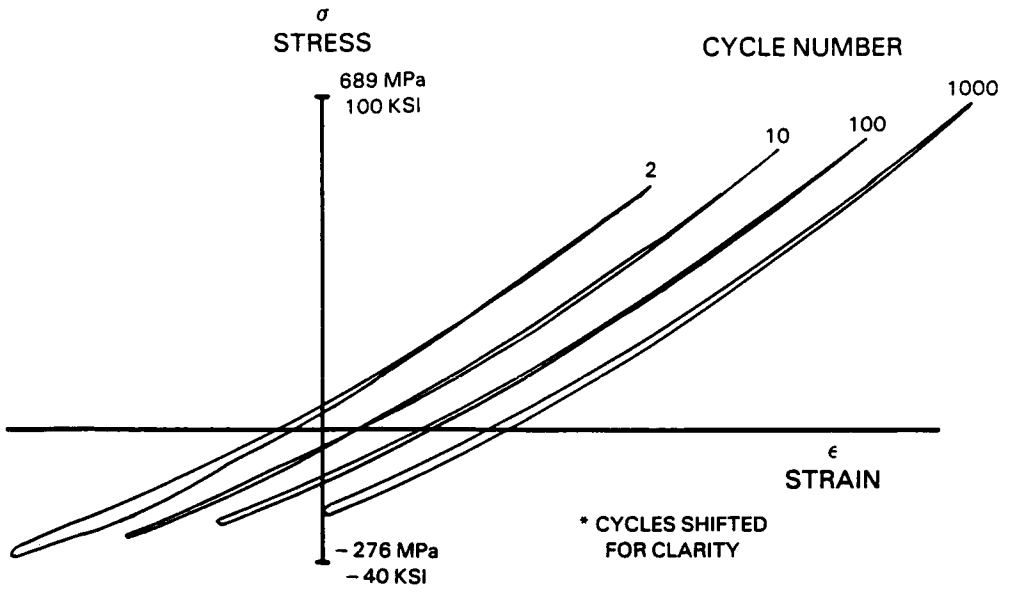


Figure 24 Cyclic Response of 427°C to 1038°C (800°F to 1900°F) Out-Of-Phase TMF Test with $\Delta\epsilon = \pm 0.38\%$, 1 cpm <001> PWA 1480

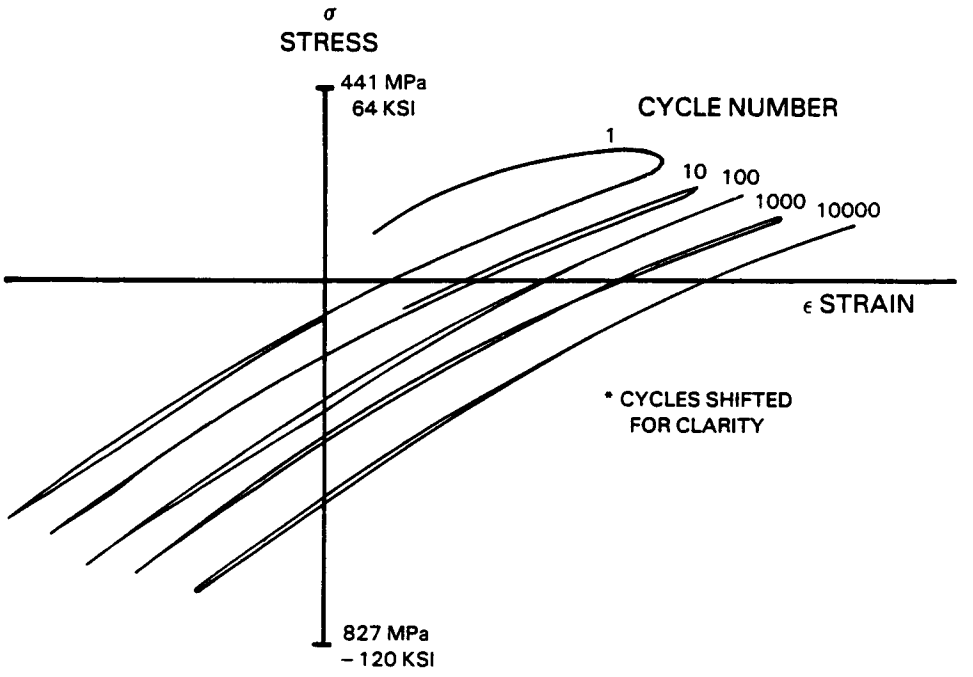


Figure 25 Cyclic Response of 427°C to 1038°C (800°F to 1900°F) In-Phase TMF Test with $\Delta\epsilon = \pm 0.395\%$, 1 cpm <001> PWA 1480

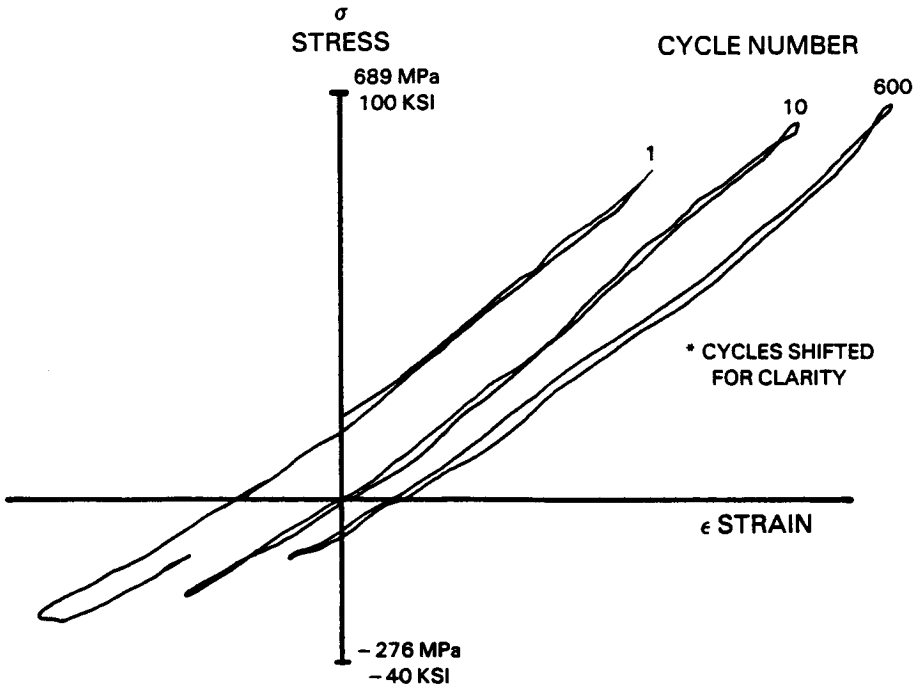


Figure 26 Cyclic Response of 427°C to 1038°C (800°F to 1900°F) Out-Of-Phase TMF Test with ± 0.15%, 1 cpm <111> PWA 1480

Table XII

Summary of PWA 1480 TEM Examinations of <001> TMF Specimens
427°C to 1038°C (800°F to 1900°F), 1 cpm

| Specimen ID | Strain Range (%) | Cycle Path | Coating Type | Life at Separation (Cycles) | Crack Initiation Site | Fracture Surface & Microstructure Characterization |
|---|---|---|---|---|---|---|
| JB-9 | ±0.4 | Out-of-Phase | PWA 286 | 1,878 | 2 OD Initiation Sites Adjacent to Each Other | Figures 27 and 29 |
| JB-19 | ±0.4 | Out-of-Phase | PWA 273 | 580 | OD Initiation | Figures 28 and 30 |
| JB-22 | ±0.275 | Out-of-Phase | PWA 273 | 3,772 | OD Initiation | Figures 31 and 32 |
| JB-11 | ±0.4 | In-Phase | PWA 286 | 10,535 | ID Initiation | Figures 33 and 34 |

TEM Observations

JB-9 Vs. JB-19, Coating Effect:

Well defined penny marks near initiation sites for JB-9. Both show fine pinpoint-like precipitates in gamma. Higher dislocation activity and more agglomeration of gamma prime in JB-9 than JB-19.

JB-22 Vs. JB-19, Strain Range Effect:

Fracture surface and dislocation structure are smaller in JB-22 and JB-19.

JB-11 Vs. JB-9, Cycle Path Effect:

Heavier oxidation and more agglomeration of gamma prime in JB-11 than in JB-9.

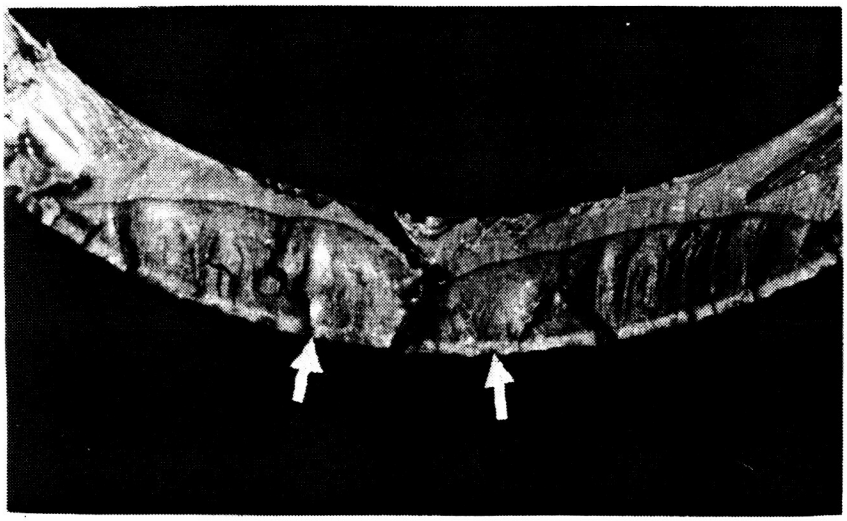

14X

Figure 27 Fracture Surface of Specimen JB-9, PWA 1480 <001> with Overlay Coating, After Being TMF Tested Between 427°C to 1038°C (800°F to 1900°F), $\varepsilon = \pm 0.4\%$, 1 cpm, Out-of-Phase for 1878 Cycles. Arrows indicate $\overline{OD}$ initiation sites.

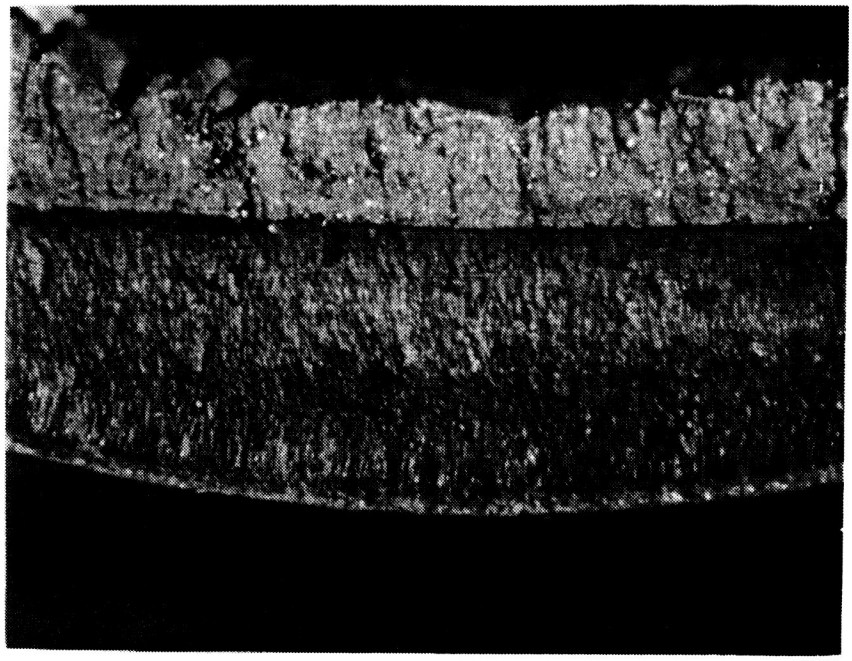

32X

Figure 28 Fracture Surface of Specimen JB-19, PWA 1480 <001> with Aluminide Coating, After Being TMF Tested Between 427°C to 1038°C (800°F to 1900°F), $\varepsilon = \pm 0.4\%$, 1 cpm, Out-of-Phase for 580 Cycles Showing OD Initiation Sites

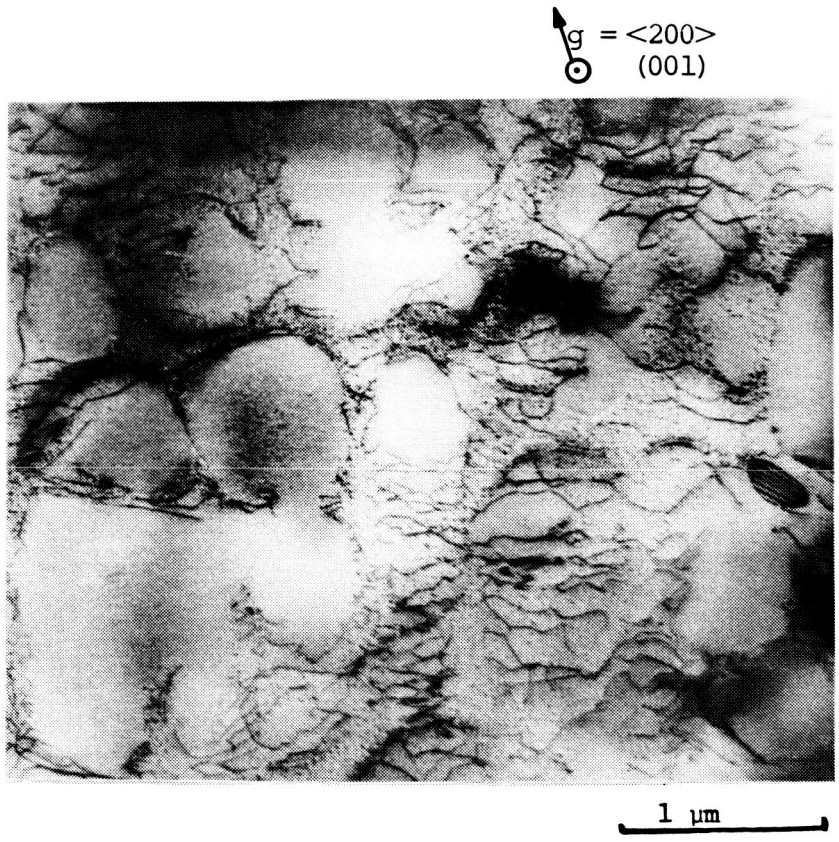


Figure 29 Dislocation Structure of Specimen JB-9

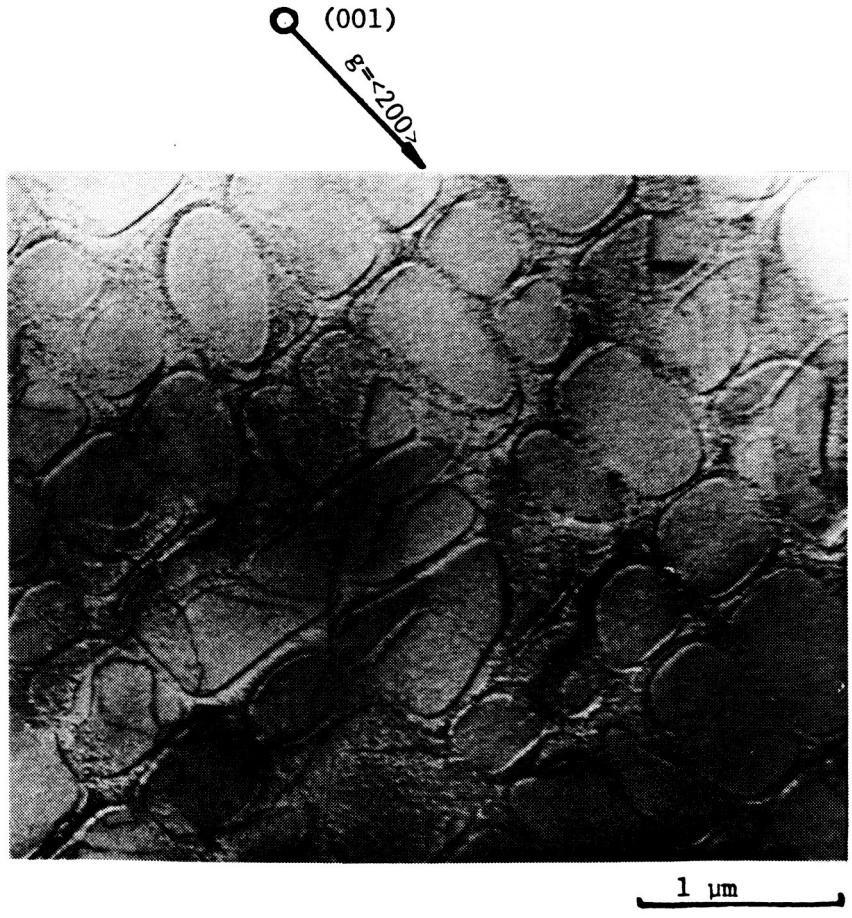


Figure 30 Dislocation Structure of Specimen JB-19

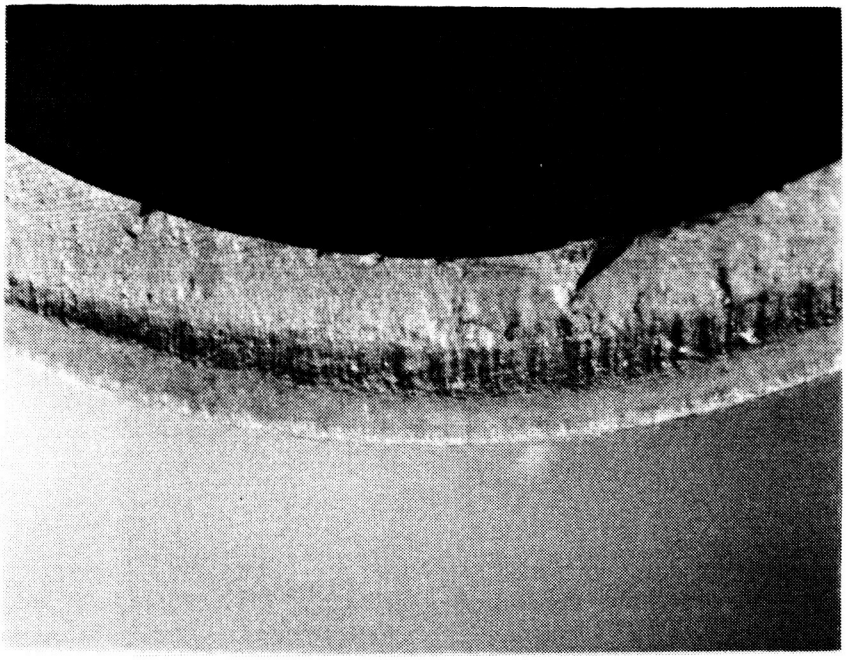

20X

Figure 31 Fracture Surface of Specimen JB-22, PWA 1480 <001> with Aluminide Coating, After Being TMF Tested Between 427°C to 1038°C (800°F to 1900°F), $\varepsilon = \pm 0.275\%$, 1 cpm, Out-of-Phase for 3772 Cycles Showing OD Initiation

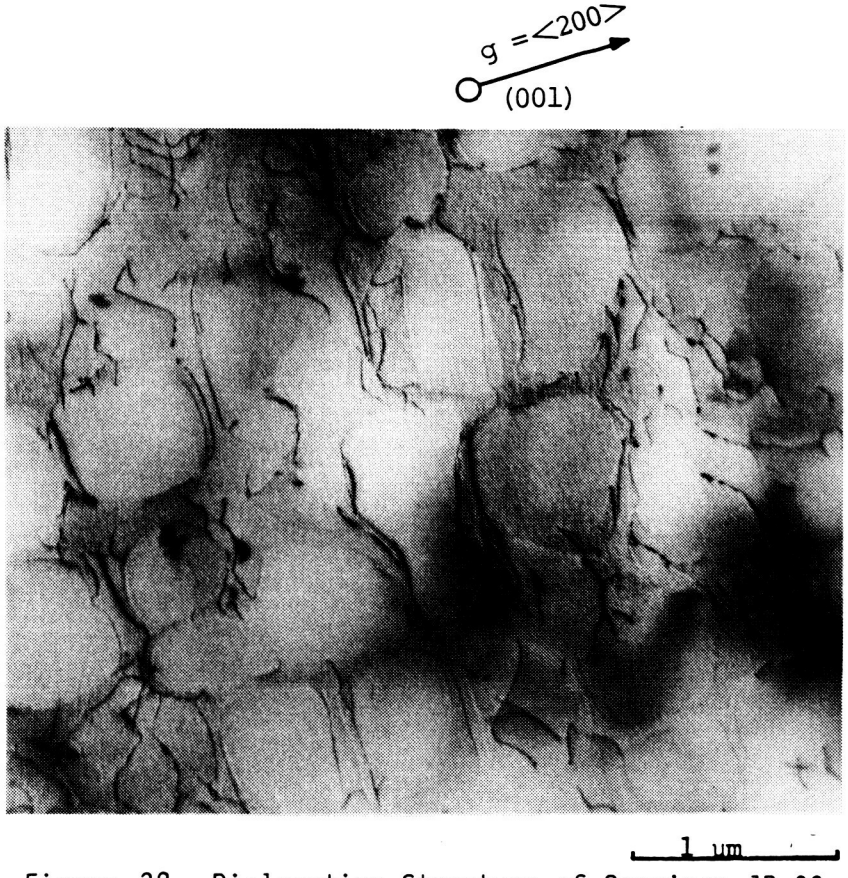


Figure 32 Dislocation Structure of Specimen JB-22

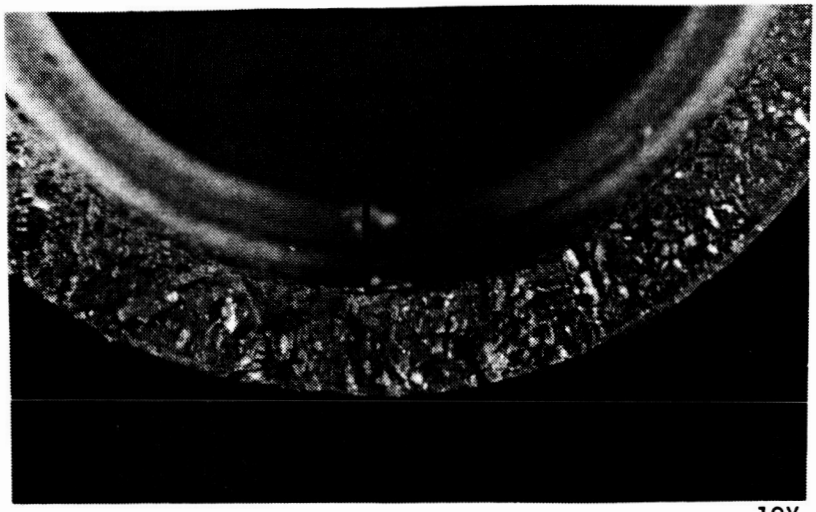


Figure 33 Fracture Surface of Specimen JB-11, PWA 1480 <001> with Overlay Coating, After Being TMF Tested Between 427°C to 1038°C (800°F to 1900°F), $\varepsilon = \pm 0.4\%$, 1 cpm, In-Phase for 10535 Cycles Showing ID Initiation

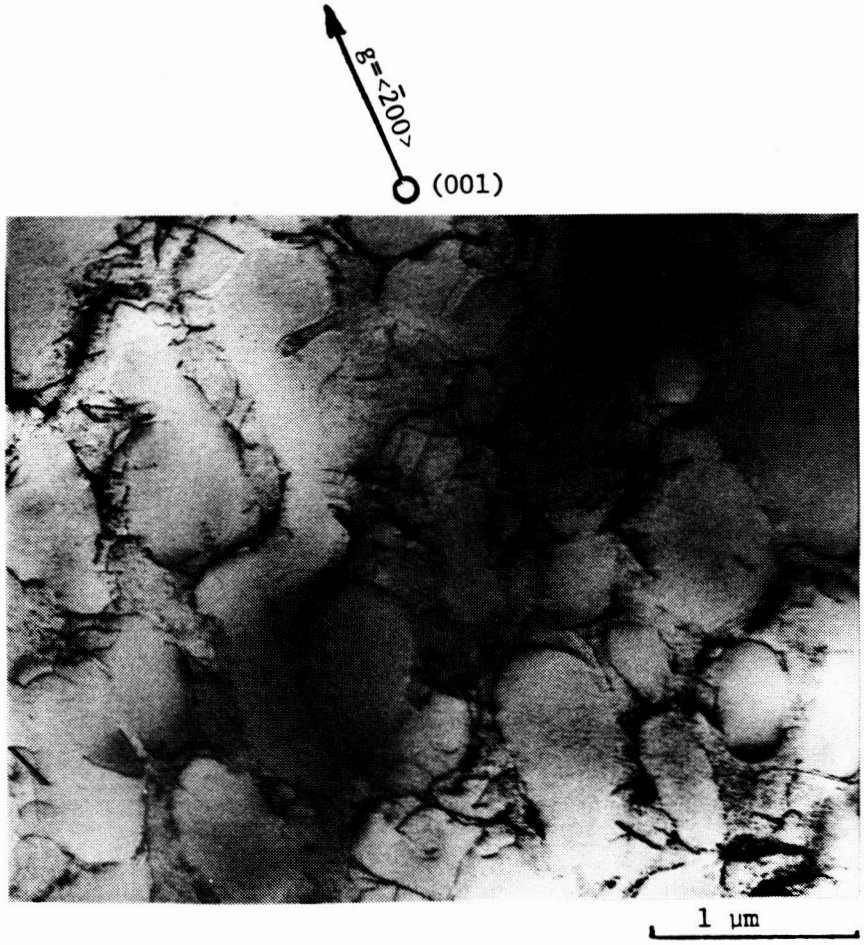


Figure 34 Dislocation Structure of Specimen JB-11

# SECTION 5.0

# TASK IV - CORRELATION OF MODELS WITH LEVEL I EXPERIMENTS

## 5.1 PWA 286 OVERLAY COATING CONSTITUTIVE MODEL

### 5.1.1 Analysis of Coated Specimens

Coated turbine airfoils are subjected to complex transient thermal mechanical fatigue loading during a typical flight cycle. At critical regions of an airfoil, the cyclic response (stress/strain/temperature/time) of each constituent of the airfoil (i.e., coating and substrate) varies considerably. A schematic representation of the potential strain-temperature responses is shown in Figure 35 for the initial cycle. The mismatch of the thermal expansion coefficients is only one of the important characteristics governing the difference in response for the cycles shown. The constitutive and failure behavior for each component of the composite under thermal mechanical fatigue must be taken into account in order to predict the useful life of a coated turbine airfoil. Potential response regimes such as alternating plasticity, shakedown, and racheting must be estimated for coating/substrate combinations (e.g., aluminide or overlay coatings and PWA 1480 crystal orientations). To effectively deal with these complex problems, it is practical to use simplified structural models (i.e., n-bar assemblies) which include the highly nonlinear behaviors of each constituent. The objective in the use of simplified structural models is to capture the first order effects which are one-dimensional in the conducted tests (uniaxial loading). Unlike nonlinear finite element analyses which require substantial amounts of central processing unit (CPU) time, simplified structural models permit extensive exploratory studies of the elastoviscoplastic responses in minimum time. A simple three-bar assembly for investigating the response of a thermal barrier coating system, consisting of the ceramic outer layer, a bond layer, and the substrate is shown in Figure 36.

The n-bar computer code utilized in this program serves two functions: (1) a single element (or bar) can be used to regress uniaxial, isothermal coating data to obtain and compare coating constitutive models, and (2) to predict the one-dimensional hysteretic response of a coating/substrate composite structure.

The regression technique obtains a least squares best fit of isothermal stress/strain/time data by optimizing each coefficient individually while holding all other coefficients constant. This simple technique has been useful in determining coefficients for the coating constitutive models. Coefficients may be perturbed singly by the user as a help to judge model sensitivities.

Once constitutive models are determined, cyclic hysteresis responses can be predicted for desired strain histories. Strain histories are input to the n-bar code by either a disk file or user interactive input. For each point of the input strain history, the corresponding stress is calculated for each of the composite constituents. Load controlled test results can also be predicted. A plotting subroutine is attached to provide desired stress and strain graphical output.

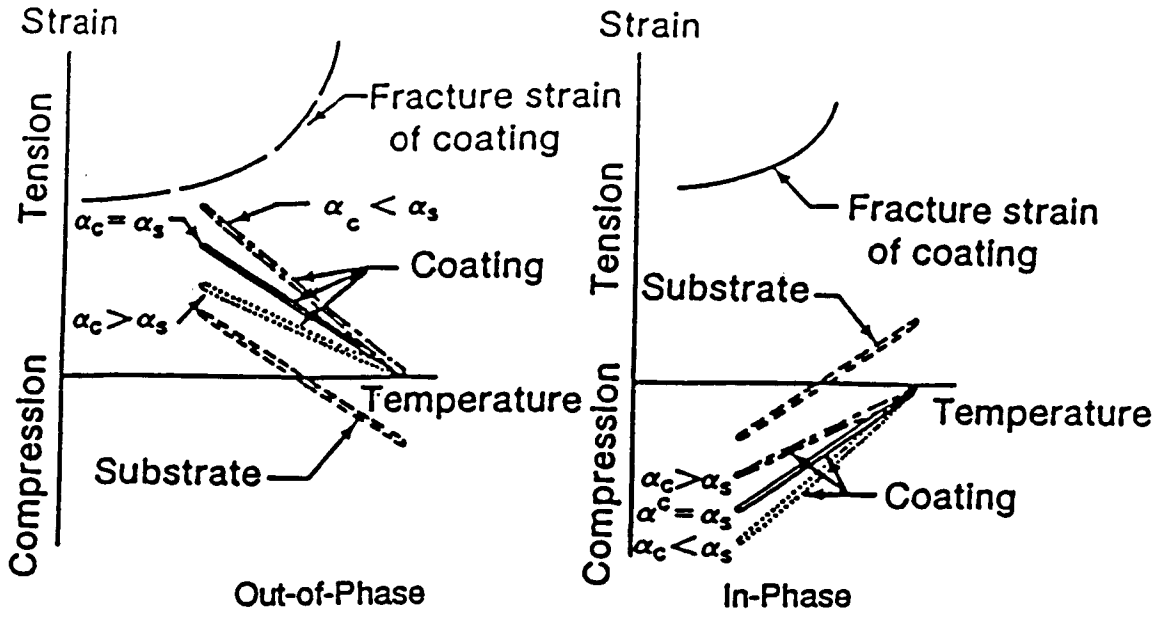


Figure 35 Mechanics of Factors Affecting Crack Initiation in Two Types of Thermal Mechanical Fatigue Cycles

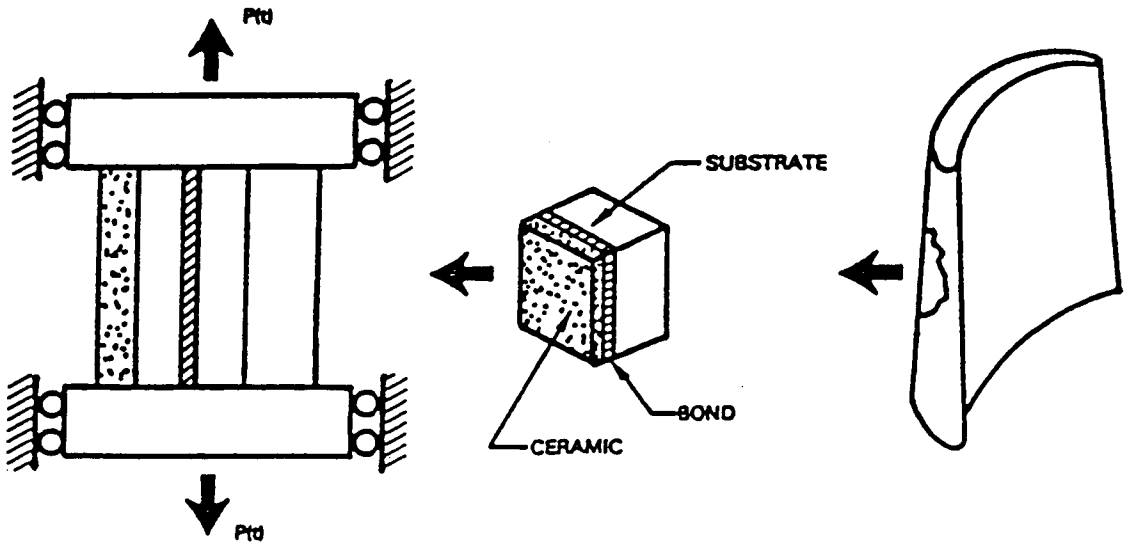


LOADING

CENTRIFUGAL P(t)
TEMPERATURE $T_S$ (t), $T_{BL}$ (t), $T_C$ (t)

Figure 36 Three Bar Simulation of Thermal Barrier Coating System

The n-bar model is being utilized to calculate the coating/substrate hysteresis response of coated PWA 1480 isothermal LCF and TMF test specimens to help determine important coating cracking life parameters. For example, Figure 37 shows the predicted response of PWA 286 overlay coating during a 427°C to 1038°C (800°F to 1900°F), ±0.4%, out-of-phase TMF test. This coating has lower high temperature creep strength and a higher thermal growth rate than the PWA 1480 substrate, which results in high coating strain range and maximum tensile stress, both of which are considered damaging by many fatigue life models. Thus, it is not surprising that this coating fails readily at this test condition which hastens substrate failure (1878 cycles to separation relative to 2589 cycles for an uncoated specimen). The overlay coating constitutive model used in this example is a Walker model with constants regressed from the first series of cyclic stress relaxation data obtained in this program. A simple thermoelastic-creep model was used for the PWA 1480 constitutive model where the creep law was determined from Larson-Miller creep property representation.

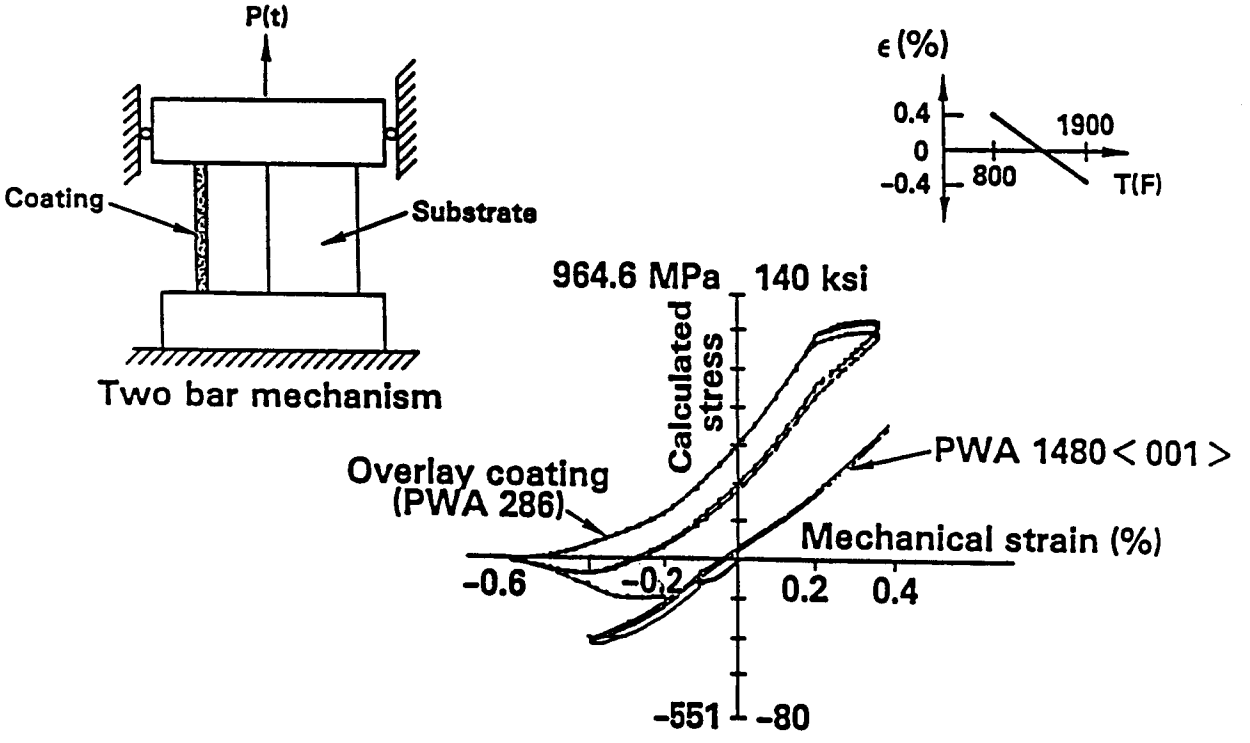


Figure 37 "Two-Bar" Mechanism and Predicted Coating/Substrate Hysteretic Response of a 427°C to 1038°C (800°F to 1900°F), ±0.4%, Out-of-Phase TMF Test

### 5.1.2 Overlay Coating Constitutive Model Correlation

Five candidate coating constitutive models were correlated with a baseline data set consisting of isothermal stress relaxation test results. Correlated were Walker, a simplified Walker, Moreno, Classical and Stowell models, as discussed below.

Constitutive model constants were determined from the first series of baseline isothermal stress relaxation tests of unexposed HIP PWA 286 conducted at 538, 760, 871, 982 and 1093°C (1000, 1400, 1600, 1800 and 2000°F) (see Section 4.1.1). A summary of model constants is presented in Table XIII. For model discussions, 538°C (1000°F) and 982°C (1800°F) regressions are presented as representative low and high temperature PWA 286 material behavior. Model constants are now being reviewed using data from the second baseline isothermal test series.

Qualitative evaluation of the prediction capabilities of each model was accomplished by application to verification data consisting of an out-of-phase thermomechanical waveform. TMF cycles include complex material behavior such as stress relaxation and plasticity which is useful for exercising the models. The out-of-phase cyclic condition is of particular interest in that such conditions are typical of gas turbine airfoil external surfaces where TMF cracks originate in the coating.

On the basis of this evaluation and the correlations, the Walker and Moreno models were selected for further development. The primary advantage of these models is the availability of a back stress formulation, which is considered necessary to duplicate the observed TMF behavior and the positive stress relaxation in the recent stress relaxation tests (Figure 10).

For brevity, the model equations are given in one-dimensional form. Expanding the models into three-dimensional forms required by nonlinear finite element computer codes was considered unnecessary until the final model is chosen. More detailed discussion of each model is documented in Reference 1.

Table XIII 6.895 kPa = 1 psi

Summary of Constitutive Model Regressed Temperature Dependent Material Constants

| | 538°C (1000°F) | 760°C (1400°F) | 871°C (1600°F) | 982°C (1800°F) | 1093°C (2000°F) |
|---|---|---|---|---|---|
| E, psi | .1850E8 | .1000E8 | .8000E7 | .3000E7 | .1000E7 |
| **Walker** | | | | | |
| n | .2685E2 | .3318E1 | .2240E1 | .2036E1 | .1649E1 |
| n1, psi | .1617E4 | .7046E3 | .8060E3 | .1316E4 | .1573E4 |
| n7 | .2369E4 | .1202E4 | .2653E4 | .1900E4 | .1843E3 |
| n9 | .2533E3 | .5850E2 | .1317E3 | .3887E2 | .1137E3 |
| n10, psi | .2389E-4 | .1469E-3 | .5504E-3 | .2184E-3 | .1340E-3 |
| n11, psi | .4955E7 | .4006E6 | .5625E6 | .7500E5 | .3312E5 |
| m0 | .1200E1 | .1200E1 | .1200E1 | .1200E1 | .1200E1 |
| K1, psi | .1736E6 | .5845E6 | .5410E6 | .2053E6 | .1435E6 |
| K2, psi | .3315E5 | .2048E6 | .3624E6 | -.1094E4 | -.4711E5 |
| **Simplified Walker** | | | | | |
| n | .2957E2 | .3554E1 | .3424E1 | .3295E1 | .3295E1 |
| n7 | .7877E3 | .7704E3 | .4053E3 | .1006E3 | .1560E3 |
| K1, psi | .1865E6 | .5164E6 | .1545E6 | .5044E5 | .1408E5 |
| K2, psi | .4351E5 | .2302E6 | .4906E5 | .2370E5 | .5820E4 |
| **Classical** | | | | | |
| A1, psi | .3054E6 | .5153E6 | .3325E6 | .8385E5 | .4753E5 |
| A2 | .7579E1 | .2711E1 | .2026E1 | .2261E1 | .2183E1 |
| A3, psi | .7778E6 | .4885E6 | .1928E6 | .4861E5 | .8368E4 |
| A4 | .7325E1 | .3627E1 | .3207E1 | .3214E1 | .3909E1 |
| **Stowell** | | | | | |
| s | .1156E-11 | .7814E-10 | .1529E-9 | .1282E-8 | .7478E-9 |
| $\Delta H$ | .2198E7 | .4471E6 | .3640E6 | .1668E7 | .1121E7 |
| $\sigma_0$, psi | .1376E5 | .4971E4 | .1682E4 | .6816E3 | .1913E3 |
| **Moreno** | | | | | |
| $\sigma_y$, psi | .1065E6 | .2392E5 | .7944E4 | .2010E4 | .5140E3 |
| Ep, psi | .2590E7 | .1120E6 | .3820E5 | .9583E4 | .4577E4 |

## Nomenclature

The following nomenclature has been used in correlating coating constitutive equations with data.

| | | | | |
|---|---|---|---|---|
| $\sigma$ | = | stress (psi) | note: | 6.895 kPa = 1 psi |
| $\epsilon_t$ | = | total strain (in/in) | note: | 1 cm/cm = 1 in/in |
| $\epsilon_e$ | = | elastic strain (in/in) | | |
| $\epsilon_{in}$ | = | $\epsilon_p + \epsilon_c$ = inelastic strain (in/in) | | |
| $\dot{\epsilon}_{in}$ | = | inelastic strain rate ($sec^{-1}$) | | |
| $\epsilon_p$ | = | plastic strain (in/in) | | |
| $\epsilon_c$ | = | creep strain (in/in) | | |
| $\epsilon_{in_{eff}}$ | = | effective inelastic strain (in/in) | | |
| $\dot{\epsilon}_{in_{eff}}$ | = | effective inelastic strain rate ($sec^{-1}$) | | |
| E | = | elastic modulus (psi) | | |
| t | = | time (sec) | | |
| T | = | absolute temperature (R) | | |
| R | = | universal gas constant (1545 ft-lbf/lbm-mole-R) | | |
| $\Delta H$ | = | apparent activation energy (ft-lbf/lbm-mole) | | |
| $\Omega$ | = | instantaneous back stress (kinematic hardening parameter) | | |
| $\Omega_2$ | = | component of instantaneous back stress (psi) | | |
| K | = | instantaneous drag stress (isotropic hardening parameter) | | |
| $\Delta\epsilon_t$ | = | total strain increment (in/in) | | |
| $\Delta\epsilon_e$ | = | elastic strain increment (in/in) | | |
| $\Delta\epsilon_p$ | = | time independent (plastic) strain increment (in/in) | | |
| $\Delta\epsilon_c$ | = | time dependent (creep) strain increment (in/in) | | |
| $\Delta\sigma$ | = | stress increment (psi) | | |

Nomenclature (continued)

$\Delta\sigma_p$ = time independent (plastic) stress increment (psi)

$\Delta\sigma_{e+c}$ = combined elastic and time dependent (creep) stress increment

$\sigma_y$ = yield stress (psi)

$\Delta t$ = time increment (sec)

Ep = strain hardening slope of monotonic stress/strain curve

Subscripts: i = beginning of increment

i+1 = end of increment

Temperature dependent material constants:

A1, A2, A3, A4, n, n1, n7, n9, n10, n11, m0, K1, K2, s, $\sigma_0$, Ep, $\sigma_y$.

Classical Model

The classical approach (e.g., Reference 8) was one of the first attempts at developing a nonlinear model which recognized the observed dissimilarity between monotonic tensile and creep inelastic material response. Time independent inelasticity (plasticity) and time dependent inelasticity (creep) are considered as uncoupled components of the total inelastic strain.

$$\varepsilon_{in} = \varepsilon_p + \varepsilon_c \tag{5-1}$$

Thus, the total strain function, neglecting thermal strain, is written:

$$\varepsilon_t = \varepsilon_e + \varepsilon_p + \varepsilon_c \tag{5-2}$$

or

$$\Delta\varepsilon_t = \Delta\varepsilon_e + \Delta\varepsilon_p + \Delta\varepsilon_c \tag{5-2A}$$

Both plastic and creep strain functions are chosen to provide adequate duplication of the material behavior. From tests of PWA 286, it was determined that both functions could be described by simple power law relationships:

$$\Delta\varepsilon_p = \frac{A_2}{A_1}\left(\frac{\sigma}{A_1}\right)^{A_2-1}\Delta\sigma \tag{5-3}$$

$$\Delta\varepsilon_c = \left(\frac{\sigma}{A_3}\right)^{A_4}\Delta t \tag{5-4}$$

Data regressions for unexposed HIP PWA 286 using the classical model are presented in Figure 38. As expected, time independent inelasticity (plasticity) dominates the low temperature response, while time dependent inelasticity (creep) dominates at high temperatures. A summary of standard deviations which describe how well the classical model fit the entire range of initial stress relaxation tests is presented in Table XIV.

Table XIV 6.895 kPa = 1 psi

Summary of Constitutive Model Regression Fit
Standard Deviation (1 std. dev., in psi)

| | 538°C (1000°F) | 760°C (1400°F) | 871°C (1600°F) | 982°C (1800°F) | 1093°C (2000°F) |
|---|---|---|---|---|---|
| Walker | 2000 | 1815 | 633 | 153 | 101 |
| Simplified Walker | 2041 | 1717 | 876 | 220 | 119 |
| Classical | 2255 | 1878 | 736 | 300 | 127 |
| Stowell | 6541 | 2091 | 1044 | 377 | 140 |

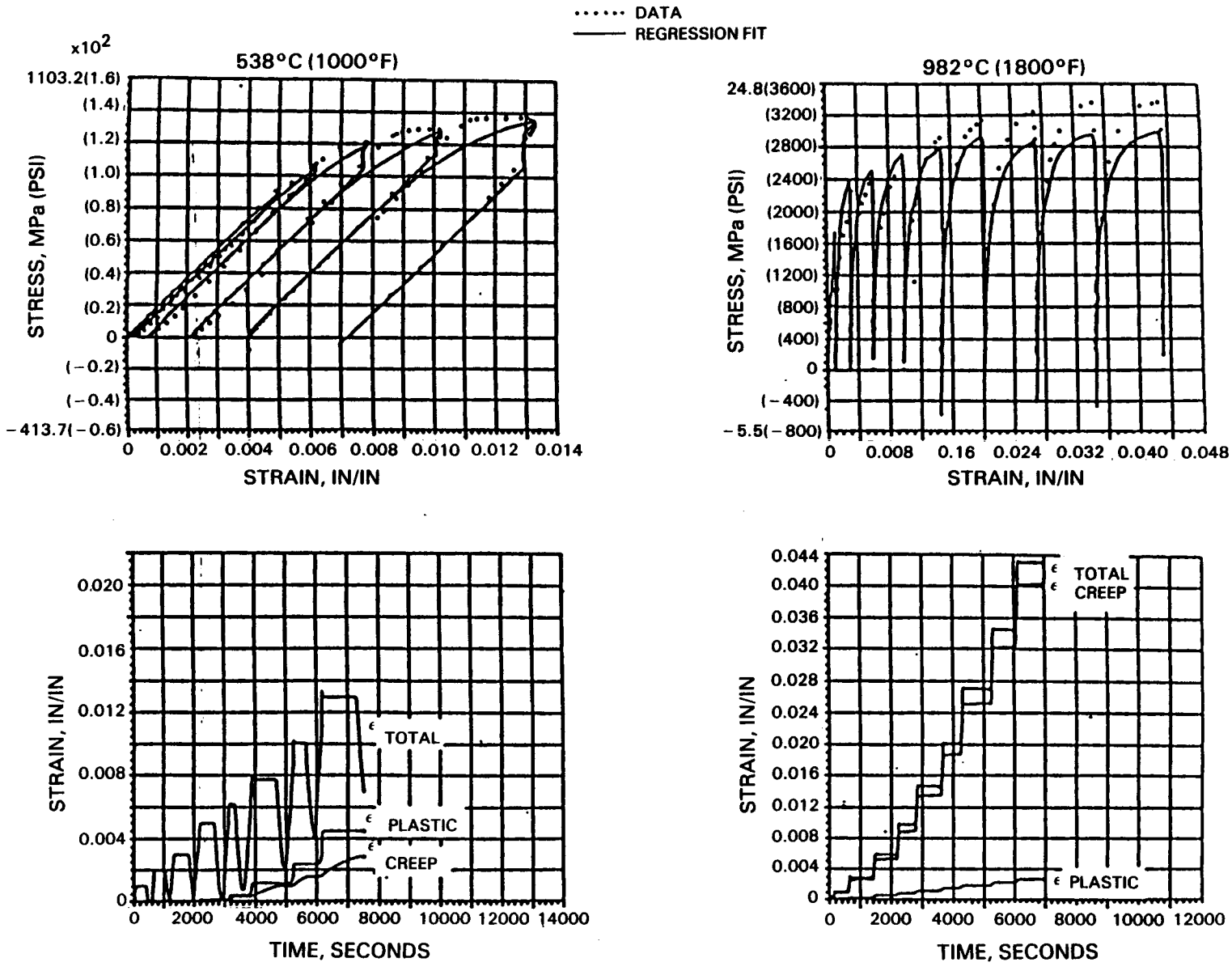


Figure 38 Classical Model Regression Fit of Unexposed PWA 286 Stress Relaxation Data

Walker Model

The Walker model (Reference 9) is among a new generation of constitutive models based on a unified viscoplastic approach which considers all nonlinear behavior as time-dependent inelasticity which includes, in the extreme, time-independent inelasticity. No distinction is made between plastic and creep inelastic action as in the Classical model. Walker, from his earlier work on Hastelloy X, chose to express inelastic behavior by a power law relationship which is written:

$$\dot{\varepsilon}_{in} = \left(\frac{\sigma - \Omega}{K}\right)^n \tag{5-5}$$

where n is a constant and $\Omega$, back stress, and K, drag stress, are strain history dependent internal state variables which describe kinematic and isotropic cyclic hardening, respectively.

The back stress term is a quantity which physically corresponds to the asymptotic stress state under relaxation conditions. Qualitatively, the evolutionary expression for back stress is a sum of opposing hardening and thermal and dynamic recovery components which can be characterized as:

$$\dot{\Omega} = f\,(\dot{\varepsilon}_{in},\ \varepsilon_{in},\ T,\ t) - g\,(\dot{\varepsilon}_{in},\ \Omega,\ T,\ t) \tag{5-6}$$

Drag stress is a quantity which represents a resistance to inelastic flow, and is considered a function of the effective inelastic strain.

$$K = K_1 - K_2 \cdot \exp(-n_7 \cdot \varepsilon in_{eff}) \tag{5-7}$$

where K1 = fully hardened/softened drag stress, and
K1 - K2 = initial drag stress.

Thus, the drag stress function is a monotonically increasing relationship describing isotropic hardening (K2 > 0) or softening (K2 < 0). The Walker model form used for this investigation is given below:

$$\dot{\varepsilon}_t = \dot{\varepsilon}_e + \dot{\varepsilon}_{in} \tag{5-8}$$

$$\dot{\varepsilon}_{in} = \left(\frac{\sigma - \Omega}{K}\right)^n \tag{5-9}$$

$$K = K_1 - K_2 \cdot \exp(-n_7 \cdot \varepsilon in_{eff}) \tag{5-10}$$

$$\Omega = n_1\ \varepsilon_{in} + \Omega_2 \tag{5-11}$$

$$\dot{\Omega}_2 = n_{11}\ \dot{\varepsilon}_{in} - \Omega_2 \left(\dot{G}_2 - \frac{1}{n_{11}}\ \frac{\partial n_{11}}{\partial T}\ \frac{dT}{dt}\right) \tag{5-12}$$

$$\dot{G}_2 = n_9\ \dot{\varepsilon} in_{eff} + n_{10}\ \Omega_2^{(M_0-1)} \tag{5-13}$$

$$\dot{\varepsilon} in_{eff} = \left|\dot{\varepsilon}_{in}\right| \tag{5-14}$$

References 9 and 10 provide a detailed discussion of Walker's and other unified approaches.

Figure 39 presents the regression fit of the Walker model to the 538°C and 982°C (1000°F and 1800°F) isothermal data sets. Again, the standard deviation describing the "goodness" of each regression throughout the entire data temperature range is presented in Table XIV.

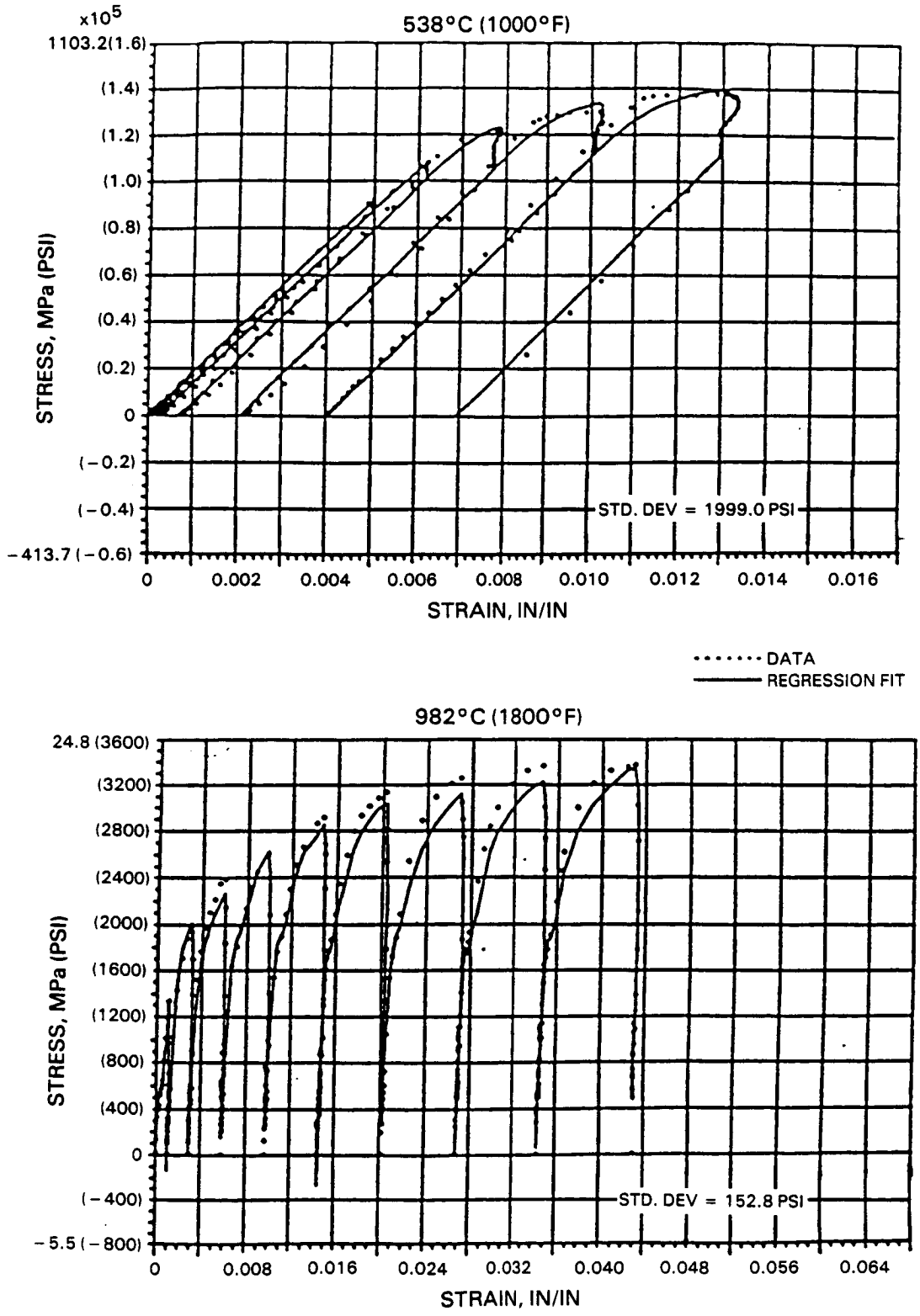


Figure 39 Walker Model Regression Fit of Unexposed PWA 286 Stress Relaxation Data

Simplified Walker Model

This model is identical to the Walker model except that all back stress terms were eliminated.

$$\dot{\epsilon}_{in} = \left(\frac{\sigma}{K}\right)^n \tag{5-15}$$

The expression for $\dot{\epsilon}_{in}$ is equivalent to the Classical model power law creep equation; however, in this case, the drag stress term, K, is not a constant, but an evolutionary variable. From a simplicity standpoint, this model is very attractive.

The regression fit of the Simplified Walker model is presented in Figure 40. Corresponding standard deviations of the data fits are presented in Table XIV.

Simplified Unified Approach (Moreno)

Recently, Moreno (Reference 11) has had success in predicting the constitutive response of Hastelloy X using a hybrid model derived from both classical and unified approaches. Basically, the model assumes that the thermoelastic response is known from previous analysis from which incremental values of strain, temperature, and time are used to calculate the actual (nonlinear) stress history.

Strain increments are considered as either time independent plastic or thermoelastic creep.

$$\Delta\epsilon_t = \Delta\epsilon_p \tag{5-16}$$

or

$$\Delta\epsilon_t = \Delta\epsilon_e + \Delta\epsilon_c \tag{5-17}$$

Expressed in terms of stress increments:

$$\Delta\sigma = \Delta\sigma_p \tag{5-18}$$

or

$$\Delta\sigma = \Delta\sigma_{e+c} \tag{5-19}$$

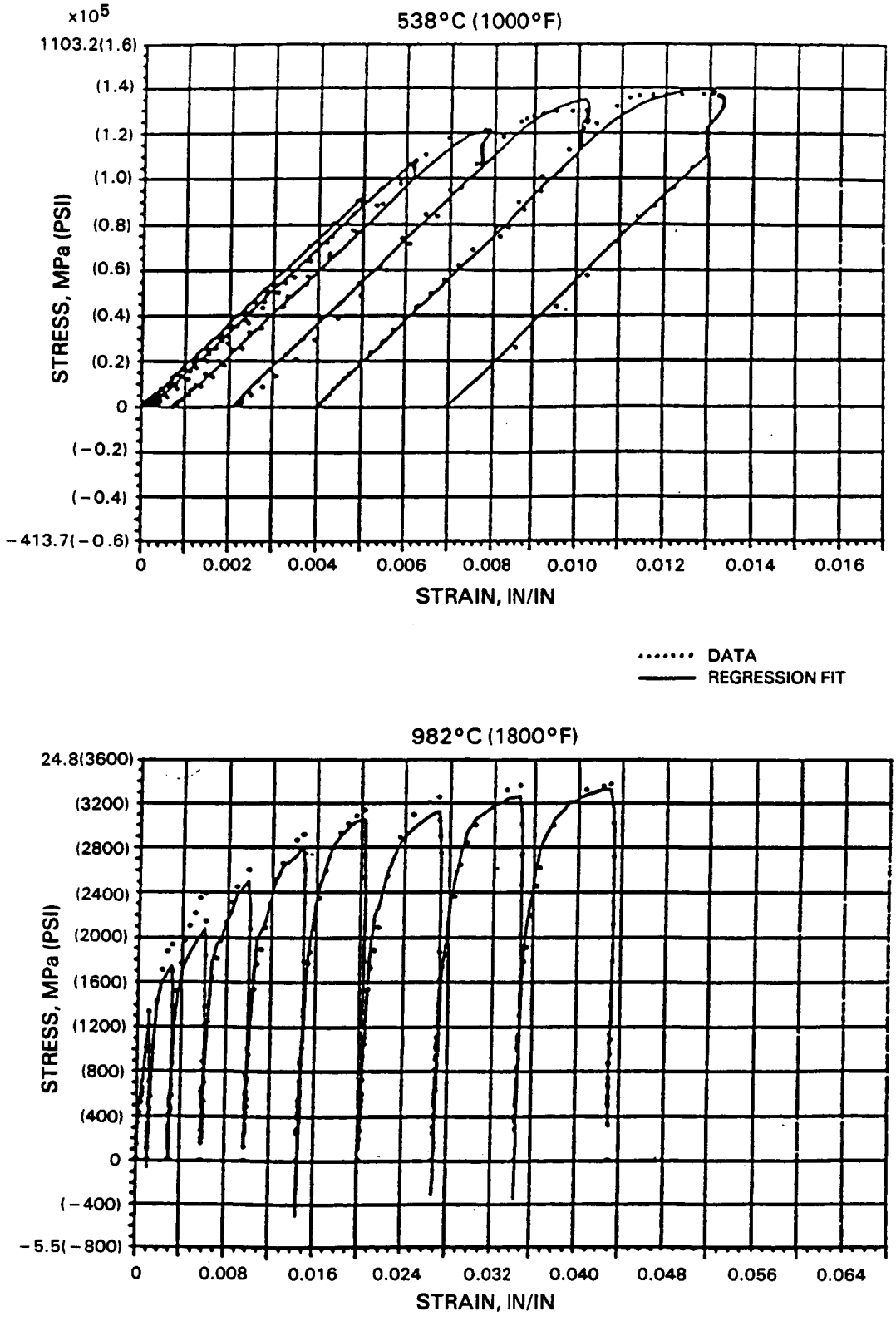


Figure 40 Simplified Walker Model Regression Fit of Unexposed PWA 286 Stress Relaxation Data

Classical yield surface criteria (Figure 41) are used to determine the onset of plastic action. Isothermal yield points are calculated from a tri-linear representation of tensile stress/strain information (Figure 42), and are assumed to be equal in tension and compression (i.e., the material is perfectly isotropic). No cyclic hardening is considered. Justification for this definition of yielding was based on observations of Hastelloy X cyclic response: (1) at elevated temperatures, little cyclic hardening/softening occurs; and (2) during thermomechanical cycling, exposure to the higher temperatures significantly reduces the amount of cyclic hardening developed at the lower temperatures.

The stress increment associated with time independent plastic action is then calculated as:

$$\sigma_{i+1} - \sigma_i = \Delta\sigma_p = \sigma_{y_{i+1}} - \sigma_{y_i} \tag{5-20}$$

for

$$\sigma_i = \sigma_{y_i}$$

$$T_{i+1} \geq T_i$$

or

$$\sigma_{i+1} - \sigma_i = \Delta\sigma_p = \frac{Ep_{i+1} + Ep_i}{2} \Delta\varepsilon_t \tag{5-20A}$$

for

$$\sigma_i = \sigma_{y_i}$$

$$T_{i+1} < T_i$$

and the stress increment associated with time dependent creep behavior is calculated as:

$$\sigma_{i+1} - \sigma_i = \Delta\sigma_{e+c} = E\,(\Delta\varepsilon_t - \Delta\varepsilon_c) \tag{5-21}$$

This model has been successful with Hastelloy X, which exhibits some behavioral similarities with overlay coating PWA 286.

Yield constants for the Simplified Unified Approach were obtained by using the cyclic stress/strain curves from the first series of baseline stress relaxation tests. This was accomplished by constructing a monotonic stress/strain curve by plotting the maximum stress and associated strain from each cycle. The resulting yield surface is presented in Figure 43. Creep law constants for the model were obtained from the Classical model creep law:

$$\Delta\varepsilon_c = \left(\frac{\sigma}{A_3}\right)^{A_4} \Delta t \tag{5-22}$$

Correlation of the isothermal stress relaxation data was not performed; however, the standard deviations of such correlations were expected to be higher than those of the Walker model.

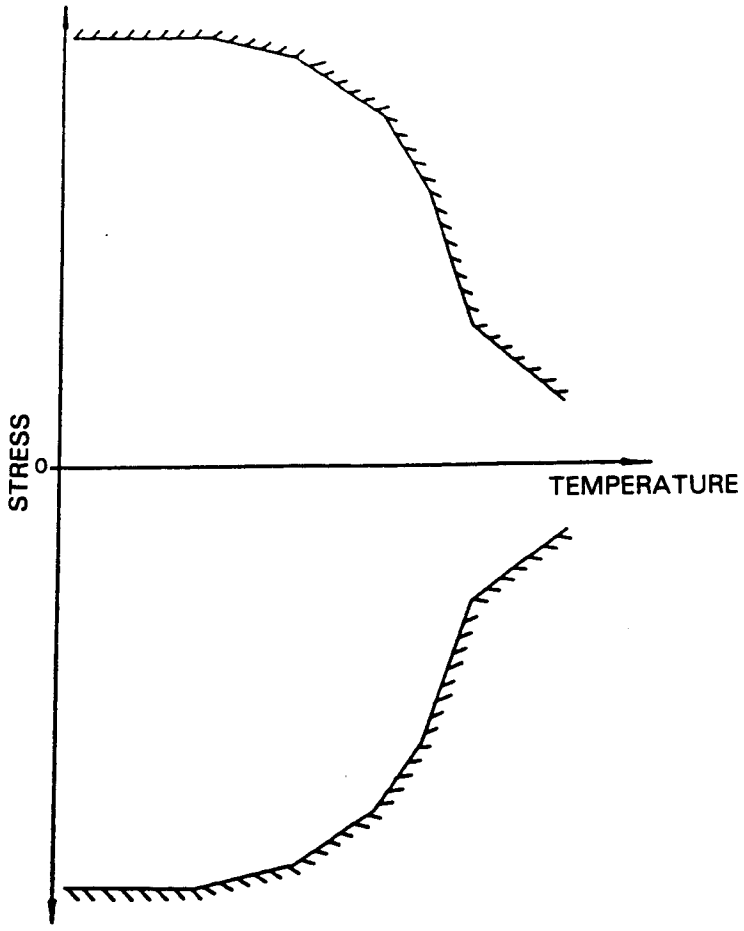


Figure 41 Classical Temperature Dependent Yield Surface for Simplified Unified Approach

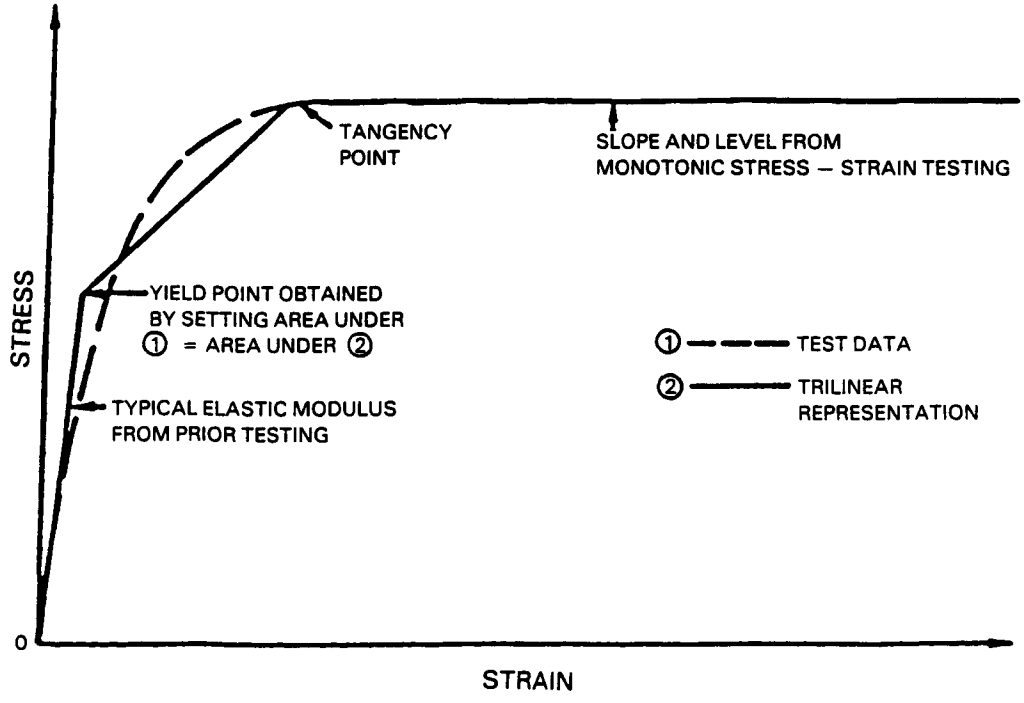


Figure 42 Construction of Tri-Linear Stress Strain Curve

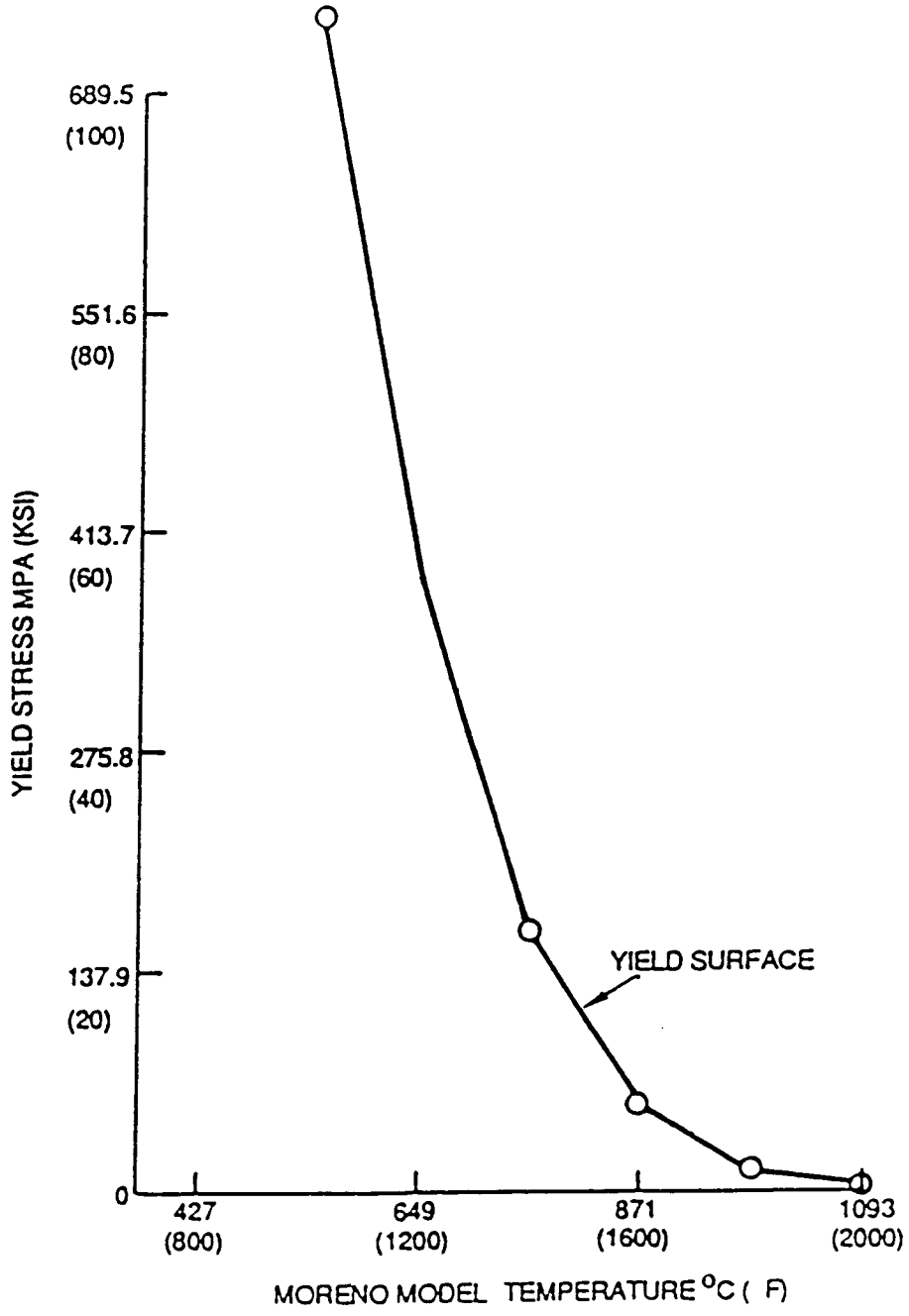


Figure 43 Moreno Model Temperature Dependent Yield Surface Obtained from Unexposed, Bulk Hot Isostatically Pressed PWA 286

Stowell Model

The Stowell model (References 12 through 14) is another form of a unified viscoplastic approach initially developed to simulate heating rate effects on yielding of metals. It considers inelastic action based on an apparent activation energy level and uses a hyperbolic sine stress function.

$$\dot{\varepsilon}_{in} = 2\ s\ T \cdot \exp\left(\frac{-\Delta H}{RT}\right) \cdot \sinh\left(\frac{\sigma}{\sigma_0}\right) \qquad (5\text{-}23)$$

Correlations using the Stowell model are presented in Figure 44 and associated standard deviations are summarized in Table XIV.

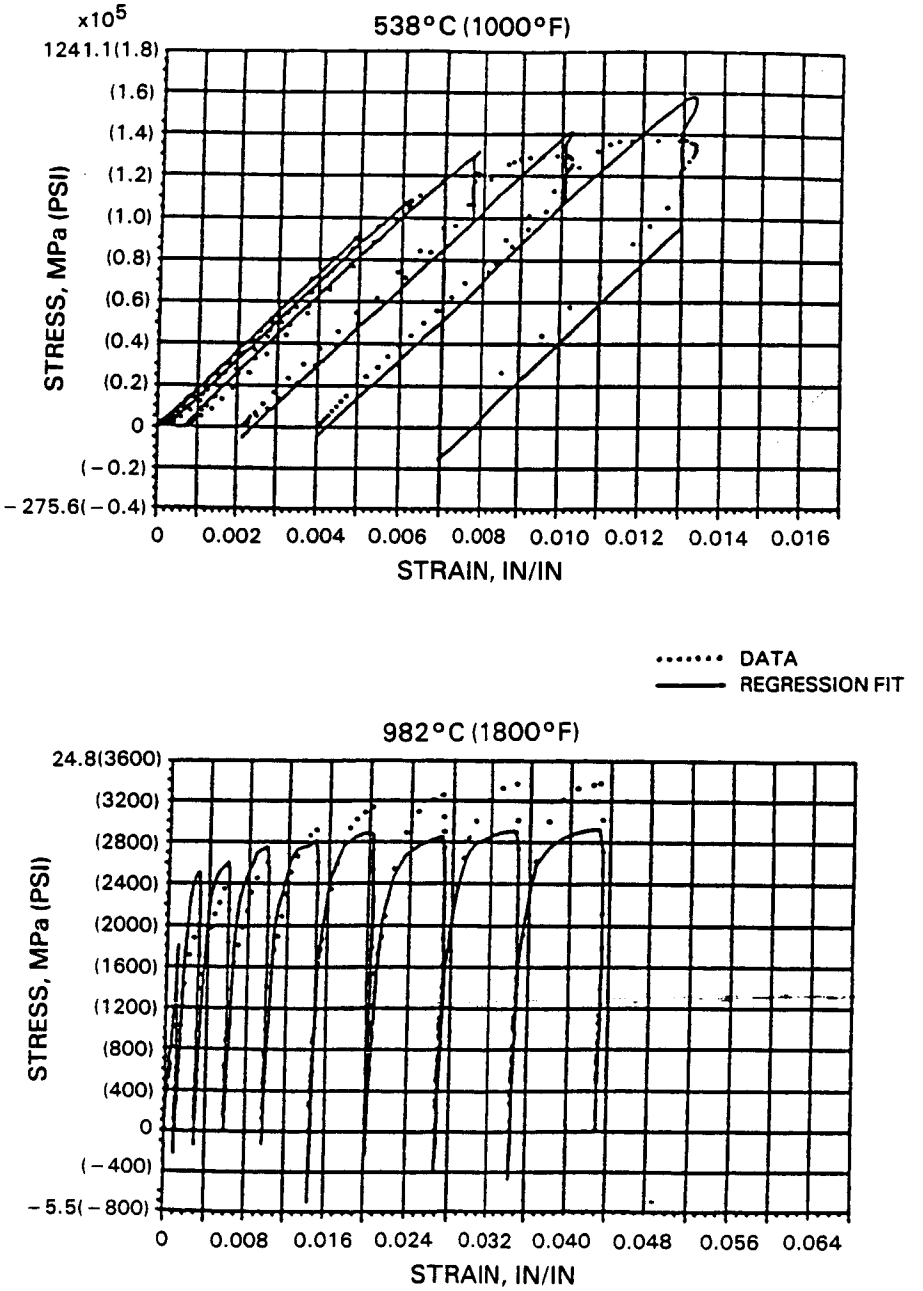


Figure 44 Stowell Model Regression Fit of Unexposed PWA 286 Stress Relaxation Data

5.1.3 Prediction of Thermomechanical Data

Experimental and predicted thermomechanical fatigue (TMF) waveforms are compared in Figures 45 and 46(A). The high temperature response of the TMF cycle was fairly well predicted by all the models, but none were able to completely predict the low temperature tensile inelasticity. In fact, only the Walker, Classical and Moreno models managed to predict any low temperature yielding. The Simplified Walker and Stowell models predicted thermoelastic tensile responses.

The ability of the Walker model to predict the observed tensile yielding trend can be explained as follows: during the compression/heating portion of the cycle (points A to B), the material relaxes, creating a compressive back stress. Then, during the tensile/cooling portion of the cycle (points B to C), the back stress moves deeper into compression due to temperature rate effects. Thus, the "effective" stress ($\sigma - \Omega$), at which yielding initiates, occurs at a lower tensile applied stress.

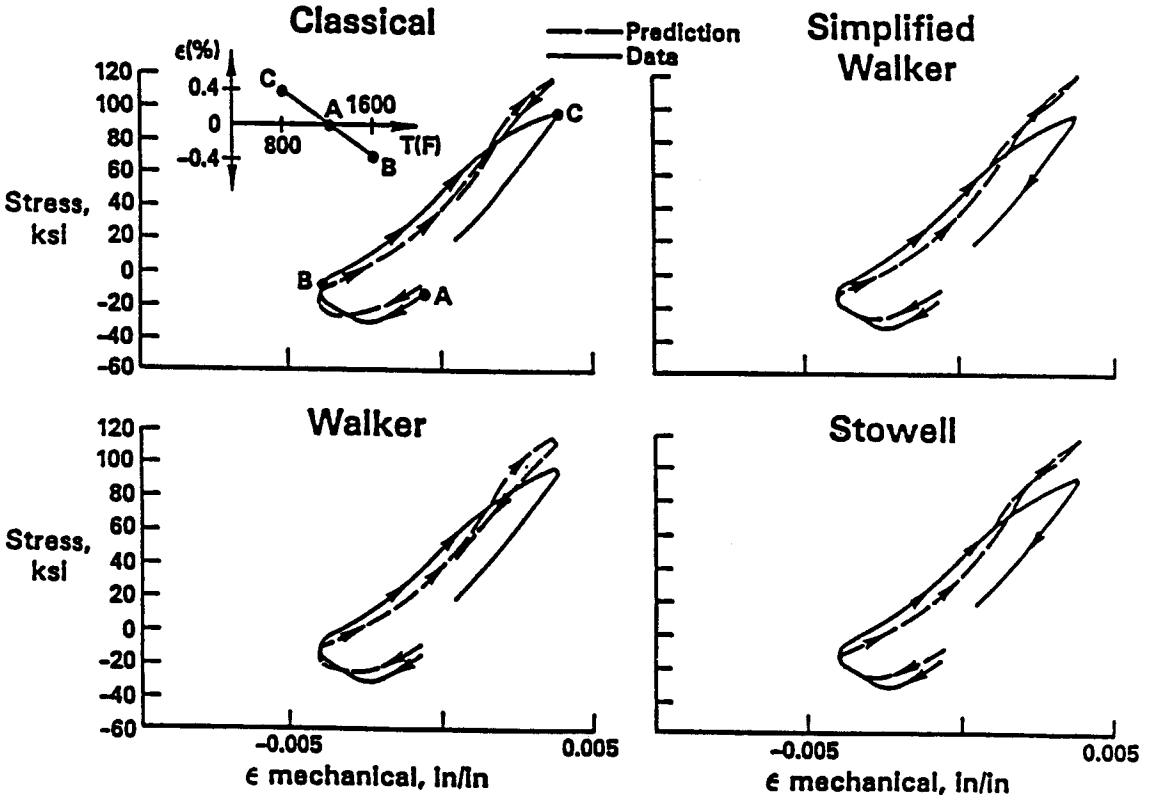


Figure 45 PWA 286 Thermomechanical Test - First Cycle Prediction Versus Test Data

(A)

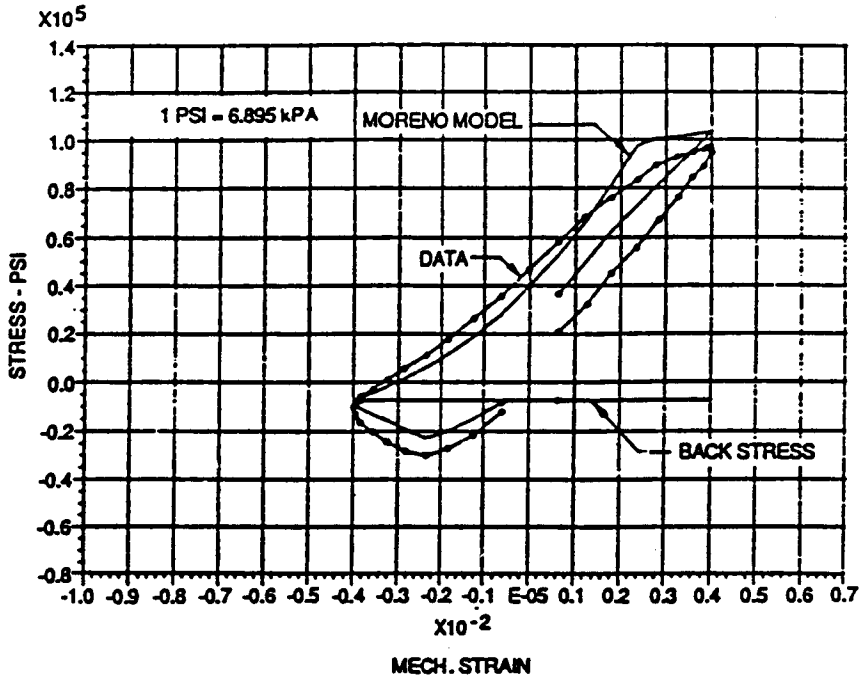


(B)

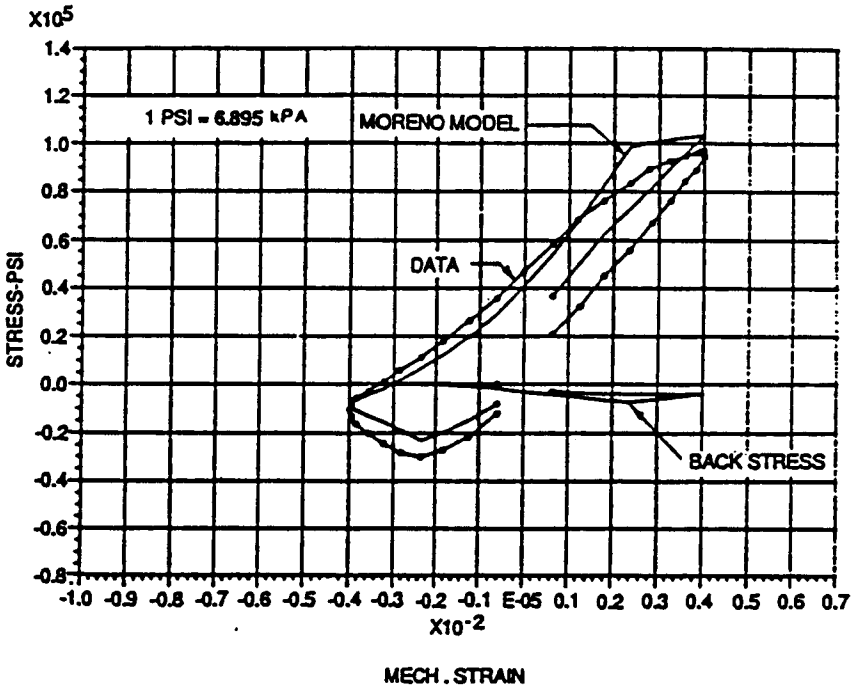


Figure 46 Moreno Model Prediction of Unexposed, Bulk Hot Isostatically Pressed PWA 286 Overlay Coating Out-of-Phase Thermomechanical Verification Test Using: (A) Constant Back Stress, and (B) Continuous Back Stress Evolution Formulation

The ability of the Classical model to correlate isothermal yielding behavior was less satisfactory than that of other models: in general, yielding is predicted to occur at much lower stresses than indicated by data (Figure 38). The prediction of low temperature yielding for the TMF cycle directly results from the low regressed yield strength. Had the Classical model correlated the 538°C (1000°F) behavior better, the low temperature tensile portion of the TMF prediction would have been more like the Simplified Walker and Stowell models, i.e., thermoelastic.

In the Simplified Unified Approach predictions, the concepts of a perfectly isotropic material and back stress were included as discussed in Reference 11. The tensile-going back stress level was held constant at about -51.7 MPa (-7.5 ksi), consistent with the technique employed by Moreno for Hastelloy X. Although this technique improved the low temperature tensile portion of the hysteresis loop, the Moreno model is not easily transformed into a general form for computer automation. Particularly, the Moreno model choice of back stress level depends on the TMF cycle type, which is generally not known a-priori. For example, out-of-phase TMF tests require a compressive back stress and in-phase cycles require a tensile back stress. Then, there is the question of how to choose a back stress for the following TMF cycle.

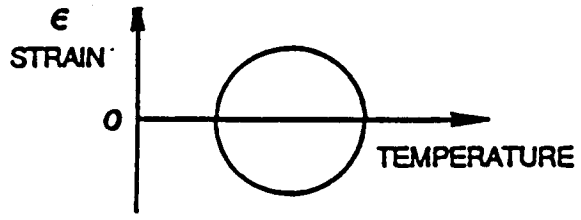


To prevent such ambiguities, a simple continuously evolving back stress formulation was adopted.

$$\Delta\Omega = n^1 \cdot \Delta\varepsilon_{in} + \Delta n^1 \cdot \varepsilon_{in} \qquad (5\text{-}24)$$

where $n^1$ is a temperature dependent material constant.

It was assumed that the material constant ($n^1$) was equivalent to the strain hardening slope (Ep) obtained from the cycled curves of the baseline isothermal data. This was based on the notion that back stress evolution during TMF occurs at saturated rates. For an isothermal tensile test, this is equivalent to the back stress growth rate during steady state inelastic straining (i.e., $\dot{\Omega}$ = constant). Thus, the back stress evolution equation is written as:

$$\Omega_{i+1} - \Omega_i = \frac{Ep_{i+1} + Ep_i}{2} (\varepsilon in_{i+1} - \varepsilon in_i) + (Ep_{i+1} - Ep_i)\, \varepsilon in_{i+1} \qquad (5\text{-}25)$$

Prediction of the TMF data using the continuously evolving back stress formulation is presented in Figure 46(B). The predicted TMF hysteresis loop shape is unchanged by using the new back stress formulation. In both cases, however, the low temperature inelasticity was not well predicted.

## 5.2 PWA 1480 SINGLE CRYSTAL CONSTITUTIVE MODELS

### 5.2.1 Overview

Two separate unified constitutive models for single crystal PWA 1480 have been formulated and are in the final stages of development. The first model, the "microscopic model," computes the inelastic quantities on the crystallographic slip systems. Development of this slip system based model began at Pratt & Whitney in 1982 and continues to be a part of a large company effort to develop constitutive models. The development has continued since 1982 through the combined efforts of Pratt & Whitney's personnel and consultants under the company program and in a complementary NASA grant NAG-512. This model achieves the required directional properties as a consequence of summing the slip system strains which have been resolved onto the global coordinate system. The second model, the "macroscopic model," uses global stresses and strains directly and employs anisotropic tensors operating on global inelastic quantities to achieve the required directional properties. The two models offer a trade between accuracy and physical significance and computing time requirements. The microscopic model is more accurate and is more physically significant in its formulation than the macroscopic model. However, the macroscopic model is more computationally efficient because integration of the evolutionary equations is required only for the six global stress/strain quantities rather than for each of the 18 slip systems.

Both models use a unified approach for computing all inelastic strain (rather than separating "plastic" and "creep" strains), and employ both a drag stress and an equilibrium (back) stress in the equations for inelastic strain rate. Each of the models is discussed in more detail below and cyclic stress strain data at 871°C (1600°F) are used to illustrate the behavior of the models. Figures 47 and 4; show test data from uniaxial bars oriented in three crystal directions: <001>, <111> and <011>. These three orientations represent the extreme ends of the possible crystal orientations. The tests were conducted under controlled strain rates ranging from 0.001% per second to 1.0% per second.

### 5.2.2 Crystallographic Slip Viscoplastic Formulation

The "microscopic" model attempts to incorporate metallurgical observations regarding the deformation of single crystals in a unified viscoplastic formulation. Details of the mathematical formulation of the micromechanical model are reported in References 1 and 2. Some of the important features of the model are discussed below and comparisons with data are presented. The model assumes that all inelastic behavior results from a homogeneous shear strain accumulation on each of the slip systems and that the resulting global or macroscopic inelastic strains are simply the sum of these slip system strains.

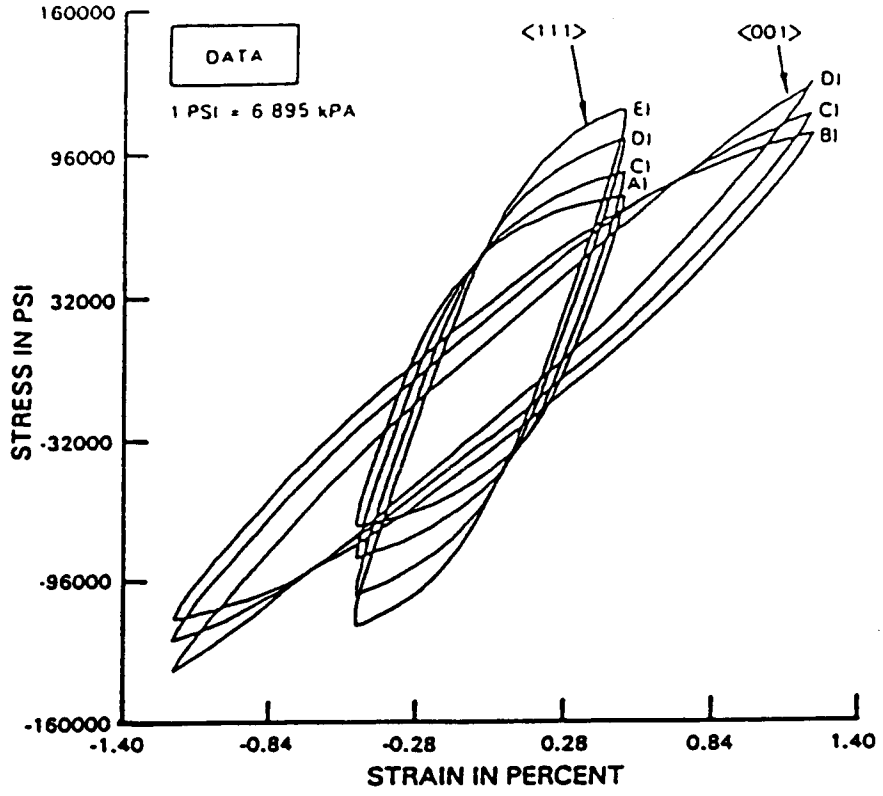


Figure 47 Experimental Loops in <001> and <111> Directions at 871°C (1600°F) at Strain Rates of: (A) 0.001% Per Second, (B) 0.0025% Per Second, (C) 0.01% Per Second, (D) 0.1% Per Second, and (E) 0.5% Per Second

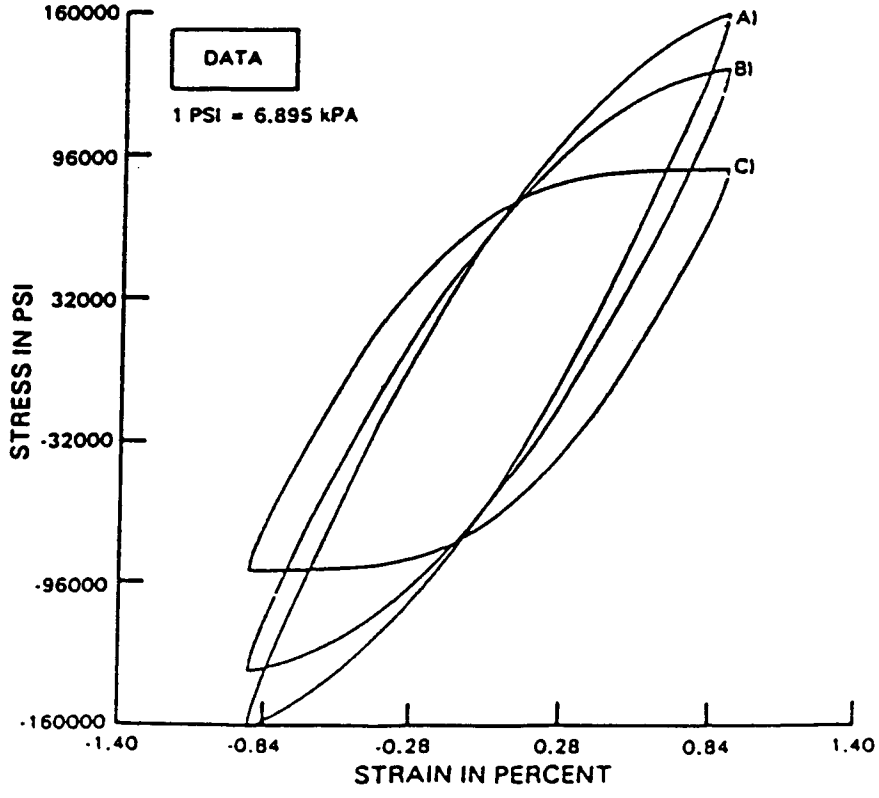


Figure 48 Experimental Loops in <001> Orientation at 871°C (1600°F) at Strain Rates of: (A) 1.0% Per Second, (B) 0.1% Per Second, and (C) 0.001% Per Second

Global stresses and strains are resolved onto coordinate systems for each of 12 octahedral and 6 cube slip systems. Figure 49 shows such a coordinate system for one of the octahedral slip systems along with some slip system stresses that are used to calculate the shear strain on that slip system. The general form of the equations governing inelastic strain on each of the octahedral slip systems is shown in the following equation:

$$\dot{\gamma}_r = \frac{(\pi_r - \omega_r)\left|\pi_r - \omega_r\right|^{P-1}}{K^P} \qquad (5\text{-}26)$$

where $\dot{\gamma}_r$ = the inelastic shear strain rate on the slip system

$\pi_r$ = the effective stress acting on the slip system

$\omega_r$ = the back stress acting on the slip system

K = the drag stress acting on the slip system.

The model has been formulated so that the effective stress, $\pi_r$, can include not only the shear stress acting in the slip direction, but other components of stress acting on the slip plane such as the stress acting normal to the slip plane ($\pi$nn in Figure 49). However, good correlation with experiment has been achieved to date by using only the shear stress acting in the slip direction ($\pi$mm in Figure 49).

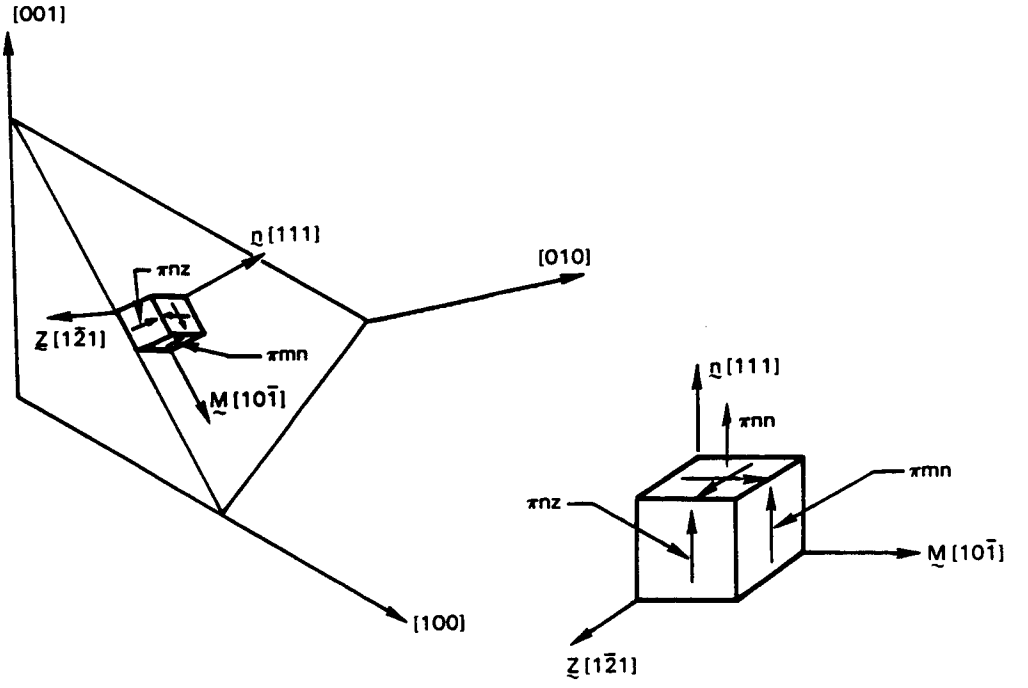


Figure 49 Coordinate System for the (111) [10$\bar{1}$] Octahedral Slip System

Both equilibrium and drag stress are evolutionary state variables. The back stress grows with the inelastic strain on the slip system and includes a dynamic recovery term to model the observed Bauschinger effect and a thermal recovery term that can be viewed as accounting for the reduction of internal stresses due to diffusion processes. The evolution of the drag stress includes terms to account for latent hardening (hardening due to simultaneous straining on slip systems other than the primary system), tension/compression asymmetry due to constriction or expansion of Shockley partial dislocations and cross slip from octahedral to cube planes. The stress $\pi nz$ in Figure 49 is assumed to control the tension/compression asymmetry. The cube cross slip is assumed to be driven by the stress $\psi$ in Figure 50. This is the shear stress acting in the slip direction but on the cube face rather than the octahedral plane.

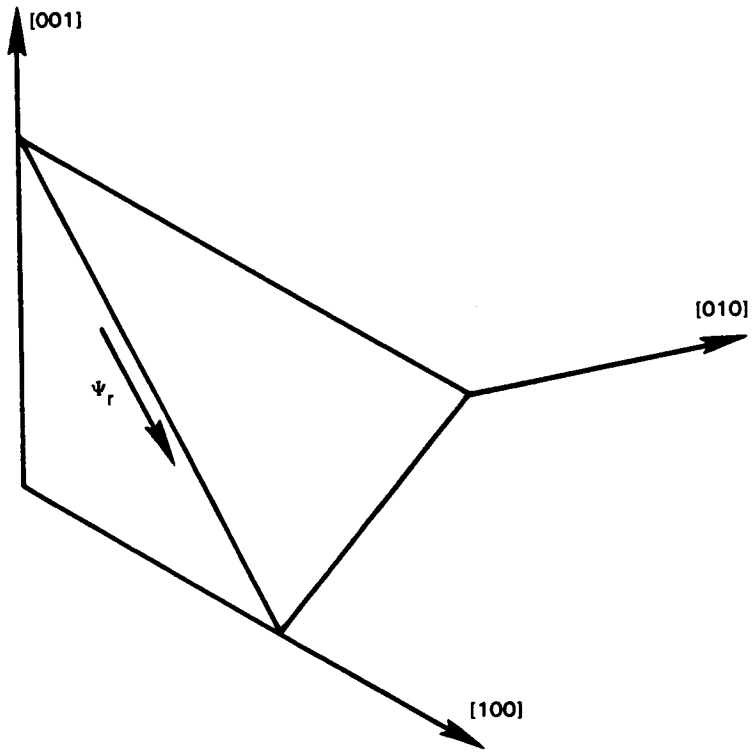


Figure 50 The Shear Stress $\psi_r$ Acting on the Cube Plane in the $[1\bar{2}1]$ Direction Is Assumed to Drive Cross Slip from the (111) $[1\bar{2}1]$ Slip System

The model includes a similar set of equations for the cube slip system, the importance of which can be shown by examining the results of inactivating the cube system terms. The model, thus modified, was fit to the <001> data (Figure 47) and subsequently used to predict the <111> behavior. Figure 51 shows the correlation with the <001> data is quite good, but the prediction for the <111> data is poor. Similarly, a prediction of the response in the <011> direction (Figure 52) is poor compared to the test data in Figure 48. The good correlation with the <001> data could have been expected since a uniaxial stress on a <001> bar produces nonzero shear stresses on the octahedral slip systems but zero shear stress on the cube slip systems. In contrast, a tensile bar oriented in the <111> direction has nonzero shear stresses on both octahedral and the cube slip systems. When cube slip terms are included in the model, the correlation with the <111> and <001> data is quite good as shown in Figure 53. The model constants in this case have been determined to best fit both the <001> and the <111> data. The accuracy of the full model is illustrated in Figure 54 by a prediction of data from a third orientation: the <011> orientation. Comparison with the test data in Figure 48 shows the prediction is very good. The maximum difference seen between the micromodel and test data for all three orientations, for stress ranges up to 21000 MPa (305 ksi) and over three orders of magnitude of strain rate is less than 62 MPa (9 ksi).

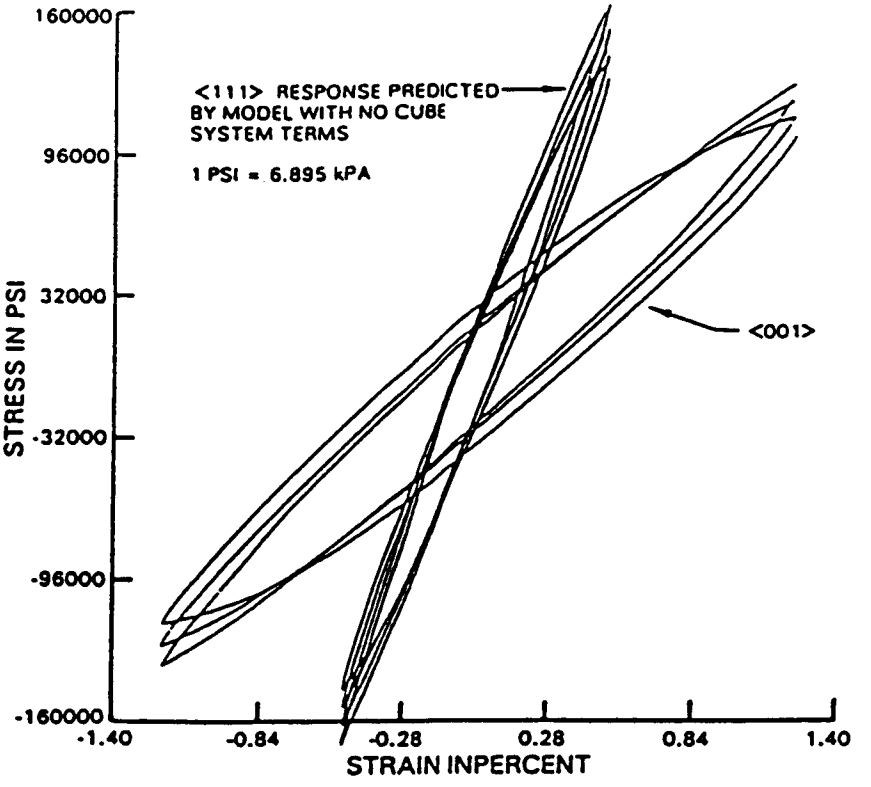


Figure 51 Using Only Octahedral Slip Terms, the <001> Data Is Correlated Well but Subsequent Prediction of <111> Response Is Poor (Compare to Data in Figure 47)

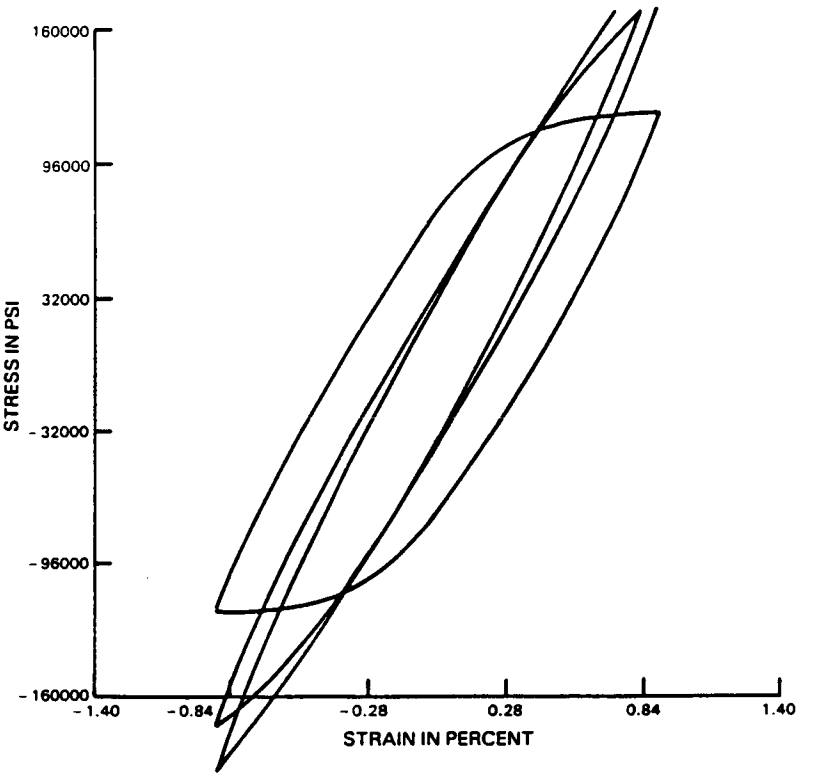


Figure 52 Predicted Loops in <011> Orientation at 871°C (1600°F) Using Only the Octahedral Slip Constants

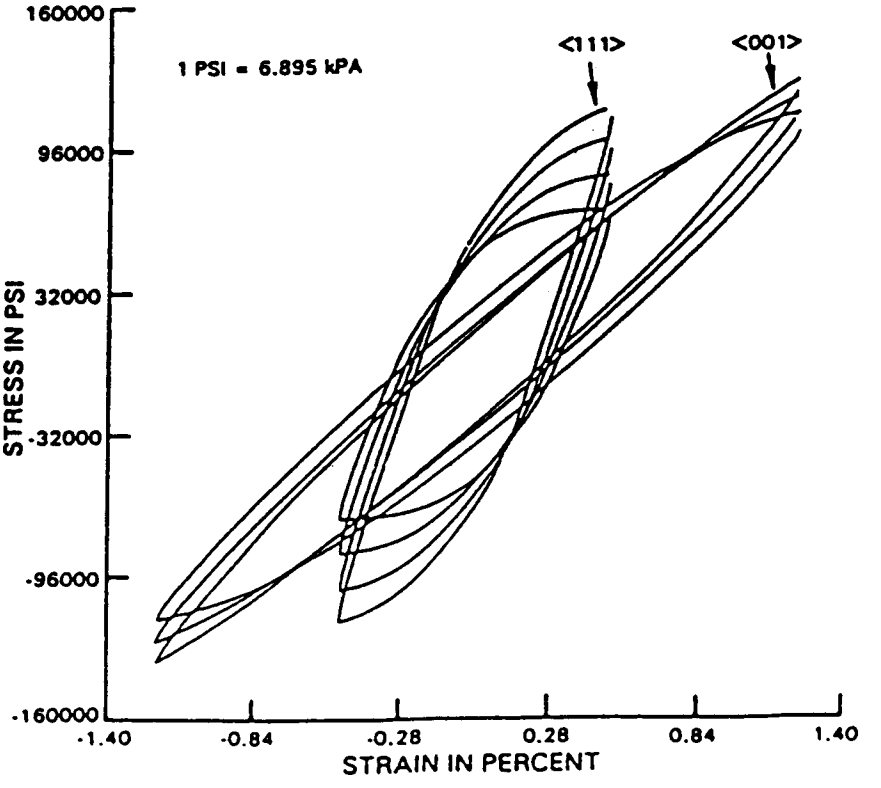


Figure 53 Micro Model with Both Octahedral and Cube Slip Terms Correlated to <111> and <001> Data (Compare to Data in Figure 47)

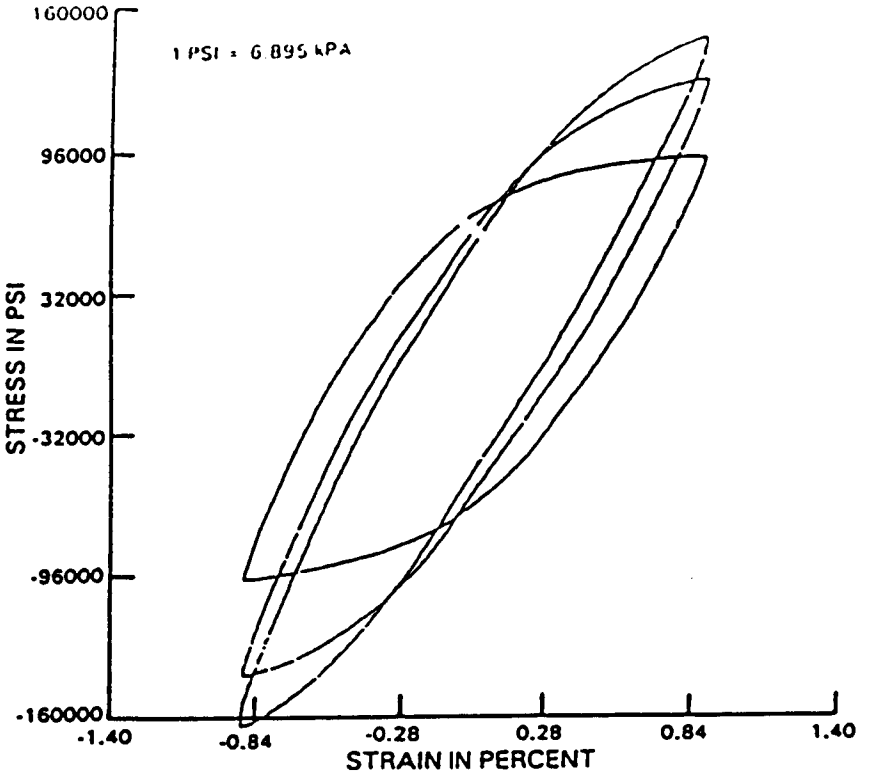


Figure 54 Predicted Loops in <011> Orientation at 871°C (1600°°F) (Compare to Data in Figure 48)

5.2.3 Macroscopic Constitutive Formulation

In the generalization of macroscopic unified viscoplastic constitutive models to account for anisotropic material behavior, the inelastic strain rate is assumed to depend on the overstress according to relation

$$\dot{\varepsilon}^{p}_{ij} = \left( \frac{\sqrt{M_{ijkl} \, (\sigma_{ij} - \Omega_{ij}) \, (\sigma_{kl} - \Omega_{kl})}}{K} \right)^{n-1} \frac{M_{ijkl} \, (\sigma_{ij} - \Omega_{ij}) \, (\sigma_{kl} - \Omega_{kl})}{K} \qquad (5\text{-}27)$$

where $\Omega_{ij}$ and K are the equilibrium and drag stress state variables, respectively. The power law expression in Equation (5-27) may be replaced by an exponential, hyperbolic sine, or any suitable functional relation according to the particular theory under consideration. The matrix form, $\underset{\sim}{M}$, of the fourth rank tensor Mijkl can be written as:

$$[M] = \begin{bmatrix} M11 & -\frac{M11}{2} & -\frac{M11}{2} & 0 & 0 & 0 \\ -\frac{M11}{2} & M11 & -\frac{M11}{2} & 0 & 0 & 0 \\ -\frac{M11}{2} & -\frac{M11}{2} & M11 & 0 & 0 & 0 \\ 0 & 0 & 0 & M44 & 0 & 0 \\ 0 & 0 & 0 & 0 & M44 & 0 \\ 0 & 0 & 0 & 0 & 0 & M44 \end{bmatrix} \quad (5\text{-}28)$$

Normally, the matrix would contain three independent components for the case of cubic symmetry appropriate to single crystal alloys, but the assumption that the inelastic strain is incompressible reduces the number of independent components to two.

The growth law governing the evolution of the equilibrium stress, $\Omega_{ij}$, may be assumed to have the form:

$$\dot{\Omega}_{ij} = n_1 \dot{\varepsilon}^P_{ij} - n_2 \Omega_{ij} \sqrt{\frac{2}{3} \dot{\varepsilon}^P_{ij} \dot{\varepsilon}^P_{ij}} - n_3 (M_{ijkl} \Omega_{ij} \Omega_{kl})^{m-1} \Omega_{ij} \quad (5\text{-}29)$$

Figure 55 shows predicted hysteresis loops for the <001> and <111> directions using the equilibrium stress growth law in equation (5-29). Comparison with the experimental data (Figure 47) shows that this type of equilibrium stress growth law does not provide the proper orientation dependence. A more appropriate growth law is:

$$\dot{\Omega}_{ij} = N_{ijkl} \dot{\varepsilon}^P_{ij} - P_{ijkl} \Omega_{kl} \sqrt{\frac{2}{3} \dot{\varepsilon}^P_{ij} \dot{\varepsilon}^P_{ij}} - Q_{ijkl} \Omega_{kl} [Q_{ijkl} \Omega_{ij} \Omega_{kl}]^{\frac{m-1}{2}} \quad (5\text{-}30)$$

where the matrix forms of the fourth rank tensors, $\underset{\sim}{N}$, $\underset{\sim}{P}$, and $\underset{\sim}{Q}$, each contain three independent material constants for materials which exhibit cubic symmetry such as single crystal superalloys. For the first evaluation of this form of the anisotropic back stress, only $\underset{\sim}{N}$ was assumed to be a non-diagonal matrix. (This is equivalent to using a single coefficient for the second and third terms of equation 5-30 as was used in equation 5-29). As shown in Figure 56, a much better correlation is achieved.

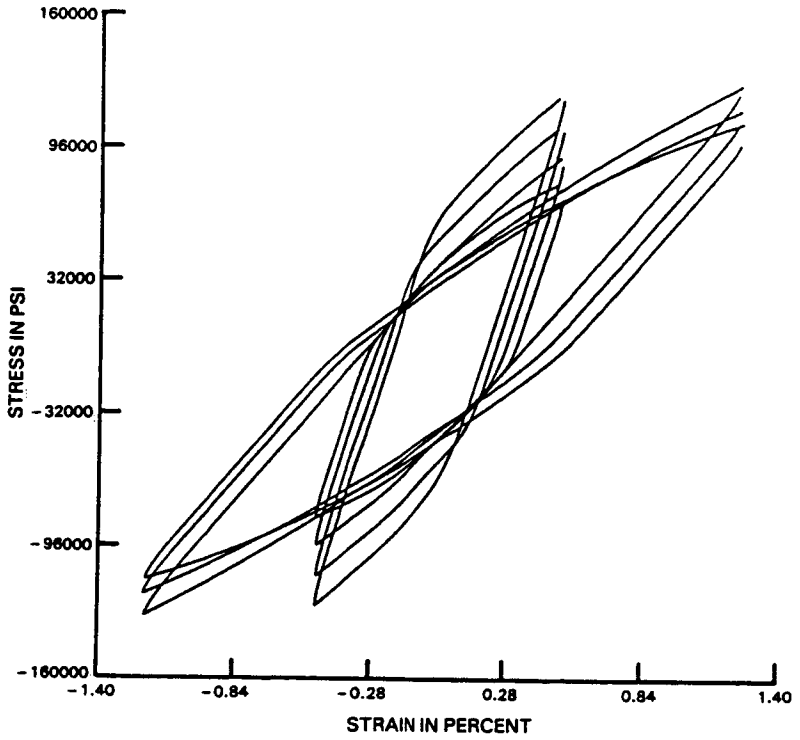


Figure 55 Correlation of <001> and <111> Data with Macroscopic Model

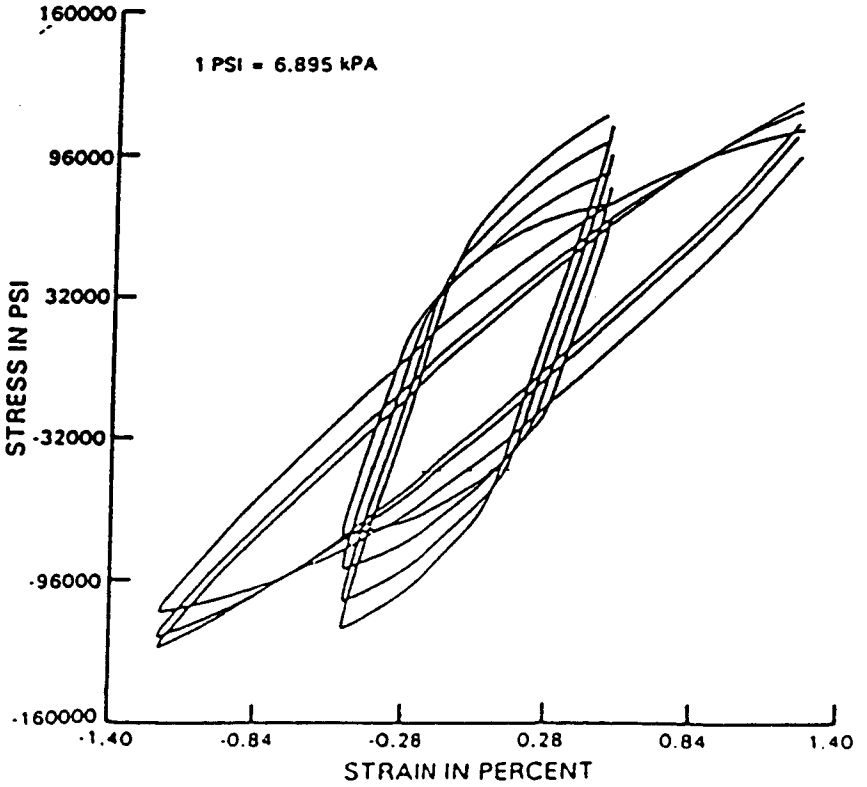


Figure 56 Correlation of <001> and <111> Data with Anisotropic Back Stress Model

## 5.3 COATED SINGLE CRYSTAL LIFE PREDICTION MODELS

Fatigue life for coated single crystal materials is defined as follows (see Section 3.2):

$$Nsep = Nc + Nsi + Nsp$$

where: Nsep = Specimen separation life (cycles)
Nc = Number of cycles to generate a crack through the coating
Nsi = Additional cycles for crack to penetrate a small distance into the substrate
Nsp = Additional cycles to grow crack to critical size.

The choice of coating crack initiation (Nc) was based on experimental observations and practical limitations of inspection techniques. Acetate replication of surface cracks during TMF tests and the post-test crack morphology exams together indicate that coating cracks rapidly penetrate through the coating. Also, crack depths less than 1/2 to 1 coating thickness are difficult to replicate and are considered near the limit of replication resolution.

Substrate reinitiation (Nsi) will include short crack behavior. Tentatively, substrate reinitiation will consider two substrate crack penetration depths, 0.13 and 0.25 mm (0.005 and 0.010 in). Replica information beyond the 0.25 mm (0.010 in) depth is not available for many specimens, and extrapolation of known data to larger crack sizes is not considered prudent.

Substrate crack propagation will not be generally addressed in this program, except to study trends and define when crack growth relationships are applicable.

### 5.3.1 Coating Life Models

The simple coating crack initiation models under initial consideration reflect the current test and analysis capability for coatings.

Coffin-Manson $$\Delta\varepsilon_{in} \cdot N_c^{B} = C_1 \qquad (5\text{-}31)$$

Ostergren $$\sigma_T \cdot \Delta\varepsilon_{in} \cdot N_c^{B} = C_2 \qquad (5\text{-}32)$$

Coating crack initiation data correlations of coated <001> PWA 1480 specimens isothermally low cycle fatigue tested at 1038°C (1900°F), using the Coffin-Manson and Ostergren relationships given above, are presented in Figures 57 through 60.

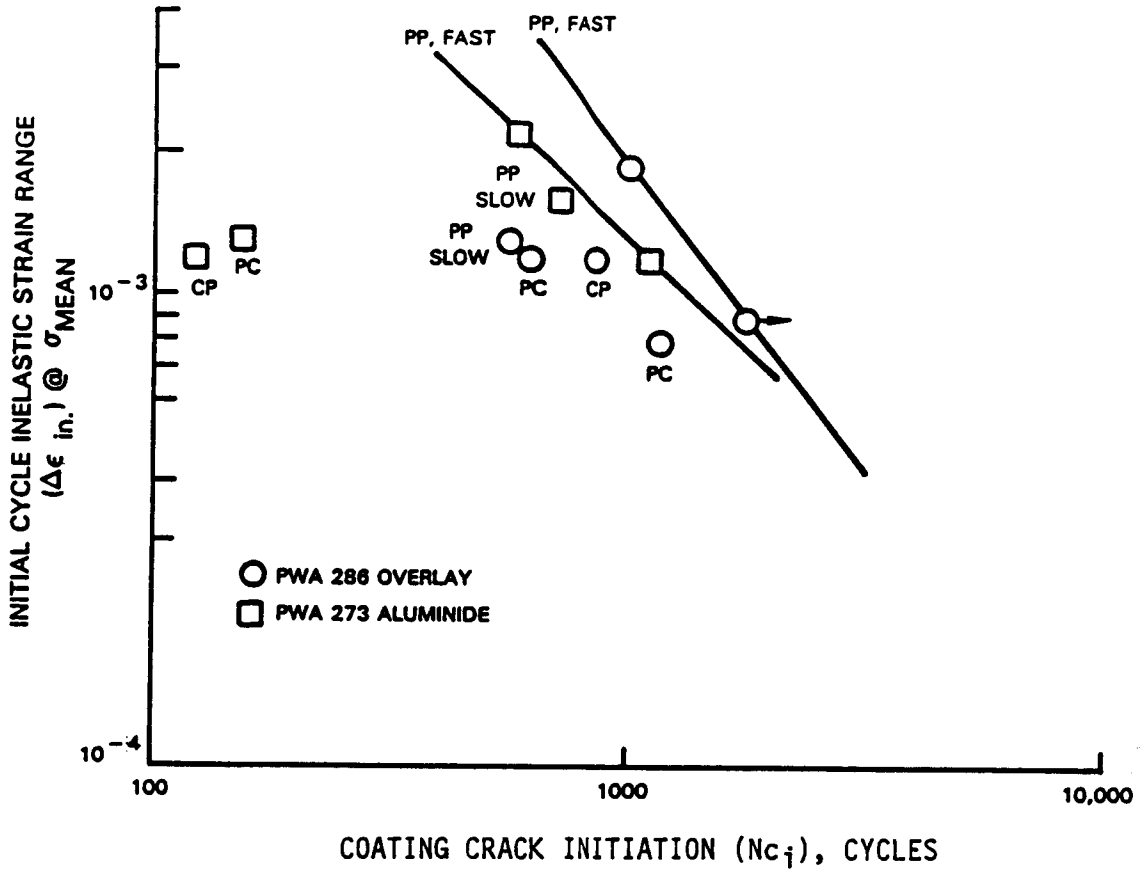


Figure 57 Coffin-Manson Correlation of Coating Cracking Lives During 1038°C (1900°F) LCF of Coated PWA 1480 <001>; $\Delta\epsilon_{in}$ Obtained from Composite Structure Hysteresis Loop Data

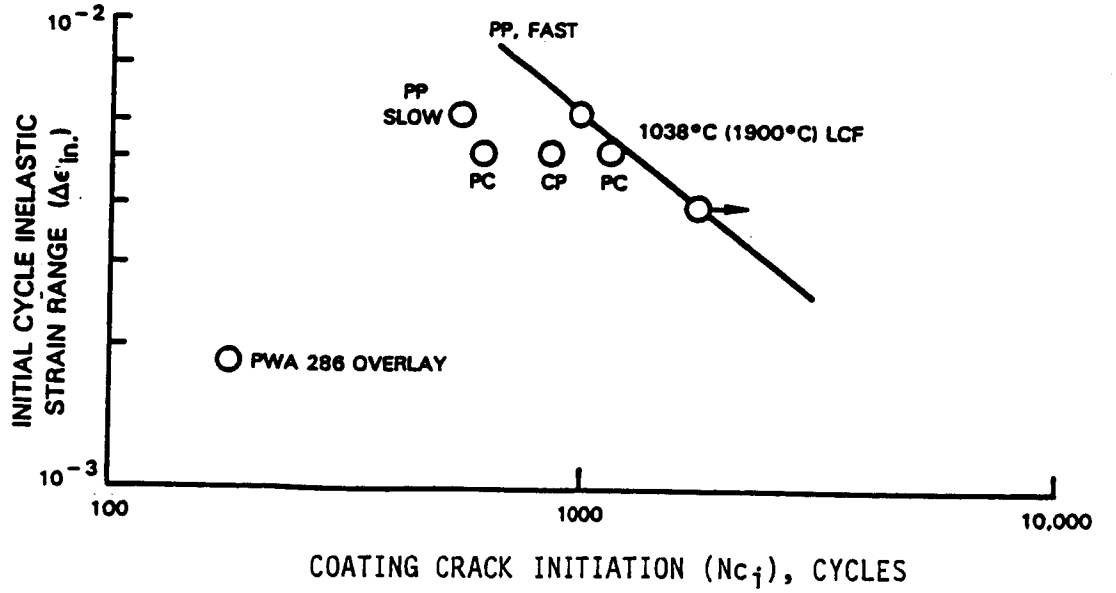


Figure 58 Coffin-Manson Correlation of Coating Cracking Lives During 1038°C (1900°F) LCF of PWA 286 Coated PWA 1480 <001>; $\Delta\epsilon_{in}$ Obtained from PWA 286 Constitutive Model

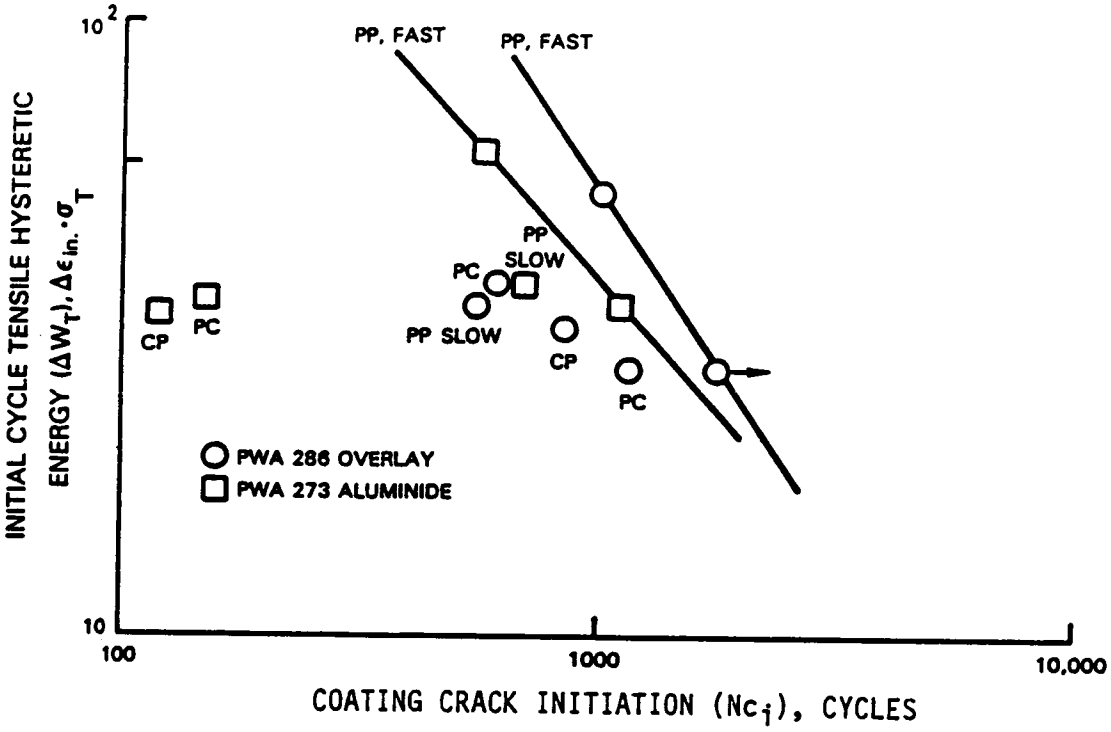


Figure 59 Ostergren Model Correlation of Coating Cracking Lives During 1038°C (1900°F) LCF of Coated PWA 1480 <001>; $\Delta\epsilon_{in}$, $\sigma_T$ Obtained from Composite Structure Hysteresis Loop Data

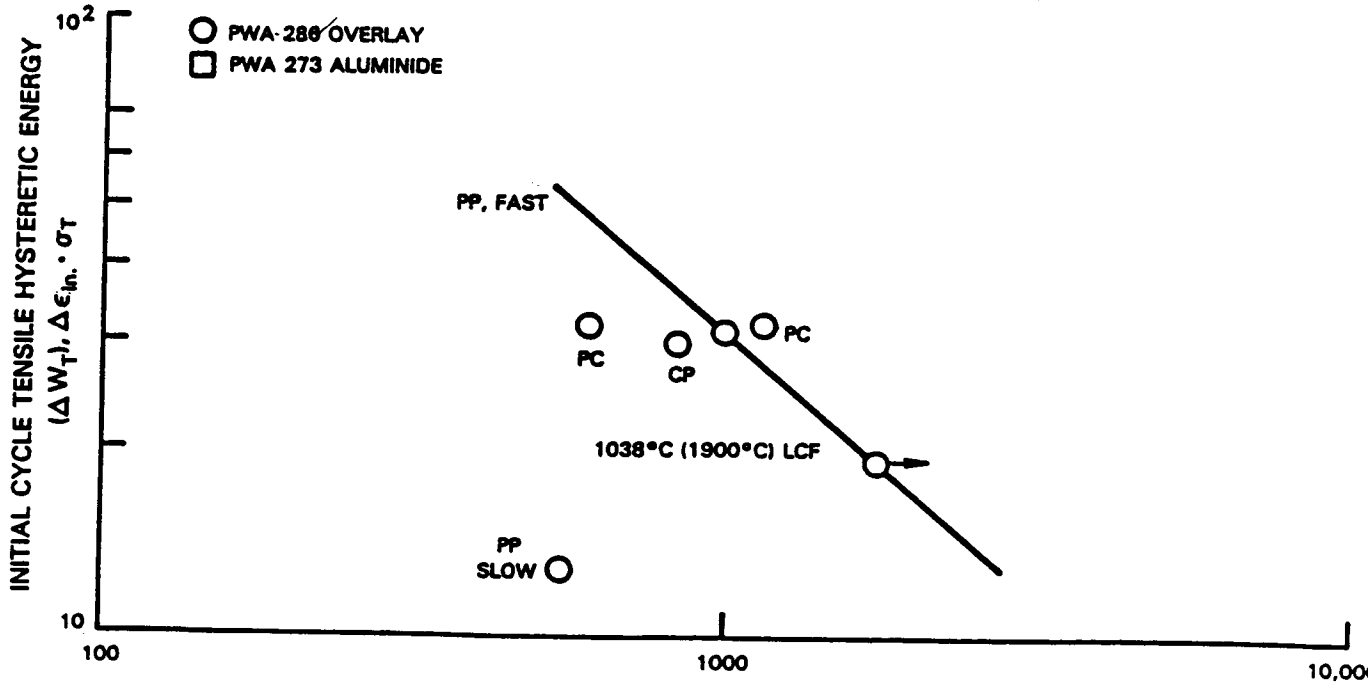


Figure 60 Ostergren Model Correlation of Coating Cracking Lives During 1038°C (1900°F) LCF of PWA 286 Coated PWA 1480 <001>; $\Delta\epsilon_{in}$, $\sigma_T$ Obtained from PWA 286 Constitutive Model

Figures 57 and 59 present correlations obtained from the coated PWA 1480 composite structure hysteresis loops. Figures 58 and 60 present correlations of the PWA 286 coated specimen lives based upon the PWA 286 Walker constitutive model predicted hysteresis loops from a uniaxial 2-bar mechanism simulation of the hollow fatigue specimens. The solid line fit in each of the figures corresponds to the fully-reversed fast cyclic rate information and is intended to serve as a reference condition. Other test conditions are marked accordingly.

There is little correlation ability of either model when considering the PWA 273 coating lives. The PWA 286 coated specimens are correlated within roughly 2X whether considering the composite or predicted PWA 286 responses. However, the model correlations based on the predicted PWA 286 response are generally better. The overlay coating life correlations suggest that overlay coating life prediction based on the coating constitutive response is a promising approach. Basing aluminide coating life predictions on the coating response requires additional work.

### 5.3.2 Single Crystal Life Models (Coated)

Initial studies of coated single crystal material fatigue life dependence on temperature were conducted using data from previous programs. These studies, which primarily considered the crack propagation portion of life, utilized data from isothermal and thermal-mechanical fatigue tests from previous Pratt & Whitney internal programs and crack propagation tests of References 15 and 16.

Fatigue data for life ranges of interest are generally presented in terms of TOTAL strain range, $\Delta\epsilon_T$, as illustrated in Figure 61. Using this representation, life is analytically described by equation 5-33, very similar in form to the Coffin-Manson life model (equation 3-3).

$$N = C \cdot \Delta\epsilon_T^{-B^1} \qquad (5\text{-}33)$$

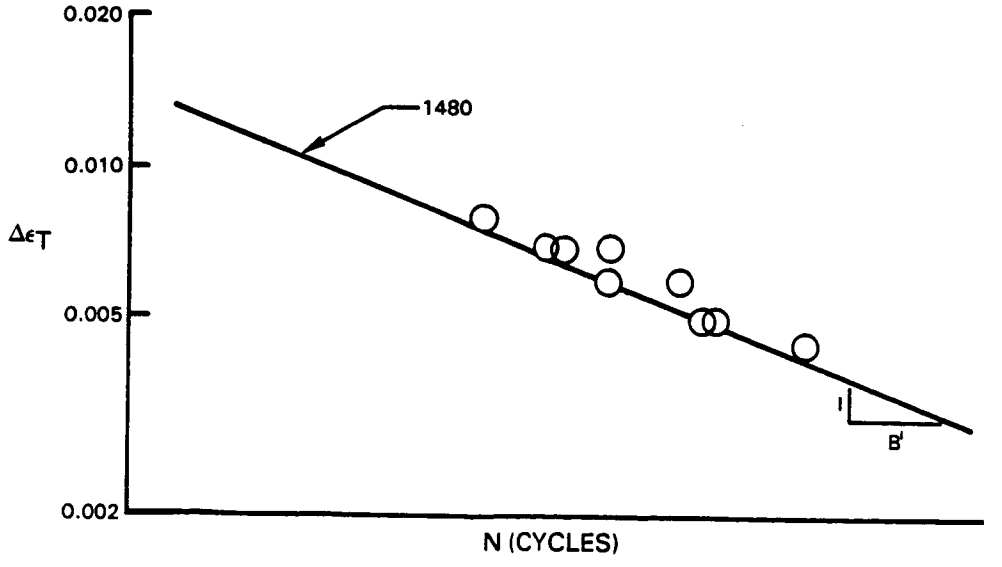


Figure 61 Typical TMF Life Representation for Coated PWA 1480

For the data set used, the specimen lives mainly consisted of substrate crack propagation time since coating cracking occurred early in the tests. This justified considering an alternate life formulation using fracture mechanics analysis and requiring knowledge of the substrate material crack growth behavior, which has been investigated in References 15 and 16 and is illustrated in Figure 62. It should be noted that under representative airfoil load conditions and in the conducted tests, the substrate remained nominally elastic, so that requirements for linear elastic fracture mechanics are satisfied. Of primary interest in coated specimens is the stable (linear) portion of the propagation law, described by equation 5-34. Also required is the strain intensity (equation 5-35).

$$da/dn = A \cdot \Delta K_{\varepsilon}^{B^{II}} \tag{5-34}$$

$$\Delta K_{\varepsilon} = G \cdot \Delta \varepsilon_T \sqrt{\pi a} \tag{5-35}$$

where a = crack size

N = number of cycles

$\Delta K_{\epsilon}$ = strain intensity

$\Delta \epsilon_T$ = total strain range

A, $B^I$, $B^{II}$, C = material constants

G = constant dependent on geometry.

A failure life expression can be derived from equations 5-34 and 5-35 by combining and integrating between initial and critical crack sizes ($a_i$ and $a_f$, respectively).

$$N = C \left[ \frac{1}{\frac{B^{II}}{2} - 1} - \frac{1}{\frac{B^{II}}{2} - 1} \right]_{a_i}^{a_f} \Delta \varepsilon_T^{-B^{II}} \tag{5-36}$$

It is interesting that this life expression (equation 5-35) is nearly identical to equation 5-33, and that slopes $B^I$ and $B^{II}$ should be expected to be equal. A comparison of slopes of the internal TMF life properties and TMF crack growth properties from References 15 and 16 shows this to be true if test cycle temperatures are considered (Figure 63). It is also shown that slopes of TMF life property curves are in close agreement with those of LCF properties at the TMF cycle maximum temperature, an indication that the peak temperature may be most critical under TMF conditions. Life curve levels could not be similarly compared because of test specimen geometry differences.

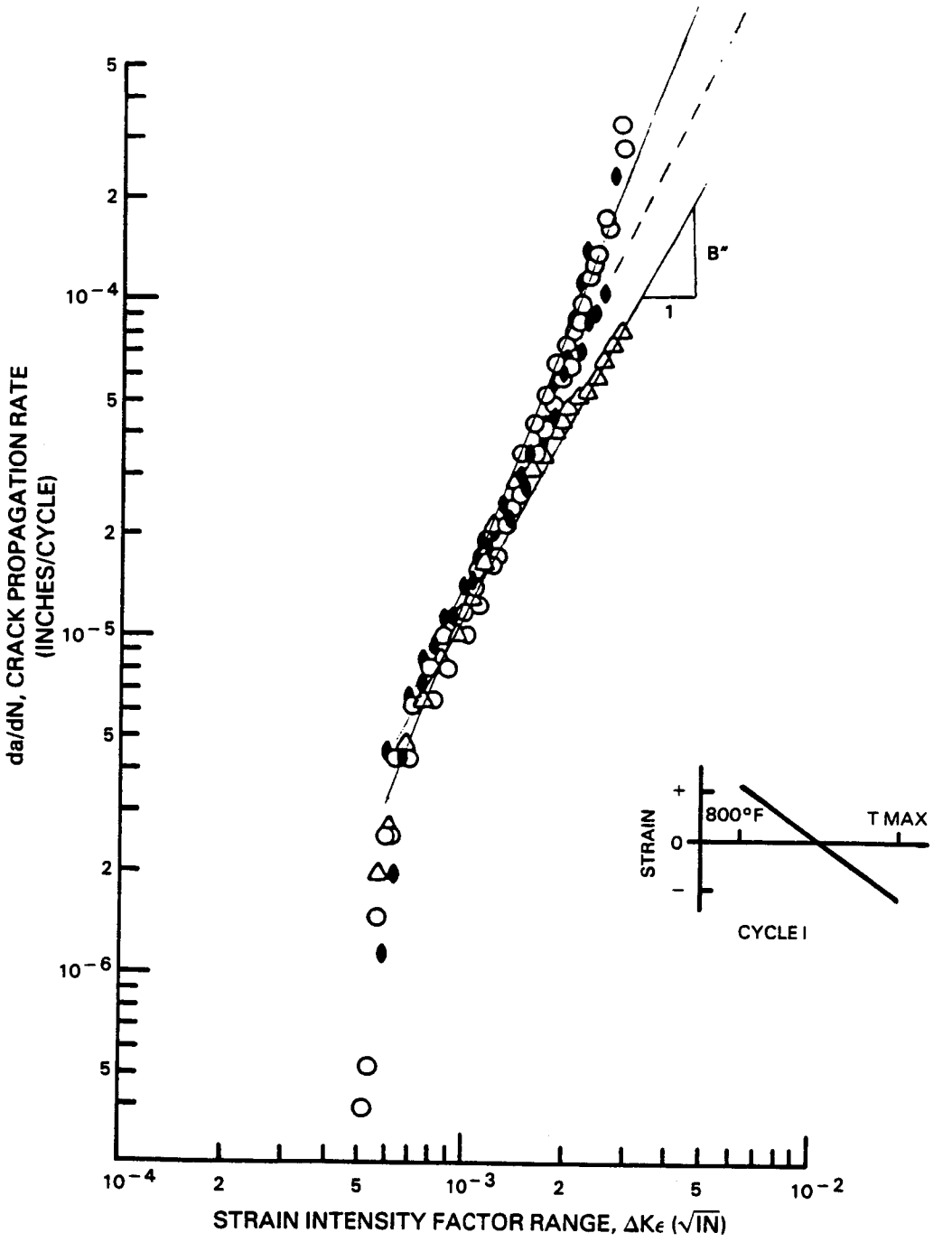


Figure 62 Typical PWA 1480 Crack Propagation Properties for Out-of-Phase TMF (Reference 16)

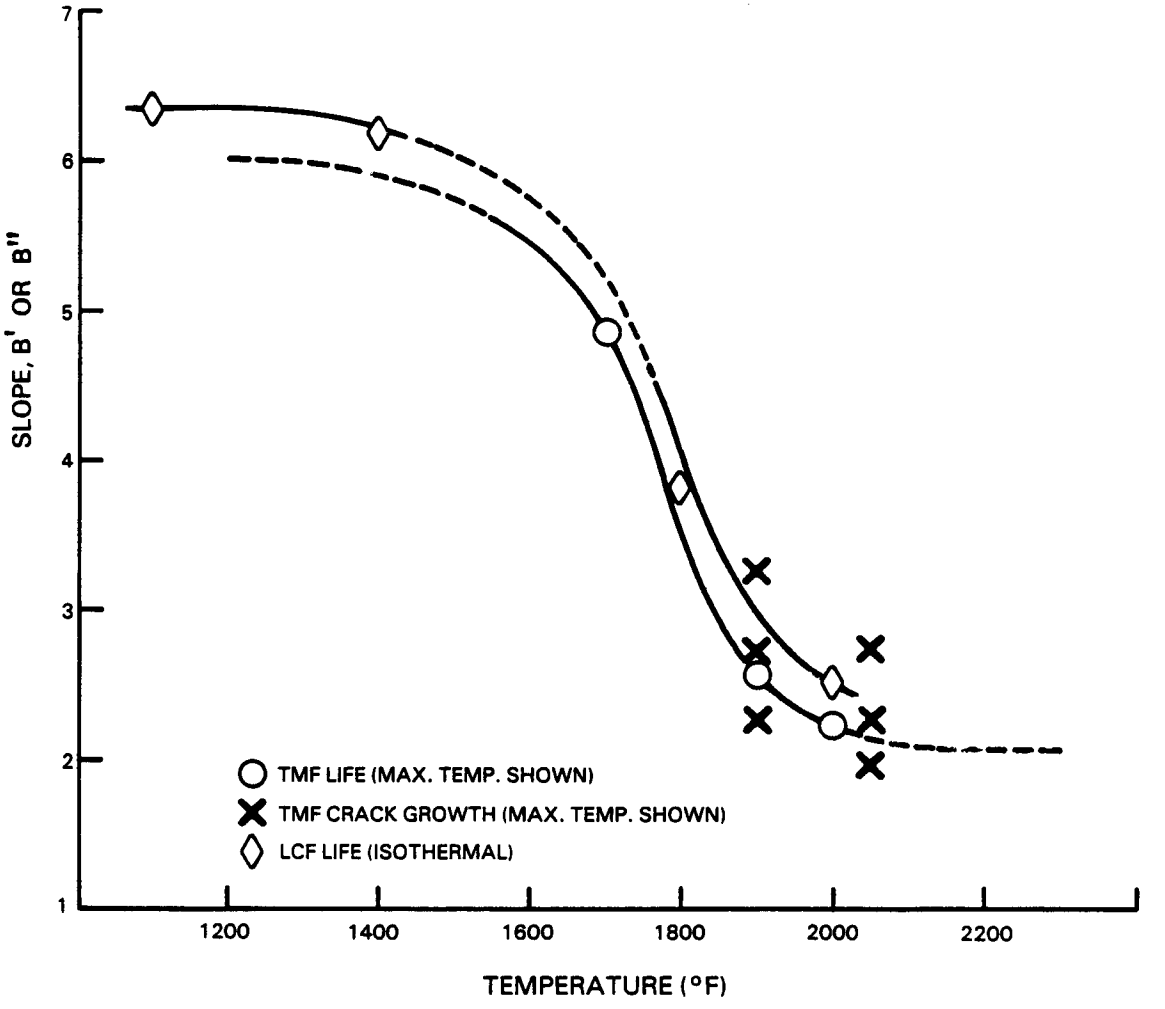


Figure 63 Comparison of Slopes for PWA 1480 TMF Life, TMF Crack Growth and LCF Life Properties

# SECTION 6.0

## TASK V - LEVEL II EXPERIMENTS

The purpose of Level II fatigue tests is to expand the constitutive and life prediction modeling data bases and to evaluate predictive capabilities of the selected models. Therefore, a prime requirement for the obtained data is that it cover a relevant range of test conditions. Level II testing has been started based on an initial test matrix. However, the test matrix is being reviewed relative to the results obtained from Level I tests and reported in Section 4.3.3. Under consideration are reduced test loads which are representative of turbine blades but which would require increased test times.

## SECTION 7.0

## SUMMARY

The following tasks were completed and results obtained during the second year effort:

- Thermal-physical and monotonic mechanical property testing for PWA 273, PWA 286 and PWA 1480 coatings and single crystal material were completed.
- Coated PWA 1480 specimen fabrication for fatigue tests was continued. The specimen geometry was redesigned for use with the MTS extensometer, eliminating the internal ridges.
- A total of 40 Level I fatigue tests were completed and Level II tests started.
- Two coating constitutive models were selected for further development from the five models initially correlated.
- PWA 1480 cyclic constitutive tests were nearly completed.
- Two separate unified constitutive models were formulated: a "microscopic" model which computes inelastic behavior based on crystallographic slip systems, and a "macroscopic" model which uses an anisotropy tensor operating on global inelastic behavior to achieve directional properties.
- A life prediction approach was defined for coated anisotropic materials of hot section components. The approach accounts for coating cracking, substrate crack initiation and substrate crack propagation.
- Initial correlations of coating fatigue life prediction models with specimen test data and predicted constitutive behavior were completed and appear promising.

C-2

# SECTION 8.0

# FUTURE WORK

During the third year of the base program, the following work will be accomplished:

- Fabrication and coating of PWA 1480 fatigue specimens will be continued and fabrication completed.
- Level II isothermal and thermal-mechanical fatigue testing of coated PWA 1480 specimens will be continued with 40 percent of tests scheduled to be completed.
- Development of PWA 1480 constitutive models for TMF loading conditions will be completed.
- Evaluation of two PWA 286 coating constitutive models will be completed using simplified analysis and a biaxial model formulated.
- Initial coating life prediction models will be formulated based on PWA 286 coating data; evaluation of the developed model for PWA 273 coating will be conducted.
- Evaluation and development of coated PWA 1480 life prediction models will be continued.

## SECTION 9.0

## REFERENCES


1. Swanson, G. A., I. Linask, D. M. Nissley, P. P. Norris, T. G. Meyer and K. P. Walker, "Life Prediction and Constitutive Models for Engine Hot Section Anisotropic Materials Program, Annual Status Report," NASA CR-174952, February, 1986.

2. Walker, K. P. and E. Jordan, "First-Annual Report on NASA Grant NAG-512," 1985.

3. Manson, S. S., et al, "Creep-Fatigue Analysis by Strain-Range Partitioning," NASA TMX-67838, 1971.

4. Gemma, A. E., Unpublished research, 1981.

5. DeLuca, D. P. and B. A. Cowles, "Fatigue and Fracture of Advanced Blade Materials," AFWAL-TR-84-4167, February, 1985.

6. Lemaitre, J. and J. L. Chaboche, "A Non-Linear Model for Creep Fatigue Damage Cumulation and Interaction," Mechanics of Viscoplastic Media and Bodies, J. Hult, Ed. Springer-Verlag, 1975, pp. 291-301.

7. Moreno, V., et al, "Creep Fatigue Life Prediction for Engine Hot Section Materials (Isotropic)," NASA CR-174844, 1984.

8. Kraus, H., Creep Analysis, Chapter 2, John Wiley & Sons, Inc., New York, 1980.

9. Walker, K. P., "Research and Development Program for Nonlinear Structural Modeling with Advanced Time-Temperature Dependent Constitutive Relationships," NASA CR-165533, November, 1981.

10. Lindholm, U. S., et al, "Constitutive Modeling for Isotropic Materials (HOST)," NASA CR-174718, May, 1984.

11. Moreno, V., "Development of a Simplified Analytical Method for Representing Material Cyclic Behavior," NASA CR-168100, January, 1983.

12. Stowell, E. Z., et al, "Predicted Behavior of Rapidly Heated Metal in Compression," NASA TR-R-59, 1960.

13. Stowell, E. Z., "The Properties of Metals Under Rapid Heating Conditions," J. Aeron. Sci., December, 1957, pp. 922-923.

14. Stowell, E. Z., "A Phenomenological Relation Between Stress, Strain Rate, and Temperature for Metals at Elevated Temperature," NASA TR-R1343, February, 1957.

15. Duhl, D. N. and N. E. Ulion, "Thermal Fatigue Crack Propagation in Single Crystal Nickel Base Superalloys," Fifth Quarterly Report to NADC, Pratt & Whitney FR-18526, 1984.

16. Duhl, D. N. and N. E. Ulion, "Thermal Fatigue Crack Propagation in Single Crystal Nickel Base Superalloys," Sixth Quarterly Report to NADC, Pratt & Whitney FR-18738, 1984.

# APPENDIX A

## THERMAL PHYSICAL PROPERTY DATA FOR PWA 1480

Tables



Note: *Specific heat equals slope of the enthalphy curve.

Table A-I

Thermal Conductivity of PWA 1480 Using Comparative Rod Apparatus with 316 Stainless Steel References

| Specimen | Mean Temperature of Specimen °F | Thermal Conductivity of Specimen $k_s$ Btu-in. / hr ft²°F | ΔT through Specimen °F | Mean Temperature of Lower Reference °F | Thermal Conductivity of Lower Reference $k_1$ Btu-in. / hr-ft²°F | ΔT through Lower Reference $\Delta T$ °F[1] | Mean Temperature of Upper Reference °F | Thermal Conductivity of Upper Reference $k_2$ Btu-in. / hr ft²°F | ΔT through Upper Reference $\Delta T_2$ °F |
|---|---|---|---|---|---|---|---|---|---|
| LED 72684-1-1480<br>Run: NOCO965-6-3 | | $l_s$ = 0.750 in. | | | Initial thickness: 1.0002 in. | | | | |
| | | Specimen Diameter = 0.7510 in. | | | Initial weight: 62.2898 gm | | | | |
| | 222 | 63.30 | 30.05 | 183 | 99.20 | 18.64 | 256 | 103.90 | 18.82 |
| | 222 | 63.30 | 30.05 | 183 | 99.20 | 18.68 | 256 | 103.90 | 18.78 |
| | 576 | 84.90 | 59.48 | 493 | 118.20 | 41.26 | 653 | 128.60 | 40.69 |
| | 577 | 85.00 | 59.45 | 494 | 118.20 | 41.23 | 654 | 128.60 | 40.70 |
| | 1030 | 109.40 | 63.80 | 940 | 146.00 | 47.79 | 1108 | 156.60 | 44.55 |
| | 1032 | 109.40 | 63.86 | 942 | 146.00 | 47.82 | 1110 | 156.60 | 44.65 |
| | 1503 | 134.70 | 93.09 | 1371 | 170.60 | 71.87 | 1625 | 183.00 | 70.08 |
| | 1504 | 134.60 | 93.16 | 1373 | 170.60 | 71.87 | 1627 | 183.00 | 70.04 |
| | 2043 | 163.30 | 103.21 | 1910 | 197.50 | 82.34 | 2186 | 211.10 | 82.61 |
| | 2044 | 163.20 | 103.29 | 1912 | 197.50 | 82.34 | 2182 | 211.10 | 82.70 |

Table A-II

Thermal Conductivity of PWA 1480 Using Comparative Rod Apparatus with 316 Stainless Steel References

| Specimen | Mean Temperature of Specimen °F | Thermal Conductivity of Specimen $k_s$ Btu-in. / hr ft²°F | ΔT through Specimen °F | Mean Temperature of Lower Reference °F | Thermal Conductivity of Lower Reference $k_1$ Btu-in. / hr-ft²°F | ΔT through Lower Reference ΔT °F[1] | Mean Temperature of Upper Reference °F | Thermal Conductivity of Upper Reference $k_2$ Btu-in. / hr ft²°F | ΔT through Upper Reference $\Delta T_2$ °F |
|---|---|---|---|---|---|---|---|---|---|
| LED 72684-2-1480<br>Run: NOC0965-6-3 | | $l_s$ = 0.750 in. | | | Initial thickness: 1.0001 in. | | | | |
| | | Specimen Diameter = 0.7510 in. | | | Initial weight: 62.3947 gm | | | | |
| | 148 | 60.40 | 30.47 | 112 | 94.60 | 19.38 | 183 | 99.20 | 18.64 |
| | 148 | 60.60 | 30.44 | 112 | 94.60 | 19.42 | 183 | 99.20 | 18.68 |
| | 418 | 76.20 | 63.05 | 343 | 108.90 | 43.50 | 793 | 118.20 | 41.26 |
| | 419 | 76.20 | 63.07 | 343 | 108.90 | 43.45 | 794 | 118.20 | 41.23 |
| | 854 | 99.30 | 70.34 | 760 | 134.90 | 51.87 | 940 | 146.00 | 47.79 |
| | 856 | 99.30 | 70.36 | 762 | 134.90 | 51.89 | 942 | 146.00 | 47.82 |
| | 1252 | 121.80 | 97.48 | 1131 | 158.00 | 72.74 | 1371 | 170.60 | 71.86 |
| | 1254 | 121.80 | 97.52 | 1132 | 158.00 | 72.75 | 1373 | 170.60 | 71.86 |
| | 1780 | 148.00 | 104.69 | 1650 | 184.60 | 79.73 | 1910 | 197.50 | 82.34 |
| | 1781 | 148.00 | 104.65 | 1652 | 184.60 | 79.74 | 1912 | 197.50 | 82.34 |

Table A-III

Thermal Expansion of PWA 1480 Measured in Quartz Dilatometer

| Specimen | Specimen Temperature - °F | | | Observed Total Elongation $10^{-3}$in. | Observed Unit Elongation $10^{-3}$ in./in. | Unit Elongation Correction for Dilatometer Motion $10^{-3}$ in./in. | Corrected Specimen Unit Elongation $10^{-3}$ in./in. |
|---|---|---|---|---|---|---|---|
| | Top | Bottom | Average | | | | |
| PWA 1480 (D9866)<br>LED 72784-1<br>Run: NOCO885-86-27 BPR | | | Initial length: 3.0000 in.<br>Final length: 3.0000 in. | | | Initial weight: 21.0660 gm<br>Final weight: 21.0668 gm | |
| | 70 | 70 | 70 | 0.0 | 0.0 | 0.0 | 0.0 |
| | 250 | 250 | 250 | 2.85 | 0.95 | 0.06 | 1.01 |
| | 500 | 500 | 500 | 8.30 | 2.77 | 0.16 | 2.93 |
| | 750 | 750 | 750 | 13.25 | 4.42 | 0.24 | 4.66 |
| | 1000 | 1000 | 1000 | 18.90 | 6.30 | 0.30 | 6.60 |
| | 1250 | 1250 | 1250 | 25.20 | 8.40 | 0.36 | 8.76 |
| | 1500 | 1500 | 1500 | 33.00 | 11.00 | 0.44 | 11.44 |
| | 70 | 70 | 70 | 0.22 | 0.07 | 0.0 | 0.07 |

Table A-IV

Thermal Expansion of PWA 1480 Measured in Graphite Dilatometer

| Specimen and Run No. | Temp °F | Observed Total Elongation ($10^{-3}$ in.) | Observed Unit Elongation ($10^{-3}$ in./in.) | Unit Correction for Dilatometer Motion ($10^{-3}$ in./in.) | Corrected Specimen Unit Elongation ($10^{-3}$ in./in.) |
|---|---|---|---|---|---|
| PWA 1480 (P9866)<br>LED 72784-1<br>Run: N0C0879-67-168 K4 | | Initial length: 3.0000 in.<br>Final length: * | Initial weight: 21.0668 gm<br>Final weight: * | | |
| | 70 | 0.0 | 0.0 | 0.0 | 0.0 |
| | 500 | 7.25 | 2.42 | 0.23 | 2.65 |
| | 1000 | 17.00 | 5.67 | 0.92 | 6.59 |
| | 1500 | 27.30 | 9.10 | 1.71 | 10.81 |
| | 1657 | 32.00 | 10.67 | 2.00 | 12.67 |
| | 1858 | 38.40 | 12.80 | 2.34 | 15.14 |
| | 2185 | 53.00 | 17.67 | 2.95 | 20.62 |
| | 2311 | 58.60 | 19.53 | 3.18 | 22.71 |
| | 2432 | 68.70 | 22.90 | 3.43 | 26.33 |
| | 2513 | 0.0 | 0.0 | 3.59 | 3.59 |

*No finals, specimen melted

Table A-V

Thermal Expansion of PWA 1480 Measured in Graphite Dilatometer

| Specimen and Run No. | Temp °F | | Observed Total Elongation ($10^{-3}$ in.) | Observed Unit Elongation ($10^{-3}$ in./in.) | Unit Correction for Dilatometer Motion ($10^{-3}$ in./in.) | Corrected Specimen Unit Elongation ($10^{-3}$ in./in.) |
|---|---|---|---|---|---|---|
| PWA 1480 (P9866)<br>LED 72784-2<br>Run: NOC0879-75-168 K4 | | Initial length: 2.9996 in.<br>Final length: 2.9990 in. | | Initial weight: 21.0670 gm<br>Final weight: 21.0687 gm | | |
| | 70 | | 0.0 | 0.0 | 0.0 | 0.0 |
| | 500 | | 5.90 | 1.97 | 0.22 | 2.19 |
| | 1038 | | 16.60 | 5.53 | 0.85 | 6.38 |
| | 1598 | | 29.30 | 9.77 | 1.78 | 11.55 |
| | 1757 | | 33.30 | 11.10 | 2.07 | 13.17 |
| | 1969 | | 40.40 | 13.47 | 2.50 | 15.97 |
| | 2160 | | 48.30 | 16.10 | 2.82 | 18.92 |
| | 2311 | | 56.70 | 18.90 | 3.13 | 22.03 |
| | 2422 | | 64.30 | 21.43 | 3.38 | 24.81 |
| | 70 | | -0.65 | -0.22 | 0.0 | -0.22 |

Table A-VI

Enthalpy of PWA 1480 (P9866) LED 73084-1
Measured in the Adiabatic Calorimeter

| Specimen | Run | Initial Cup Temp °F | Final Cup Temp °F | Change in Cup Temp °F | Initial Sample Temp °F | Initial Weight of Sample gm | Final Weight of Sample gm | Enthalpy h = (K/Ws)(t2-t1) Btu/lb | Enthalpy Btu/lb Above 85°F Ref. | Enthalpy Btu/lb Above 32°F Ref. |
|---|---|---|---|---|---|---|---|---|---|---|
| | C0827 | | | | | | | | | |
| HC-1 | 37 | 65.783 | 69.318 | 3.535 | 215 | 31.1746 | 31.1744 | 13.65 | 12.18 | 17.15 |
| HC-3 | 40 | 75.909 | 80.318 | 4.409 | 1027 | 5.2751 | 5.2752 | 100.62 | 100.13 | 105.75 |
| HC-3 | 40 | 79.826 | 85.044 | 5.218 | 1214 | 5.2753 | 5.2752 | 119.077 | 119.077 | 124.66 |
| HC-4 | 62 | 69.818 | 79.261 | 9.443 | 500 | 27.1655 | 27.1649 | 41.85 | 41.28 | 46.55 |

Table A-VII

Enthalpy of PWA 1480 Measured in the Ice Calorimeter

| Specimen Number | SRI Run Number | Drop Temperature °F | Initial Weight gm | Final Weight gm | Enthalpy from Drop Temperature to 32°F Btu/lb |
|---|---|---|---|---|---|
| HC-1 | 58 | 1605 | 31.1744 | 31.1757 | 169.41 |
| HC-1 | 59 | 2011 | 31.1757 | 31.1775 | 235.84 |
| HC-2 | 64 | 1923 | 28.4596 | 28.4620 | 222.22 |
| HC-4 | 72 | 2110 | 27.1677 | 27.1697 | 276.44 |
| HC-1 | 72 | 2250 | 31.1775 | 31.1841 | 305.76 |
| HC-2 | 68 | 2320 | 28.4620 | 28.4696 | 314.92 |
| HC-4 | 68 | 1539 | 27.1649 | 27.1677 | 168.22 |

## APPENDIX B

## THERMAL PHYSICAL PROPERTY DATA FOR PWA 273 AND PWA 286 COATINGS

Table



Note: *Specific heat equals slope of the enthalpy curve.

Table B-I

Thermal Conductivity of PWA 273 Using Comparative Rod Apparatus with SS316 References

| Specimen | Mean Temperature of Specimen °F | Thermal Conductivity of Specimen $k_s$ Btu in. / hr ft² °F | ΔT through Specimen °F | Mean Temperature of Lower Reference °F | Thermal Conductivity of Lower Reference $k_1$ Btu in. / hr ft² °F | ΔT through Lower Reference $\Delta T_1$ °F | Mean Temperature of Upper Reference °F | Thermal Conductivity of Upper Reference $k_2$ Btu in. / hr ft² °F | ΔT through Upper Reference $\Delta T_2$ °F |
|---|---|---|---|---|---|---|---|---|---|
| Spec: LED 72684-2 | | $l_s$ = 0.750 | | Initial Thickness: 1.0132 in. | | | Initial Weight: 47.0290 gm | | |
| Run: NOD0250-117-3 | | $l_1$ and $l_2$ = 0.750 | | Final Thickness: 1.0137 in. | | | Final Weight: 47.0405 gm | | |
| | | Specimen Diameter = 0.8051 | | | | | | | |
| | 182 | 145.2 | 15.95 | 149 | 97.0 | 23.76 | 219 | 101.4 | 22.96 |
| | 182 | 144.3 | 16.04 | 149 | 97.0 | 23.79 | 219 | 101.4 | 22.91 |
| | 394 | 176.7 | 29.23 | 331 | 108.0 | 47.19 | 463 | 116.3 | 45.00 |
| | 396 | 176.4 | 29.26 | 332 | 108.0 | 47.19 | 464 | 116.3 | 44.93 |
| | 842 | 238.4 | 38.67 | 753 | 134.5 | 68.05 | 935 | 145.6 | 63.75 |
| | 844 | 238.6 | 38.63 | 755 | 134.5 | 68.00 | 938 | 145.6 | 63.79 |
| | 1315 | 289.6 | 53.87 | 1197 | 162.0 | 92.56 | 1442 | 174.0 | 93.17 |
| | 1316 | 289.9 | 53.84 | 1198 | 162.0 | 92.58 | 1443 | 174.0 | 93.22 |
| | 1925 | 299.9 | 56.32 | 1824 | 193.3 | 83.76 | 2030 | 203.6 | 86.40 |
| | 1923 | 299.7 | 56.31 | 1822 | 193.3 | 83.69 | 2029 | 203.6 | 86.34 |

## Table B-II

Thermal Conductivity of PWA 273 Using Comparative Rod Apparatus with SS316 References

| Specimen | Mean Temperature of Specimen °F | Thermal Conductivity of Specimen $k_s$ Btu in./hr ft² °F | ΔT through Specimen °F | Mean Temperature of Lower Reference °F | Thermal Conductivity of Lower Reference $k_1$ Btu in./hr ft² °F | ΔT through Lower Reference $\Delta T_1$ °F | Mean Temperature of Upper Reference °F | Thermal Conductivity of Upper Reference $k_1$ Btu in./hr ft² °F | ΔT through Upper Reference $\Delta T_2$ °F |
|---|---|---|---|---|---|---|---|---|---|
| Spec: LED 72684-1 | | $l_s$ = 0.750 | | Initial Thickness: 1.0217 in. | | | Initial Weight: 47.4602 gm | | |
| Run: NOD0250-117-3 | | $l_1$ and $l_2$ = 0.750 | | Final Thickness: 1.0226 in. | | | | Final Weight: 47.4893 gm | |
| | | Specimen Diameter = 0.8023 | | | | | | | |
| | 248 | 154.9 | 15.13 | 219 | 101.4 | 22.96 | 281 | 105.1 | 22.43 |
| | 248 | 155.4 | 15.07 | 219 | 101.4 | 22.91 | 281 | 105.1 | 22.46 |
| | 518 | 192.4 | 27.39 | 463 | 116.3 | 45.00 | 581 | 124.0 | 42.78 |
| | 519 | 192.6 | 27.35 | 464 | 116.3 | 44.93 | 582 | 124.0 | 42.83 |
| | 1013 | 253.3 | 37.20 | 935 | 145.6 | 63.75 | 1098 | 155.8 | 61.39 |
| | 1015 | 254.6 | 37.20 | 938 | 145.6 | 63.79 | 1100 | 155.8 | 61.34 |
| | 1554 | 300.0 | 56.82 | 1442 | 174.0 | 93.17 | 1681 | 186.0 | 96.27 |
| | 1556 | 300.1 | 56.86 | 1443 | 174.0 | 93.22 | 1683 | 186.0 | 96.27 |
| | 2133 | 276.1 | 65.14 | 2030 | 203.6 | 86.40 | 2244 | 214.0 | 85.90 |
| | 2132 | 275.9 | 65.14 | 2029 | 203.6 | 86.34 | 2242 | 214.0 | 85.81 |

Table B-III

Thermal Conductivity of PWA 286 Using Comparative Rod Apparatus with SS316 References

| Specimen | Mean Temperature of Specimen °F | Thermal Conductivity of Specimen $k_S$ Btu in. / hr ft² °F | ΔT through Specimen °F | Mean Temperature of Lower Reference °F | Thermal Conductivity of Lower Reference $k_1$ Btu in. / hr ft² °F | ΔT through Lower Reference $\Delta T_1$ °F | Mean Temperature of Upper Reference °F | Thermal Conductivity of Upper Reference $k_1$ Btu in. / hr ft² °F | ΔT through Upper Reference $\Delta T_2$ °F |
|---|---|---|---|---|---|---|---|---|---|
| Spec: LED 72684-2 | | $l_S$ = 0.750 | | Initial Thickness: 1.0004 in. | | | Initial Weight: 51.1827 gm | | |
| Run: NODO250-110-5 | | $l_1$ and $l_2$ = 0.750 | | Final Thickness: 0.9998 in. | | | Final Weight: N/A | | |
| | | Specimen Diameter = 0.7506 | | | | | | | |
| | 166 | 79.4 | 23.22 | 135 | 96.1 | 18.61 | 199 | 100.4 | 18.92 |
| | 166 | 79.8 | 23.17 | 135 | 96.1 | 18.65 | 200 | 100.4 | 18.96 |
| | 372 | 95.6 | 52.18 | 302 | 106.3 | 45.25 | 448 | 115.1 | 44.88 |
| | 373 | 95.7 | 52.18 | 303 | 106.2 | 45.34 | 449 | 115.1 | 44.91 |
| | 868 | 134.3 | 74.21 | 763 | 135.1 | 72.00 | 976 | 148.1 | 68.98 |
| | 869 | 134.4 | 74.16 | 764 | 135.1 | 71.91 | 977 | 148.1 | 68.96 |
| | 1345 | 168.5 | 82.46 | 1229 | 163.8 | 80.45 | 1471 | 175.2 | 83.44 |
| | 1347 | 168.6 | 82.44 | 1230 | 163.8 | 80.51 | 1472 | 175.2 | 83.39 |
| | 1849 | 203.0 | 92.62 | 1722 | 188.4 | 96.45 | 1981 | 201.1 | 96.60 |
| | 1848 | 203.6 | 92.32 | 1722 | 188.4 | 96.50 | 1981 | 201.1 | 96.54 |

Table B-IV

Thermal Conductivity of PWA 286 Using Comparative Rod Apparatus with SS316 References

| Specimen | Mean Temperature of Specimen °F | Thermal Conductivity of Specimen $k_s$ $\frac{Btu\ in.}{hr\ ft^2\ °F}$ | ΔT through Specimen °F | Mean Temperature of Lower Reference °F | Thermal Conductivity of Lower Reference $k_1$ $\frac{Btu\ in.}{hr\ ft^2\ °F}$ | ΔT through Lower Reference $\Delta T_1$ °F | Mean Temperature of Upper Reference °F | Thermal Conductivity of Upper Reference $k_1$ $\frac{Btu\ in.}{hr\ ft^2\ °F}$ | ΔT through Upper Reference $\Delta T_2$ °F |
|---|---|---|---|---|---|---|---|---|---|
| Spec: LED 72684-1<br>Run: NOD0250-110-5 | | $l_s$ = 0.750<br>$l_1$ and $l_2$ = 0.750<br>Specimen Diameter = 0.7505 | | Initial Thickness: 1.0001 in.<br>Final Thickness: N/A | | | Initial Weight: 51.2472 gm<br>Final Weight: N/A | | |
| | 229 | 83.7 | 22.65 | 199 | 100.4 | 18.92 | 257 | 104.0 | 18.18 |
| | 229 | 83.6 | 22.66 | 200 | 100.4 | 18.96 | 258 | 104.0 | 18.13 |
| | 516 | 105.5 | 50.71 | 448 | 115.1 | 44.88 | 584 | 124.1 | 44.61 |
| | 517 | 105.6 | 50.70 | 449 | 115.1 | 44.91 | 585 | 124.1 | 44.62 |
| | 1078 | 148.7 | 72.30 | 976 | 148.1 | 68.98 | 1181 | 161.0 | 70.13 |
| | 1079 | 148.7 | 72.29 | 977 | 148.1 | 68.96 | 1182 | 161.0 | 70.13 |
| | 1593 | 185.1 | 82.78 | 1471 | 175.2 | 83.44 | 1722 | 188.2 | 85.14 |
| | 1595 | 185.0 | 82.75 | 1472 | 175.2 | 83.39 | 1723 | 188.2 | 85.09 |
| | 2092* | 187.7* | 53.62* | 1981 | 201.1 | 96.60 | 2242 | 214.0 | 97.36 |
| | 2092* | 187.8* | 53.58* | 1981 | 201.1 | 96.54 | 2242 | 214.0 | 97.40 |

Note: * Values are for lower half of specimen, top 1/3 of specimen deformed and melting

Table B-V

Thermal Expansion of PWA 273 Measured in Quartz Dilatometer

Specimen and Run Number

Spec: LED 72784-1
Run: NODO394-20-HR-1
Initial Length: 2.7102 in.
Final Length: 2.7128 in.
Initial Weight: 14.1415 gm
Final Weight: 14.1469 gm

| Temp °F | Observed Total Elongation $10^{-3}$ in. | Observed Unit Elongation $10^{-3}$ in./in. | Unit Correction for Dilatometer Motion $10^{-3}$ in./in. | Corrected Specimen Unit Elongation $10^{-3}$ in./in. |
|---|---|---|---|---|
| 70 | 0 | 0 | 0 | 0 |
| 100 | 0.40 | 0.15 | 0.01 | 0.16 |
| 200 | 2.30 | 0.85 | 0.04 | 0.89 |
| 300 | 4.30 | 1.59 | 0.07 | 1.66 |
| 400 | 6.20 | 2.29 | 0.11 | 2.40 |
| 500 | 8.20 | 3.03 | 0.14 | 3.17 |
| 600 | 10.20 | 3.76 | 0.18 | 3.94 |
| 700 | 12.50 | 4.61 | 0.22 | 4.83 |
| 800 | 14.80 | 5.46 | 0.24 | 5.70 |
| 900 | 16.50 | 6.09 | 0.27 | 6.36 |
| 1000 | 18.70 | 6.90 | 0.29 | 7.19 |
| 1100 | 20.90 | 7.71 | 0.32 | 8.03 |
| 1200 | 23.20 | 8.56 | 0.34 | 8.90 |
| 1300 | 25.50 | 9.41 | 0.36 | 9.77 |
| 1400 | 27.90 | 10.29 | 0.38 | 10.67 |
| 1500 | 30.70 | 11.33 | 0.41 | 11.74 |
| 1600 | 32.90 | 12.14 | 0.43 | 12.57 |
| 1700 | 35.30 | 13.02 | 0.44 | 13.46 |
| 1800 | 38.00 | 14.02 | 0.47 | 14.49 |
| 1900 | 40.50 | 14.94 | 0.48 | 15.42 |
| 2000 | 43.40 | 16.01 | 0.50 | 16.51 |
| 2100 | 46.50 | 17.16 | 0.52 | 17.68 |
| 70 | 2.20 | 0.81 | 0 | 0.81 |

Table B-VI

Thermal Expansion of PWA 273 Measured in Quartz Dilatometer

Specimen and Run Number

Spec: LED 72784-2
Run: NODO394-18-HR-1
Initial Length: 1.4935 in.
Final Length: 1.4950 in.
Initial Weight: 7.4560 gm
Final Weight: 7.4589 gm

| Temp °F | Observed Total Elongation $10^{-3}$ in. | Observed Unit Elongation $10^{-3}$ in./in. | Unit Correction for Dilatometer Motion $10^{-3}$ in./in. | Corrected Specimen Unit Elongation $10^{-3}$ in./in. |
|---|---|---|---|---|
| 70 | 0 | 0 | 0 | 0 |
| 100 | 0.23 | 0.15 | 0.01 | 0.16 |
| 200 | 1.20 | 0.80 | 0.04 | 0.84 |
| 300 | 2.40 | 1.61 | 0.07 | 1.67 |
| 400 | 3.50 | 2.34 | 0.11 | 2.45 |
| 500 | 4.60 | 3.08 | 0.14 | 3.22 |
| 600 | 5.70 | 3.82 | 0.18 | 4.00 |
| 700 | 6.85 | 4.59 | 0.22 | 4.81 |
| 800 | 7.90 | 5.29 | 0.24 | 5.53 |
| 900 | 9.15 | 6.13 | 0.27 | 6.40 |
| 1000 | 10.40 | 6.96 | 0.29 | 7.25 |
| 1100 | 11.60 | 7.77 | 0.32 | 8.09 |
| 1200 | 12.84 | 8.60 | 0.34 | 8.94 |
| 1300 | 14.25 | 9.54 | 0.36 | 9.90 |
| 1400 | 15.30 | 10.24 | 0.38 | 10.62 |
| 1500 | 16.60 | 11.11 | 0.41 | 11.52 |
| 1600 | 17.85 | 11.95 | 0.43 | 12.38 |
| 1700 | 19.10 | 12.79 | 0.44 | 13.23 |
| 1800 | 20.30 | 13.59 | 0.47 | 14.06 |
| 1900 | 21.60 | 14.46 | 0.48 | 14.94 |
| 2000 | 22.92 | 15.35 | 0.50 | 15.85 |
| 2100 | 24.43 | 16.36 | 0.52 | 16.88 |
| 70 | 1.30 | 0.87 | 0 | 0.87 |

Table B-VII

Thermal Expansion of PWA 286 Measured in Quartz Dilatometer

| Specimen and Run Number | Specimen Temperature - °F | | | Observed Total Elongation $10^{-3}$ in. | Observed Unit Elongation $10^{-3}$ in./in. | Unit Elongation Correction for Dilatometer Motion $10^{-3}$ in./in. | Corrected Specimen Unit Elongation $10^{-3}$ in./in. |
|---|---|---|---|---|---|---|---|
| | Top | Bottom | Average | | | | |
| Spec: LED 72784-1 | 77 | 77 | 77 | 0 | 0 | 0 | 0 |
| Run: NOD0394-15-HR-1 | 100 | 100 | 100 | 0.15 | 0.05 | 0.01 | 0.06 |
| Initial Length: 3.0008 in. | 200 | 200 | 200 | 2.10 | 0.70 | 0.04 | 0.74 |
| Final Length: 3.0022 in. | 300 | 300 | 300 | 4.20 | 1.40 | 0.07 | 1.47 |
| Initial Weight: 17.2062 gm | 400 | 400 | 400 | 6.40 | 2.13 | 0.11 | 2.24 |
| Final Weight: 17.2093 gm | 500 | 500 | 500 | 8.60 | 2.87 | 0.14 | 3.01 |
| | 600 | 600 | 600 | 10.90 | 3.63 | 0.18 | 3.81 |
| | 700 | 700 | 700 | 13.40 | 4.47 | 0.22 | 4.69 |
| | 800 | 800 | 800 | 16.00 | 5.33 | 0.24 | 5.57 |
| | 900 | 900 | 900 | 18.70 | 6.23 | 0.27 | 6.50 |
| | 1000 | 1000 | 1000 | 21.30 | 7.10 | 0.29 | 7.39 |
| | 1100 | 1100 | 1100 | 24.30 | 8.10 | 0.32 | 8.42 |
| | 1200 | 1200 | 1200 | 27.20 | 9.07 | 0.34 | 9.41 |
| | 1300 | 1300 | 1300 | 30.20 | 10.07 | 0.36 | 10.43 |
| | 1400 | 1400 | 1400 | 33.50 | 11.17 | 0.38 | 11.55 |
| | 1500 | 1500 | 1500 | 37.30 | 12.43 | 0.41 | 12.84 |
| | 1600 | 1600 | 1600 | 40.70 | 13.57 | 0.43 | 14.00 |
| | 1700 | 1700 | 1700 | 44.40 | 14.80 | 0.44 | 15.24 |
| | 1800 | 1800 | 1800 | 49.00 | 16.33 | 0.47 | 16.80 |
| | 1900 | 1900 | 1900 | 52.80 | 17.60 | 0.48 | 18.08 |
| | 2000 | 2000 | 2000 | 56.90 | 18.97 | 0.50 | 19.47 |
| | 2100 | 2100 | 2100 | 60.50 | 20.17 | 0.52 | 20.69 |
| | 70 | 70 | 70 | 0.80 | 0.27 | 0 | 0.27 |

Table B-VIII

Thermal Expansion of PWA 286 Measured in Quartz Dilatometer

Specimen and Run Number

Spec: LED 72784-2
Run: NOD0394-16-HR-1
Initial Length: 3.0008 in.
Final Length: 3.0024 in.
Initial Weight: 17.2082 gm
Final Weight: 17.2114 gm

| Specimen Temperature - °F | | | Observed Total Elongation $10^{-3}$ in. | Observed Unit Elongation $10^{-3}$ in./in. | Unit Elongation Correction for Dilatometer Motion $10^{-3}$ in./in. | Corrected Specimen Unit Elongation $10^{-3}$ in./in. |
|---|---|---|---|---|---|---|
| Top | Bottom | Average | | | | |
| 77 | 77 | 77 | 0 | 0 | 0 | 0 |
| 100 | 100 | 100 | 0.21 | 0.07 | 0.01 | 0.08 |
| 200 | 200 | 200 | 2.10 | 0.70 | 0.04 | 0.74 |
| 300 | 300 | 300 | 4.20 | 1.40 | 0.07 | 1.47 |
| 400 | 400 | 400 | 6.40 | 2.13 | 0.11 | 2.24 |
| 500 | 500 | 500 | 8.60 | 2.87 | 0.14 | 3.01 |
| 600 | 600 | 600 | 10.90 | 3.63 | 0.18 | 3.81 |
| 700 | 700 | 700 | 13.20 | 4.40 | 0.22 | 4.62 |
| 800 | 800 | 800 | 15.50 | 5.17 | 0.24 | 5.41 |
| 900 | 892 | 896 | 18.10 | 6.03 | 0.27 | 6.30 |
| 1000 | 980 | 990 | 20.70 | 6.90 | 0.29 | 7.19 |
| 1100 | 1082 | 1091 | 23.60 | 7.87 | 0.32 | 8.19 |
| 1200 | 1180 | 1190 | 26.50 | 8.83 | 0.34 | 9.17 |
| 1300 | 1278 | 1289 | 29.20 | 9.73 | 0.36 | 10.09 |
| 1400 | 1376 | 1388 | 32.60 | 10.87 | 0.38 | 11.25 |
| 1500 | 1468 | 1484 | 36.10 | 12.03 | 0.41 | 12.44 |
| 1600 | 1574 | 1587 | 39.80 | 13.27 | 0.43 | 13.70 |
| 1700 | 1672 | 1686 | 43.40 | 14.47 | 0.44 | 14.91 |
| 1800 | 1772 | 1786 | 47.10 | 15.70 | 0.47 | 16.17 |
| 1900 | 1863 | 1881 | 50.60 | 16.87 | 0.48 | 17.35 |
| 2000 | 1857 | 1979 | 54.60 | 18.20 | 0.50 | 18.70 |
| 2100 | 2052 | 2076 | 58.80 | 19.60 | 0.52 | 20.12 |
| 70 | 70 | 70 | 1.30 | 0.43 | 0 | 0.43 |

Table B-IX

Enthalpy of PWA 273 Measured in the Adiabatic Calorimeter

| Specimen | Run | Initial Cup Temp °F | Final Cup Temp °F | Change in Cup Temp °F | Initial Sample Temp °F | Initial Weight of Sample gm | Final Weight of Sample gm | Enthalpy $h=(K/W_S)(t2-t1)$ Btu/lb | Enthalpy Btu/lb Above 85°F Ref. | Enthalpy Btu/lb Above 32°F Ref |
|---|---|---|---|---|---|---|---|---|---|---|
| PWA 273-1 | D0349 | | | | | | | | | |
| HC-1 | 86 | 70.130 | 73.455 | 3.325 | 260.5 | 16.0459 | 16.0460 | 24.95 | 23.41 | 30.48 |
| HC-2 | 86 | 73.455 | 74.913 | 1.458 | 262 | 7.4509 | 7.4509 | 23.56 | 22.29 | 28.96 |
| HC-3 | 87 | 74.696 | 79.091 | 4.395 | 524 | 8.4974 | 8.4950 | 62.28 | 61.45 | 68.87 |
| HC-2 | 87 | 78.478 | 83.739 | 5.261 | 714 | 7.4509 | 7.4505 | 85.00 | 84.83 | 91.98 |
| HC-3 | 88 | 81.913 | 91.044 | 8.131 | 1039.5 | 8.4950 | 8.4933 | 129.42 | 130.24 | 137.48 |
| HC-4 | 88 | 77.455 | 80.364 | 2.909 | 1232 | 2.0922 | 2.0922 | 167.38 | 166.71 | 174.41 |
| HC-3 | 89 | 75.318 | 78.217 | 2.899 | 1246 | 2.0922 | 2.0921 | 166.82 | 165.85 | 173.42 |

Table B-X

Enthalpy of PWA 273 Measured in the Ice Calorimeter

| Specimen Number | SoRI Run Number | Drop Temp °F | Initial Weight grams | Final Weight grams | Enthalpy from Drop Temp to 32°F Btu/lb |
|---|---|---|---|---|---|
| PWA 273 | D0349 | | | | |
| HC-5 | 117 | 1519 | 24.5353 | 24.5344 | 218.49 |
| HC-1 | 118 | 1742 | 16.0420 | 16.0383 | 258.25 |
| HC-1 | 118 | 2099 | 16.0383 | 16.0399 | 323.38 |
| HC-6 | 119 | 1960 | 36.3034 | 36.3000 | 299.67 |

Table B-XI

Enthalpy of PWA 286 Measured in the Adiabatic Calorimeter

| Specimen | Run | Initial Cup Temp °F | Final Cup Temp °F | Change in Cup Temp °F | Initial Sample Temp °F | Initial Weight of Sample gm | Final Weight of Sample gm | Enthalpy $h=(K/W_S)(t2-t1)$ Btu/lb | Enthalpy Btu/lb Above 85°F Ref. | Enthalpy Btu/lb Above 32°F Ref |
|---|---|---|---|---|---|---|---|---|---|---|
| PWA 286 | D0349 | | | | | | | | | |
| HC-286-1 | 58 | 79.044 | 80.227 | 1.183 | 537 | 2.8650 | 2.8650 | 49.71 | 49.19 | 54.96 |
| HC-286-1 | 59 | 79.783 | 82.304 | 2.521 | 916 | 2.8649 | 2.8647 | 105.94 | 105.60 | 111.97 |
| HC-286-1 | 60 | 70.304 | 70.783 | 0.479 | 220 | 2.8650 | 2.8649 | 20.13 | 18.21 | 25.36 |
| HC-286-1 | 65 | 88.609 | 90.217 | 1.608 | 724.5 | 2.8649 | 2.8647 | 67.57 | 68.12 | 73.77 |
| HC-286-1 | 71 | 77.727 | 81.348 | 3.621 | 1230.5 | 2.8647 | 2.8649 | 152.15 | 151.67 | 158.69 |
| HC-286-1 | 109 | 72.391 | 74.435 | 2.044 | 734 | 2.8649 | 2.8649 | 85.89 | 84.82 | 91.39 |

Table B-XII

Enthalpy of PWA 286 Measured in the Ice Calorimeter

| Specimen Number | SoRI Run Number | Drop Temp °F | Initial Weight grams | Final Weight grams | Enthalpy from Drop Temp to 32°F Btu/lb |
|---|---|---|---|---|---|
| PWA 286 | D0349 | | | | |
| HC-3 | 105 | 1978 | 41.1550 | 41.1659 | 292.01 |
| HC-2 | 82 | 2102 | 21.1602 | 21.1633 | 313.81 |
| HC-2 | 80 | 1532 | 21.1599 | 21.1602 | 204.01 |
| HC-2 | 80 | 1750 | 21.1602 | 21.1602 | 250.34 |

## APPENDIX C

## OVERLAY COATING CONSTITUTIVE TEST RESULTS, ISOTHERMAL

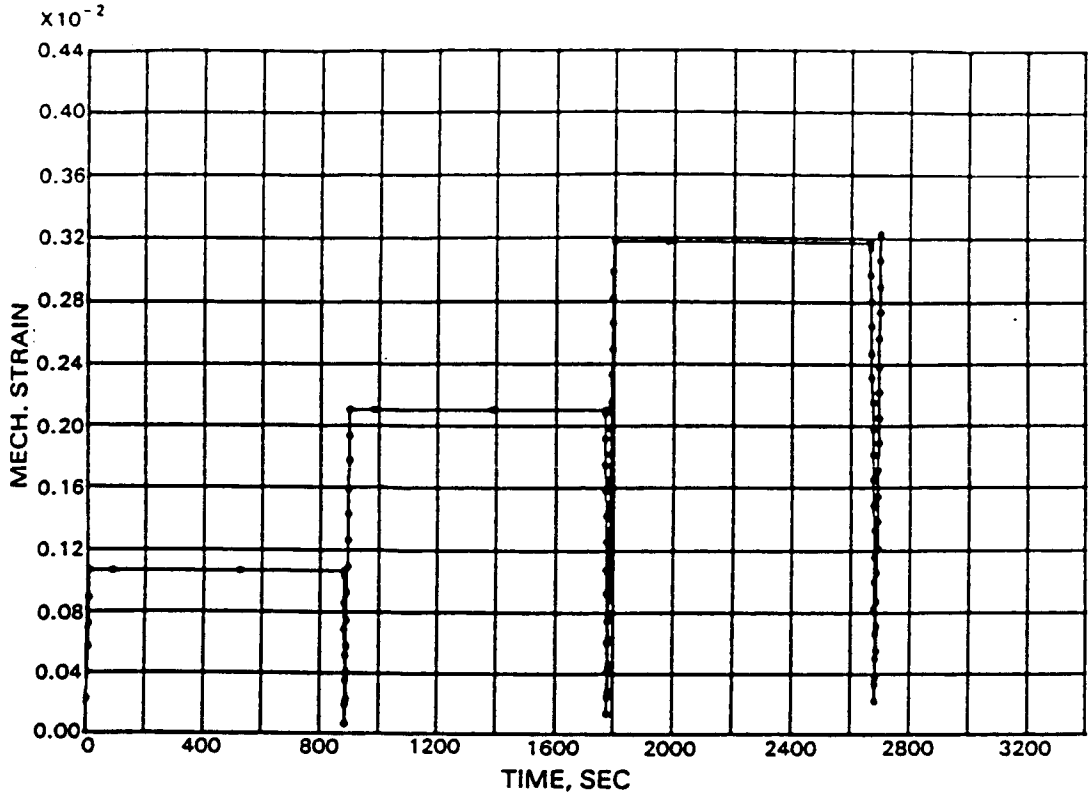


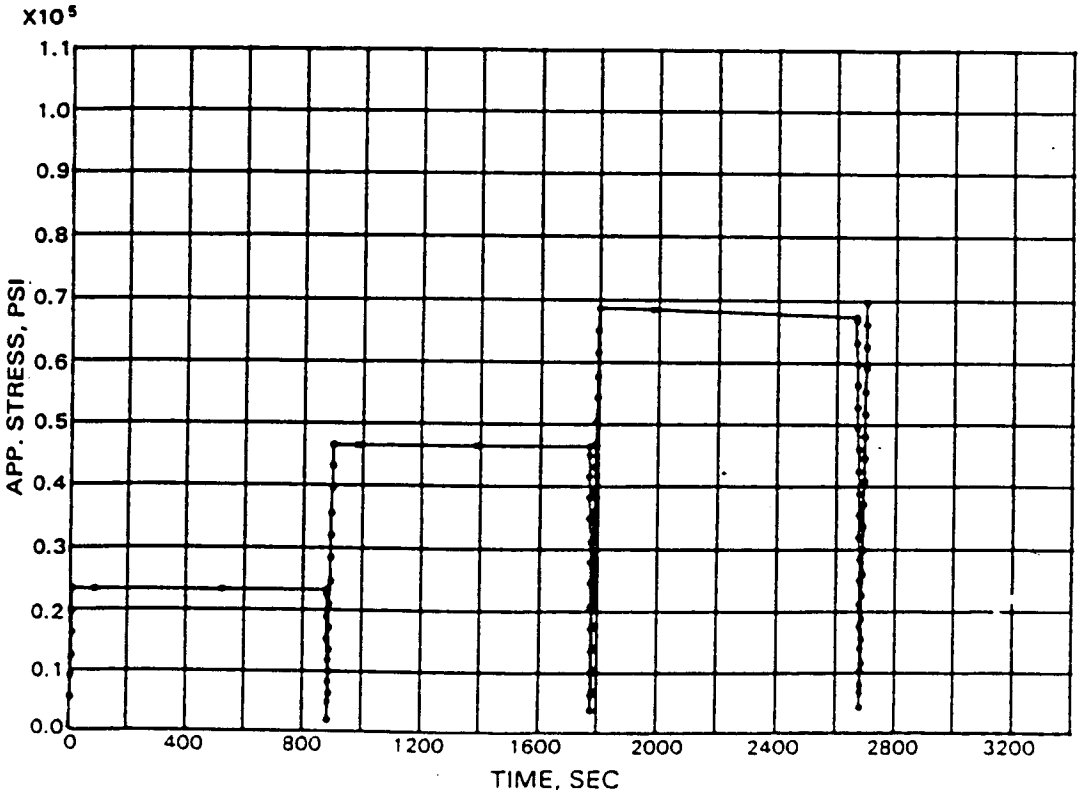


Figure C-1 PWA 286 Coating Stress Relaxation During Strain Hold Tests at 427°C (800°F)

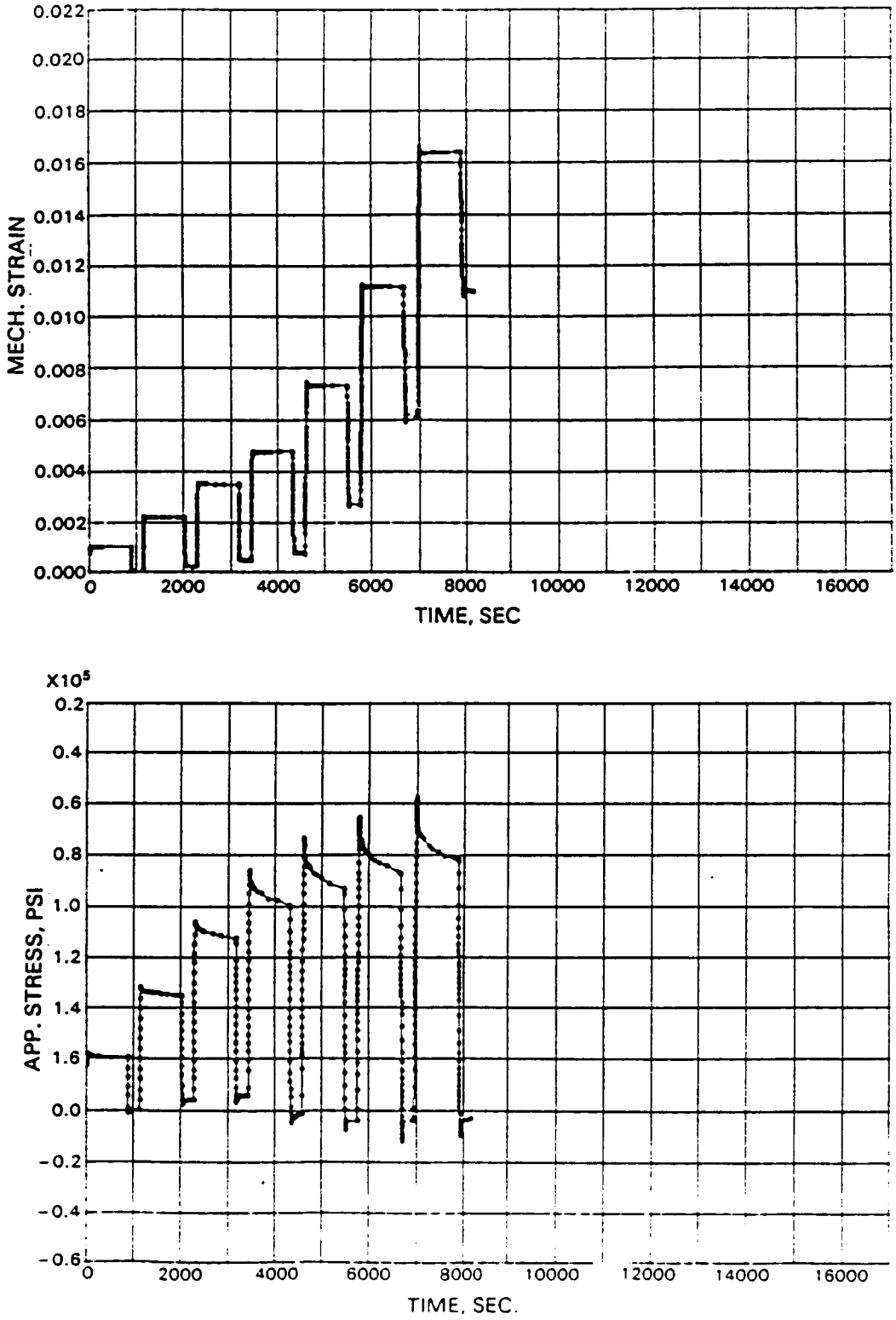


Figure C-2 PWA 286 Coating Stress Relaxation During Strain Hold Tests at 538°C (1000°F)

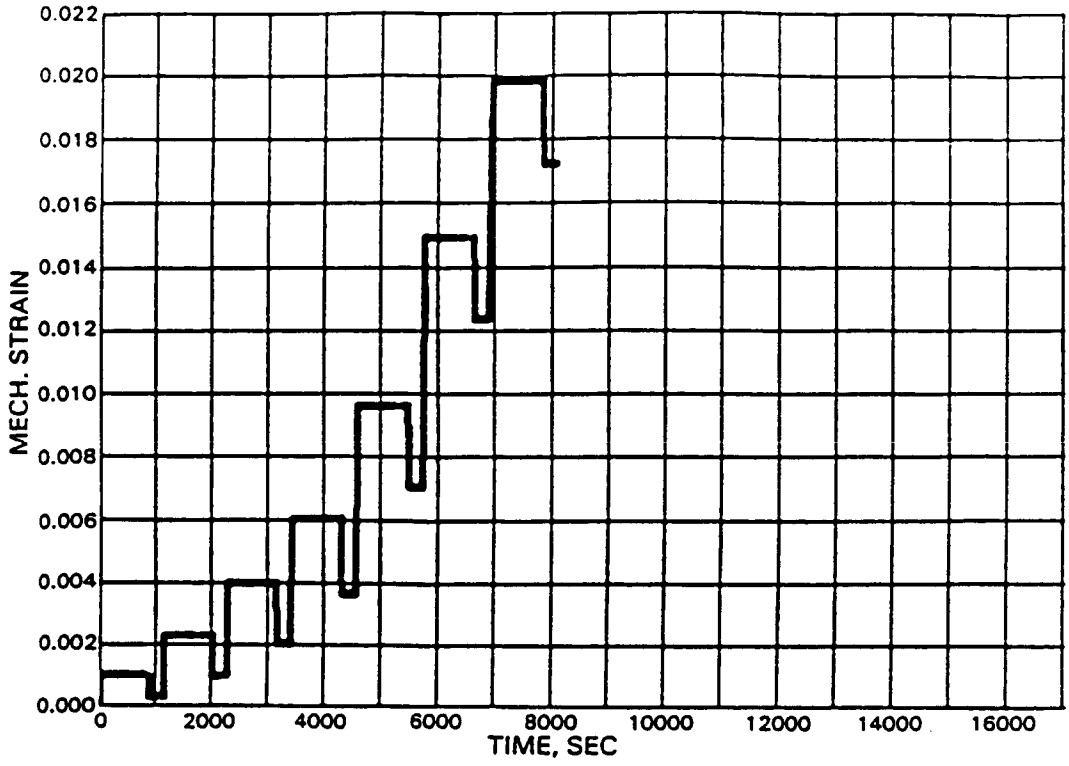


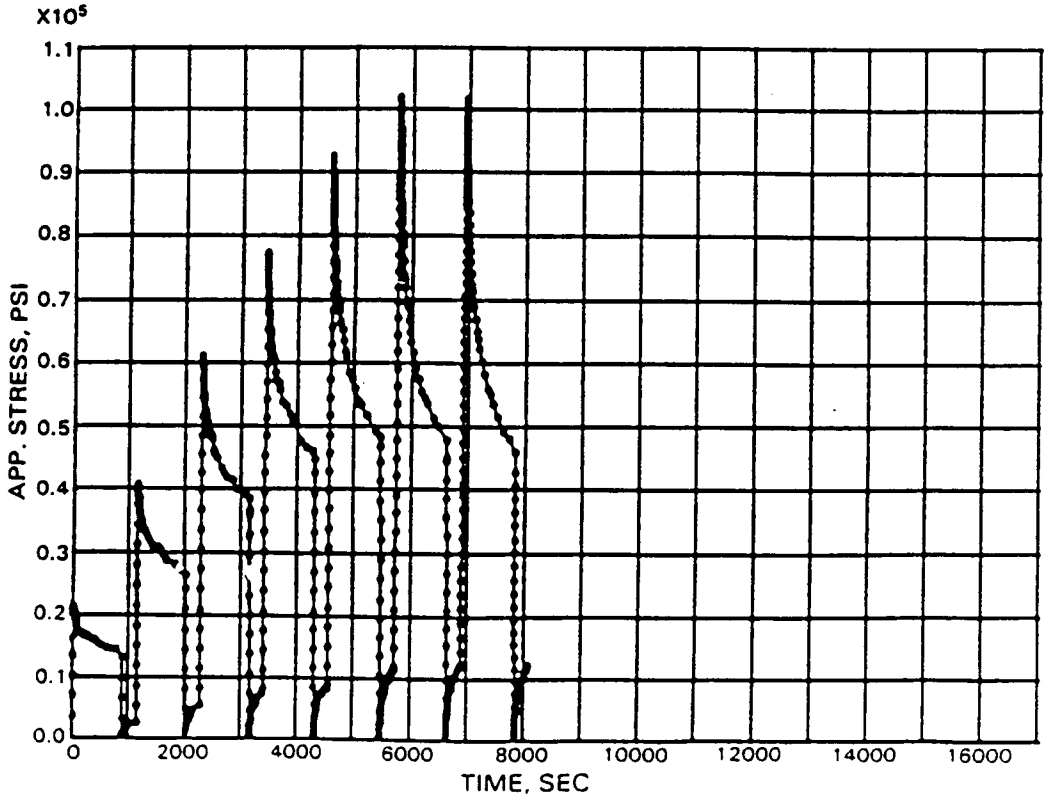


Figure C-3 PWA 286 Coating Stress Relaxation During Strain Hold Tests at 649°C (1200°F)

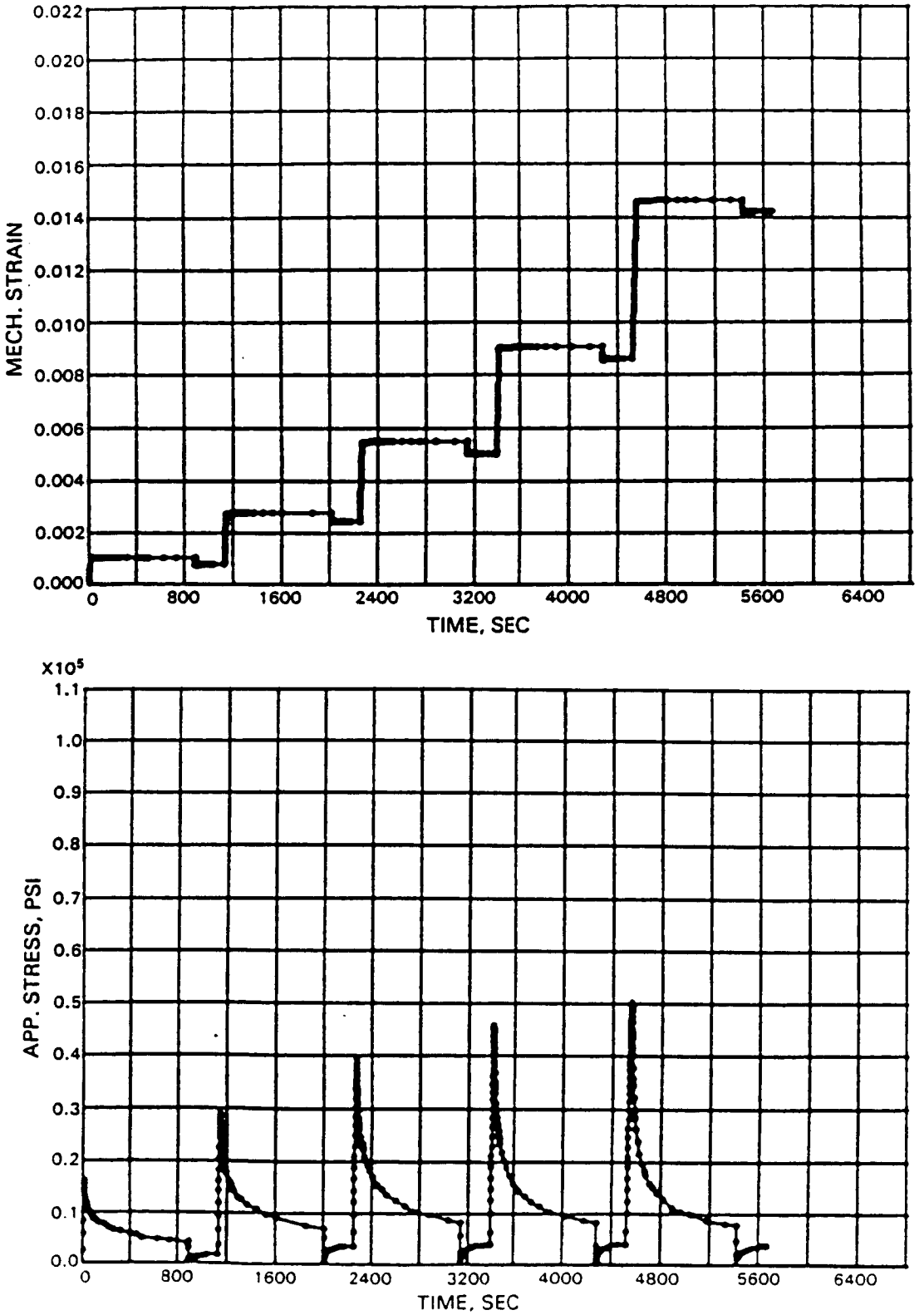


Figure C-4 PWA 286 Coating Stress Relaxation During Strain Hold Tests at 760°C (1400°F)

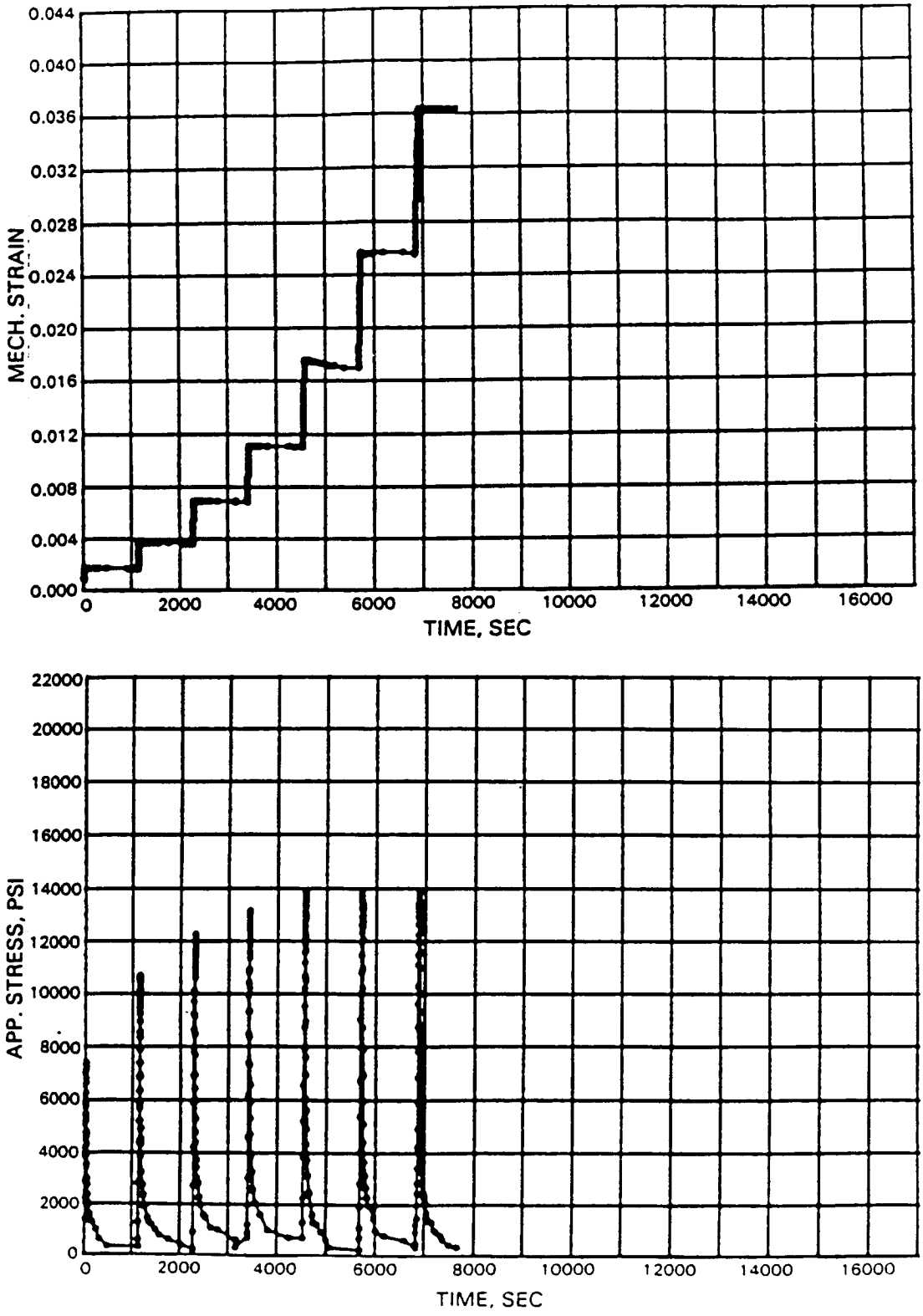


Figure C-5 PWA 286 Coating Stress Relaxation During Strain Hold Tests at 871°C (1600°F)

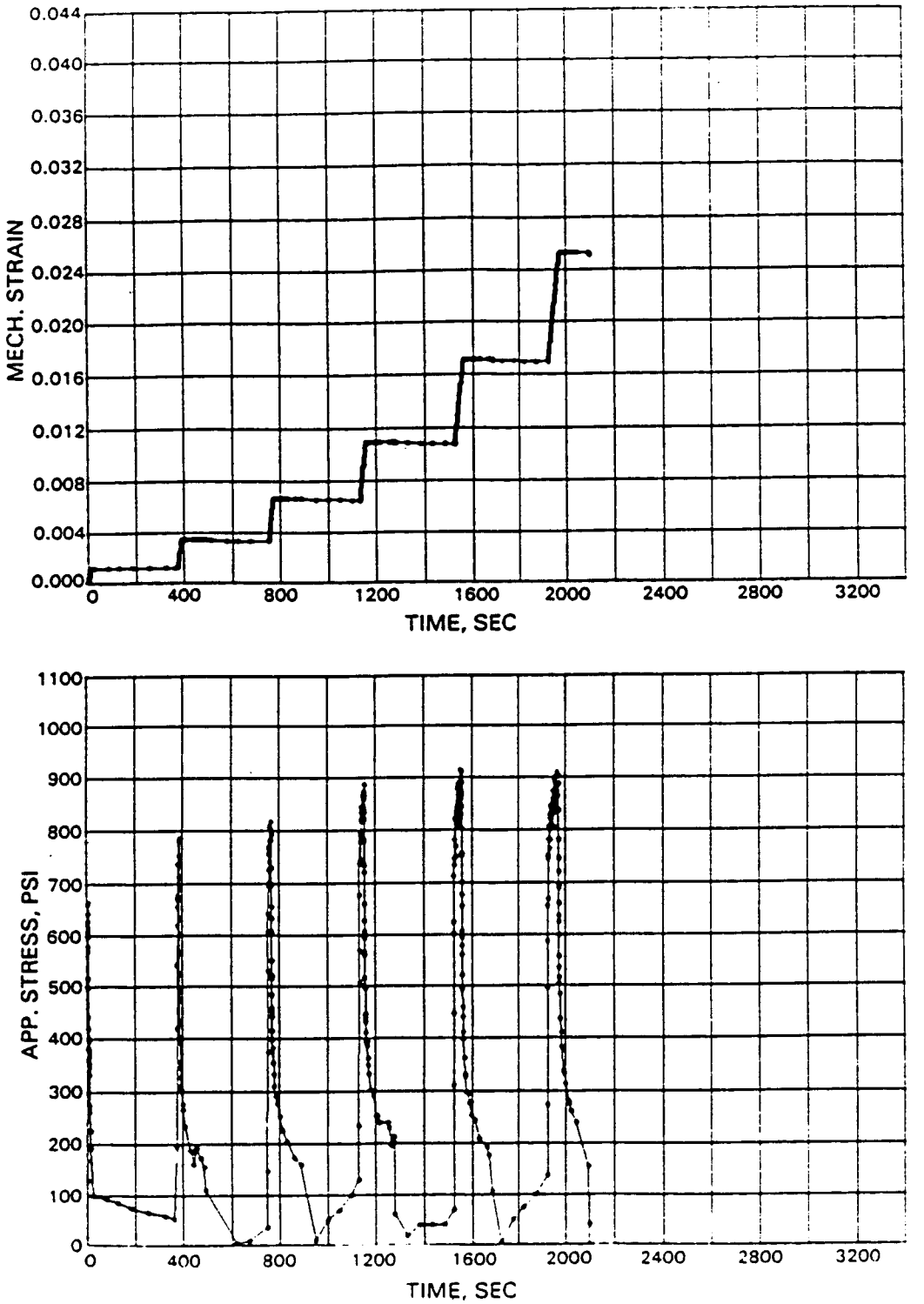


Figure C-6 PWA 286 Coating Stress Relaxation During Strain Hold Tests at 1093°C (2000°F)

APPENDIX D

OVERLAY COATING CONSTITUTIVE TEST RESULTS, TMF

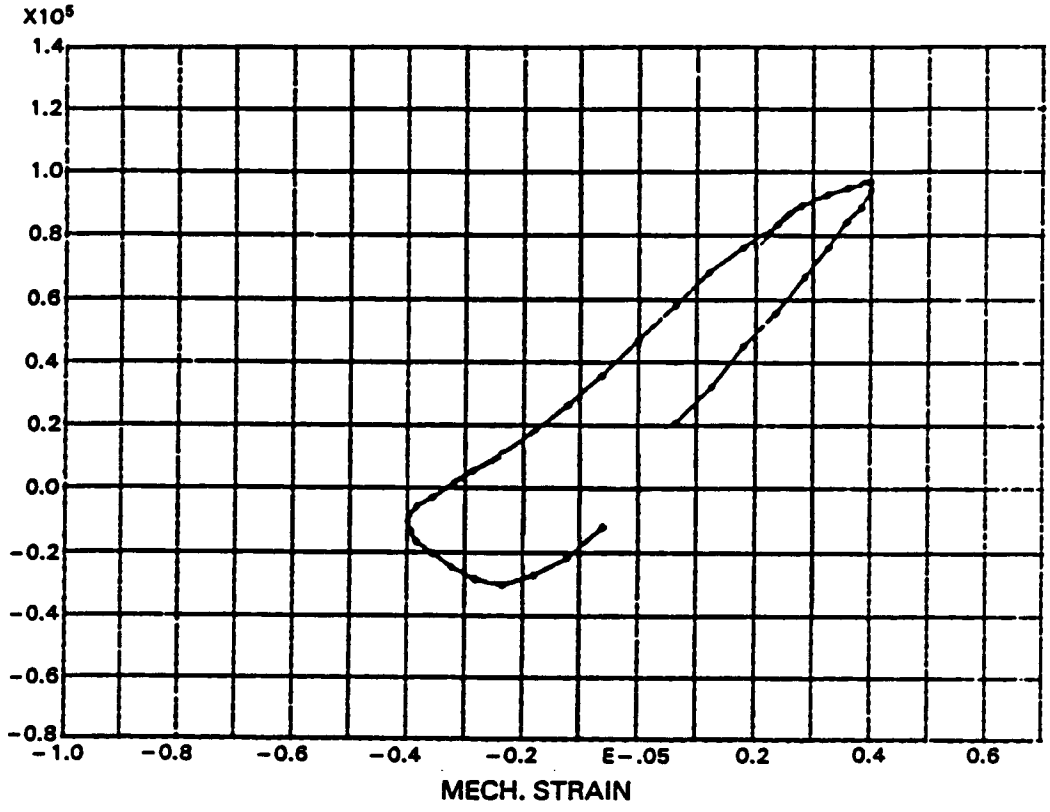


Figure D-1 PWA 286 Coating Stress/Strain Cycle for In-Phase TMF Test at 427°C to 871°C (800°F to 1600°F), ±0.4% Strain Load

APPENDIX E

TEST SEQUENCE OF CYCLIC CONSTITUTIVE TESTS

The sequence of testing for each test is listed in this appendix. The orientation of each specimen is also given in terms of deviation from the nominal orientation and in terms of Eulerian angles defined in Figure E-1.

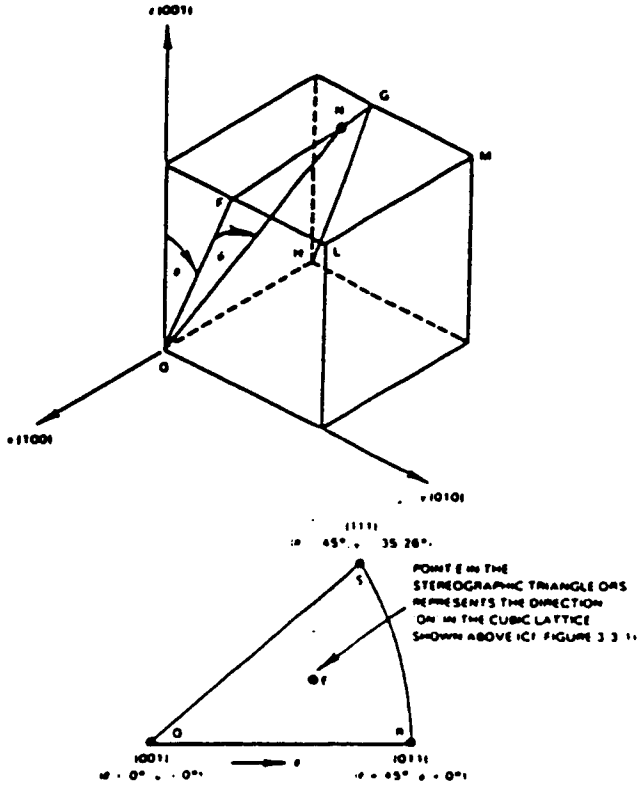


Figure E-1 A Single Crystal Bar Orientated Along ON at Angles $\theta$ and $\psi$ with Respect to the Crystal Axes X, Y, Z Is located at Point E in the Stereographic Triangle ORS

Specimen Number = MA27 Nominal Orientation = <123>

Test Temperature = 821°C
( 70°F)

Deviation from Nominal Orientation = 2.9 degrees

Actual Orientation: Theta = 35.89 degrees
Psi = 13.53 degrees

Test Conditions

| Order of Test | Strain Rate (%/sec) | Nominal Strain Limits (%) | Number of Creep and Relaxation Tests |
|---|---|---|---|
| 1 | 0.1 | $\pm$ 0.4 | 0 |
| 2 | 0.1 | $\pm$ 0.5 | 0 |
| 3 | 0.02 | $\pm$ 0.5 | 0 |

Specimen Number = JA61

Nominal Orientation = <100>

Test Temperature = 427°C (800°F)

Deviation from Nominal Orientation = 6.7 degrees

Actual Orientation: Theta = 6.50 degrees
Psi = 0.68 degrees

Test Conditions

| Order of Test | Strain Rate (%/sec) | Nominal Strain Limits (%) | Number of Creep and Relaxation Tests |
|---|---|---|---|
| 1 | 0.1 | ± 0.6 | 0 |
| 2 | 0.1 | ± 0.8 | 0 |
| 3 | 0.1 | ± 0.9 | 0 |
| 4 | 0.1 | ± 1.0 | 0 |

Specimen Number = KA27 Nominal Orientation = <110>

Test Temperature = 427°C (800°F)

Deviation from Nominal Orientation = 1.5 degrees

Actual Orientation: Theta = 43.60 degrees
Psi = 0.50 degrees

Test Conditions

| Order of Test | Strain Rate (%/sec) | Nominal Strain Limits (%) | Number of Creep and Relaxation Tests |
|---|---|---|---|
| 1 | 0.1 | ± 0.3 | 0 |
| 2 | 0.1 | ± 0.4 | 0 |
| 3 | 0.1 | ± 0.45 | 0 |
| 4 | 0.1 | ± 0.5 | 0 |
| 5 | 0.01 | ± 0.5 | 0 |
| 6 | 0.01 | ± 0.53 | 0 |

Specimen Number = LA66 Nominal Orientation = <111>

Test Temperature = 427°C (800°F)

Deviation from Nominal Orientation = 2.8 degrees

Actual Orientation: Theta = 42.56 degrees
Psi = 33.28 degrees

Test Conditions

| Order of Test | Strain Rate (%/sec) | Nominal Strain Limits (%) | Number of Creep and Relaxation Tests |
|---|---|---|---|
| 1 | 0.1 | ± 0.3 | 0 |
| 2 | 0.1 | ± 0.35 | 0 |
| 3 | 0.1 | ± 0.4 | 0 |
| 4 | 0.1 | ± 0.45 | 0 |
| 5 | 0.1 | ± 0.5 | 0 |
| 6 | 0.1 | ± 0.53 | 0 |
| 7 | 0.1 | ± 0.56 | 0 |
| 8 | 0.1 | ± 0.61 | 0 |
| 9 | 0.1 | ± 0.7 | 0 |
| 10 | 0.1 | ± 0.4 | 0 |
| 11 | 0.1 | ± 0.7 | 0 |
| 12 | 0.1 | ± 0.5 | 0 |
| 13 | 0.1 | ± 0.7 | 0 |
| 14 | 0.1 | ± 0.6 | 0 |
| 15 | 0.1 | ± 0.5 | 0 |
| 16 | 0.1 | ± 0.35 | 0 |

Specimen Number = MA26

Nominal Orientation = <123>

Test Temperature = 427°C (800°F)

Deviation from Nominal Orientation = 1.2 degrees

Actual Orientation: Theta = 34.93 degrees
Psi = 15.40 degrees

Test Conditions

| Order of Test | Strain Rate (%/sec) | Nominal Strain Limits (%) | Number of Creep and Relaxation Tests |
|---|---|---|---|
| 1 | 0.1 | ± 0.3 | 0 |
| 2 | 0.1 | ± 0.4 | 0 |
| 3 | 0.1 | ± 0.45 | 2 |
| 4 | 0.1 | ± 0.5 | 0 |
| 5 | 0.1 | ± 0.53 | 1 |

Specimen Number = MA30 Nominal Orientation = <123>

Test Temperature = 427°C and 982°C
(800°F and 1800°F)

Deviation from Nominal Orientation = 4.4 degrees

Actual Orientation: Theta = 38.25 degrees
Psi = 16.05 degrees

Test Conditions

| Order of Test | Strain Rate (%/sec) | Nominal Strain Limits (%) | Temp. (°C) | Number of Creep and Relaxation Tests |
|---|---|---|---|---|
| 1 | 0.1 | ± 0.2 | 982 | 0 |
| 2 | 0.1 | ± 0.3 | 982 | 0 |
| 3 | 0.1 | ± 0.4 | 427 | 0 |
| 4 | 0.1 | ± 0.3 | 982 | 0 |
| 5 | 0.1 | ± 0.6 | 982 | 0 |
| 6 | 0.1 | ± 0.4 | 427 | 0 |
| 7 | 0.1 | ± 0.45 | 427 | 0 |

Specimen Number = MA28 Nominal Orientation = <123>

Test Temperature = 427°C (800°F)

Deviation from Nominal Orientation = 1.2 degrees

Actual Orientation: Theta = 34.61 degrees
Psi = 14.70 degrees

Test Conditions

| Order of Test | Strain Rate (%/sec) | Nominal Strain Limits (%) | Number of Creep and Relaxation Tests |
|---|---|---|---|
| 1 | 0.1 | 0.0 to +0.8 | 0 |

Specimen Number = JA64 Nominal Orientation = <100>

Test Temperature = 649°C (1200°F)

Deviation from Nominal Orientation = 4.4 degrees

Actual Orientation: Theta = 3.68 degrees
Psi = 0.96 degrees

Test Conditions

| Order of Test | Strain Rate (%/sec) | Nominal Strain Limits (%) | Number of Creep and Relaxation Tests |
|---|---|---|---|
| 1 | 0.1 | ± 0.6 | 0 |
| 2 | 0.1 | ± 0.8 | 0 |
| 3 | 0.1 | ± 1.0 | 0 |
| 4 | 0.1 | ± 1.2 | 0 |
| 5 | 0.1 | ± 1.3 | 0 |

Specimen Number = KA31 Nominal Orientation = <110>

Test Temperature = 649°C (1200°F)

Deviation from Nominal Orientation = 4.8 degrees

Actual Orientation: Theta = 41.82 degrees
Psi = 3.54 degrees

Test Conditions

| Order of Test | Strain Rate (%/sec) | Nominal Strain Limits (%) | Number of Creep and Relaxation Tests |
|---|---|---|---|
| 1 | 0.1 | $\pm$ 0.6 | 0 |
| 2 | 0.1 | $\pm$ 0.2 | 5 |
| 3 | 0.01 | -0.5 to +0.3 | 2 |
| 4 | 0.01 | 0.0 to +0.6 | 0 |

Specimen Number = LA71 Nominal Orientation = <111>

Test Temperature = 649°C (1200°F)

Deviation from Nominal Orientation = 2.5 degrees

Actual Orientation: Theta = 43.88 degrees
Psi = 32.97 degrees

Test Conditions

| Order of Test | Strain Rate (%/sec) | Nominal Strain Limits (%) | Number of Creep and Relaxation Tests |
|---|---|---|---|
| 1 | 0.1 | $\pm$ 0.35 | 0 |
| 2 | 1.0 | $\pm$ 0.35 | 0 |
| 3 | 0.01 | $\pm$ 0.35 | 0 |
| 4 | 0.1 | 0.0 to +0.6 | 0 |
| 5 | 0.1 | $\pm$ 0.6 | 0 |
| 6 | 0.01 | $\pm$ 0.6 | 0 |

Specimen Number = JA44 Nominal Orientation = <100>

Test Temperature = 760°C (1400°F)

Deviation from Nominal Orientation = 5.7 degrees

Actual Orientation: Theta = 4.89 degrees
Psi = 2.59 degrees

Test Conditions

| Order of Test | Strain Rate (%/sec) | Nominal Strain Limits (%) | Number of Creep and Relaxation Tests |
|---|---|---|---|
| 1 | 0.1 | ± 0.6 | 0 |
| 2 | 0.1 | ± 0.7 | 0 |
| 3 | 0.1 | ± 0.8 | 5 |
| 4 | 0.1 | ± 0.9 | 0 |
| 5 | 0.1 | ± 1.0 | 0 |
| 6 | 0.1 | ± 1.1 | 5 |
| 7 | 0.005 | ± 1.1 | 0 |
| 8 | 0.1 | ± 1.3 | 0 |

Specimen Number = KA26 Nominal Orientation = <110>

Test Temperature = 760°C (1400°F)

Deviation from Nominal Orientation = 2.1 degrees

Actual Orientation: Theta = 43.20 degrees
Psi = 1.03 degrees

Test Conditions

| Order of Test | Strain Rate (%/sec) | Nominal Strain Limits (%) | Number of Creep and Relaxation Tests |
|---|---|---|---|
| 1 | 0.1 | ± 0.2 | 0 |
| 2 | 0.1 | ± 0.3 | 0 |
| 3 | 0.1 | ± 0.4 | 0 |
| 4 | 0.1 | ± 0.5 | 0 |
| 5 | 0.1 | ± 0.6 | 0 |
| 6 | 0.01 | ± 0.6 | 0 |
| 7 | 0.1 | ± 0.6 | 10 |
| 8 | 0.1 | ± 0.7 | 0 |
| 9 | 0.1 | ± 0.8 | 0 |

Specimen Number = LA63 Nominal Orientation = <111>

Test Temperature = 760°C (1400°F)

Deviation from Nominal Orientation = 5.0 degrees

Actual Orientation: Theta = 41.36 degrees
Psi = 31.31 degrees

Test Conditions

| Order of Test | Strain Rate (%/sec) | Nominal Strain Limits (%) | Number of Creep and Relaxation Tests |
|---|---|---|---|
| 1 | 0.1 | $\pm$ 0.4 | 10 |
| 2 | 0.01 | $\pm$ 0.4 | 0 |
| 3 | 1.0 | $\pm$ 0.4 | 0 |
| 4 | 0.1 | $\pm$ 0.4 | 0 |
| 5 | 0.1 | $\pm$ 0.5 | 0 |
| 6 | 0.1 | $\pm$ 0.6 | 7 |

Specimen Number = LA67 Nominal Orientation = <111>

Test Temperature = 760°C (1400°F)

Deviation from Nominal Orientation = 3.2 degrees

Actual Orientation: Theta = 42.21 degrees
Psi = 33.00 degrees

Test Conditions

| Order of Test | Strain Rate (%/sec) | Nominal Strain Limits (%) | Number of Creep and Relaxation Tests |
|---|---|---|---|
| 1 | 0.1 | 0.0 to -0.4 | 0 |

Specimen Number = MA25 Nominal Orientation = <123>

Test Temperature = 760°C (1400°F)

Deviation from Nominal Orientation = 2.0 degrees

Actual Orientation: Theta = 35.75 degrees
Psi = 15.36 degrees

Test Conditions

| Order of Test | Strain Rate (%/sec) | Nominal Strain Limits (%) | Number of Creep and Relaxation Tests |
|---|---|---|---|
| 1 | 0.1 | $\pm$ 0.4 | 0 |
| 2 | 0.1 | $\pm$ 0.5 | 0 |
| 3 | 0.1 | $\pm$ 0.6 | 11 |

Specimen Number = JA67 Nominal Orientation = <100>

Test Temperature = 872°C (1600°F)

Deviation from Nominal Orientation = 3.2 degrees

Actual Orientation: Theta = 3.58 degrees
Psi = 1.31 degrees

Test Conditions

| Order of Test | Strain Rate (%/sec) | Nominal Strain Limits (%) | Number of Creep and Relaxation Tests |
|---|---|---|---|
| 1 | 0.1 | | 0 |
| 2 | 0.1 | ± 0.8 | 0 |
| 3 | 0.1 | ± 1.22 | 0 |
| 4 | 0.01 | ± 1.22 | 0 |
| 5 | 0.0025 | ± 1.22 | 0 |
| 6 | 0.1 | ± 1.22 | 0 |
| 7 | 0.1 | ± 1.22 | 6 |

Specimen Number = KA33 Nominal Orientation = <100>

Test Temperature = 872°C (1600°F)

Deviation from Nominal Orientation = 4.8 degrees

Actual Orientation: Theta = 44.80 degrees
Psi = 4.83 degrees

Test Conditions

| Order of Test | Strain Rate (%/sec) | Nominal Strain Limits (%) | Number of Creep and Relaxation Tests |
|---|---|---|---|
| 1 | 0.1 | ± 0.01 | 0 |
| 2 | 0.01 | ± 0.01 | 0 |
| 3 | 0.1 | ± 0.9 | 0 |
| 4 | 0.01 | ± 0.9 | 0 |
| 5 | 0.001 | ± 0.9 | 0 |
| 6 | 0.5 | ± 0.9 | 0 |
| 7 | 0.1 | ± 0.9 | 0 |
| 8 | 1.0 | ± 0.9 | 0 |
| 9 | 0.00012 | ± 0.9 | 0 |

Specimen Number = LA68 Nominal Orientation = <111>

Test Temperature = 872°C (1600°F)

Deviation from Nominal Orientation = 1.4 degrees

Actual Orientation: Theta = 43.97 degrees
Psi = 34.19 degrees

Test Conditions

| Order of Test | Strain Rate (%/sec) | Nominal Strain Limits (%) | Number of Creep and Relaxation Tests |
|---|---|---|---|
| 1 | 0.1 | ± 0.2 | 0 |
| 2 | 0.1 | ± 0.3 | 9 |
| 3 | 0.1 | ± 0.4 | 0 |
| 4 | 0.1 | ± 0.5 | 9 |
| 5 | 0.001 | ± 0.5 | 0 |
| 6 | 0.01 | ± 0.5 | 0 |
| 7 | 0.1 | ± 0.5 | 0 |
| 8 | 0.5 | ± 0.5 | 0 |
| 9 | 0.1 | ± 0.5 | 0 |
| 10 | 0.1 | ± 0.6 | 12 |
| 11 | 0.1 | ± 1.0 | 0 |

Specimen Number = MA35 Nominal Orientation = <123>

Test Temperature = 872°C (1600°F)

Deviation from Nominal Orientation = 2.5 degrees

Actual Orientation: Theta = 36.26 degrees
Psi = 15.63 degrees

Test Conditions

| Order of Test | Strain Rate (%/sec) | Nominal Strain Limits (%) | Number of Creep and Relaxation Tests |
|---|---|---|---|
| 1 | 0.1 | ± 0.4 | 0 |
| 2 | 0.1 | ± 0.6 | 0 |
| 3 | 1.0 | ± 0.6 | 0 |
| 4 | 0.01 | ± 0.6 | 0 |
| 5 | 1.0 | ± 0.6 | 0 |

Specimen Number = JA63 Nominal Orientation = <100>

Test Temperature = 872°C (1600°F)

Deviation from Nominal Orientation = 6.6 degrees

Actual Orientation: Theta = 6.73 degrees
Psi = 0.23 degrees

Test Conditions

| Order of Test | Strain Rate (%/sec) | Nominal Strain Limits (%) | Number of Creep and Relaxation Tests |
|---|---|---|---|
| 1 | 0.1 | 0.0 to +0.8 | 0 |
| 2 | 0.1 | 0.0 to +1.0 | 0 |
| 3 | 0.01 | 0.0 to +1.0 | 0 |
| 4 | 0.1 | 0.0 to +1.0 | 5 |
| 5 | 0.1 | 0.0 to +1.0 | 0 |
| 6 | 0.1 | $\pm$ 1.0 | 0 |
| 7 | 0.1 | $\pm$ 1.2 | 0 |
| 8 | 0.01 | $\pm$ 1.2 | 0 |
| 9 | 0.1 | $\pm$ 1.2 | 0 |
| 10 | 0.1 | 0.0 to +1.2 | 2 |
| 11 | 0.1 | 0.0 to +1.2 | 0 |

Specimen Number = KA23 Nominal Orientation = <110>

Test Temperature = 872°C (1600°F)

Deviation from Nominal Orientation = 5.0 degrees

Actual Orientation: Theta = 40.36 degrees
Psi = 1.83 degrees

Test Conditions

| Order of Test | Strain Rate (%/sec) | Nominal Strain Limits (%) | Number of Creep and Relaxation Tests |
|---|---|---|---|
| 1 | 0.1 | 0.0 to -0.8 | 0 |
| 2 | 0.1 | 0.0 to +0.8 | 0 |
| 3 | 0.1 | ± 0.8 | 0 |
| 4 | 0.1 | 0.0 to +0.8 | 0 |
| 5 | 0.1 | ± 0.9 | 0 |
| 6 | 0.1 | 0.0 to -0.9 | 0 |
| 7 | 0.1 | 0.0 to +0.9 | 0 |
| 8 | 0.1 | ± 0.9 | 0 |
| 9 | 0.1 | ± 0.8 | 0 |
| 10 | 0.1 | ± 0.7 | 0 |
| 11 | 0.1 | ± 0.6 | 0 |
| 12 | 0.1 | ± 0.5 | 0 |
| 13 | 0.1 | ± 0.4 | 0 |
| 14 | 0.1 | ± 0.3 | 0 |
| 15 | 0.1 | ± 1.0 | 0 |
| 16 | 0.1 | ± 1.2 | 0 |

Specimen Number = LA65 Nominal Orientation = <111>

Test Temperature = 872°C (1600°F)

Deviation from Nominal Orientation = 2.7 degrees

Actual Orientation: Theta = 42.68 degrees
Psi = 33.42 degrees

Test Conditions

| Order of Test | Strain Rate (%/sec) | Nominal Strain Limits (%) | Number of Creep and Relaxation Tests |
|---|---|---|---|
| 1 | 0.1 | 0.0 to -0.3 | 0 |
| 2 | 0.1 | 0.0 to -0.5 | 0 |
| 3 | 0.1 | 0.0 to +0.5 | 0 |
| 4 | 0.1 | $\pm$ 0.5 | 0 |
| 5 | 0.1 | $\pm$ 0.4 | 0 |
| 6 | 0.1 | $\pm$ 0.3 | 0 |
| 7 | 0.1 | $\pm$ 0.2 | 0 |
| 8 | 0.1 | $\pm$ 0.2 | 5 |

Specimen Number = JA58 Nominal Orientation = <100>

Test Temperature = 982°C (1800°F)

Deviation from Nominal Orientation = 5.0 degrees

Actual Orientation: Theta = 3.86 degrees
Psi = 2.90 degrees

Test Conditions

| Order of Test | Strain Rate (%/sec) | Nominal Strain Limits (%) | Number of Creep and Relaxation Tests |
|---|---|---|---|
| 1 | 0.1 | $\pm$ 1.2 | 6 |
| 2 | 0.01 | $\pm$ 1.2 | 2 |

Specimen Number = JA66 Nominal Orientation = <100>

Test Temperature = 982°C (1800°F)

Deviation from Nominal Orientation = 2.8 degrees

Actual Orientation: Theta = 42.56 degrees
Psi = 33.28 degrees

Test Conditions

| Order of Test | Strain Rate (%/sec) | Nominal Strain Limits (%) | Number of Creep and Relaxation Tests |
|---|---|---|---|
| 1 | 0.1 | ± 0.3 | 0 |
| 2 | 0.1 | ± 0.4 | 10 |
| 3 | 1.0 | ± 0.4 | 0 |
| 4 | 0.01 | ± 0.4 | 0 |
| 5 | 0.001 | ± 0.4 | 0 |
| 6 | 0.1 | ± 0.4 | 0 |
| 7 | 0.1 | ± 0.6 | 0 |
| 8 | 0.1 | ± 0.8 | 12 |
| 9 | 1.0 | ± 0.8 | 0 |
| 10 | 0.01 | ± 0.8 | 3 |
| 11 | 0.005 | ± 0.8 | 0 |

Specimen Number = JA68 Nominal Orientation = <100>

Test Temperature = 982°C (1800°F)

Deviation from Nominal Orientation = 6.5 degrees

Actual Orientation: Theta = 6.39 degrees
Psi = 0.47 degrees

Test Conditions

| Order of Test | Strain Rate (%/sec) | Nominal Strain Limits (%) | Number of Creep and Relaxation Tests |
|---|---|---|---|
| 1 | 0.1 | 0.0 to -0.6 | 0 |
| 2 | 0.1 | 0.0 to -0.8 | 0 |
| 3 | 0.1 | 0.0 to -1.0 | 0 |
| 4 | 0.1 | 0.0 to -1.2 | 0 |
| 5 | variable | 0.0 to -0.7 | 0 |
| 6 | 0.1 | 0.0 to -1.2 | 0 |
| 7 | 0.1 | 0.0 to +1.2 | 0 |
| 8 | 0.1 | $\pm$ 1.2 | 0 |
| 9 | 0.01 | $\pm$ 1.2 | 0 |
| 10 | 0.5 | $\pm$ 1.2 | 0 |
| 11 | 0.0025 | $\pm$ 1.2 | 0 |

Specimen Number = KA22 Nominal Orientation = <110>

Test Temperature = 982°C (1800°F)

Deviation from Nominal Orientation = 5.4 degrees

Actual Orientation: Theta = 41.55 degrees
Psi = 4.15 degrees

Test Conditions

| Order of Test | Strain Rate (%/sec) | Nominal Strain Limits (%) | Number of Creep and Relaxation Tests |
|---|---|---|---|
| 1 | 0.1 | ± 0.3 | 0 |
| 2 | 0.1 | ± 0.4 | 12 |
| 3 | 1.0 | ± 0.4 | 0 |
| 4 | 0.01 | ± 0.4 | 0 |
| 5 | 0.1 | ± 0.5 | 0 |
| 6 | 0.1 | ± 0.6 | 10 |
| 7 | 0.001 | ± 0.6 | 0 |

Specimen Number = LA64 Nominal Orientation = <111>

Test Temperature = 982°C (1800°F)

Deviation from Nominal Orientation = 3.4 degrees

Actual Orientation: Theta = 41.86 degrees
Psi = 33.07 degrees

Test Conditions

| Order of Test | Strain Rate (%/sec) | Nominal Strain Limits (%) | Number of Creep and Relaxation Tests |
|---|---|---|---|
| 1 | 0.1 | ± 0.3 | 7 |
| 2 | 0.1 | ± 0.3 | 1 |
| 3 | 0.01 | ± 0.3 | 0 |
| 4 | 0.001 | ± 0.3 | 0 |
| 5 | 0.1 | ± 0.3 | 5 |

Specimen Number = LA69 Nominal Orientation = <111>

Test Temperature = 982°C (1800°F)

Deviation from Nominal Orientation = 2.0 degrees

Actual Orientation: Theta = 43.11 degrees
Psi = 34.02 degrees

Test Conditions

| Order of Test | Strain Rate (%/sec) | Nominal Strain Limits (%) | Number of Creep and Relaxation Tests |
|---|---|---|---|
| 1 | 0.1 | ± 0.15 | 7 |
| 2 | 0.1 | ± 0.2 | 6 |
| 3 | 0.1 | ± 0.3 | 7 |
| 4 | 0.1 | ± 0.4 | 12 |
| 5 | 0.1 | ± 0.5 | 9 |
| 6 | 0.1 | ± 0.4 | 0 |
| 7 | 0.1 | ± 0.3 | 0 |
| 8 | 0.1 | ± 0.2 | 3 |
| 9 | 0.1 | ± 0.15 | 0 |
| 10 | 0.001 | ± 0.5 | 0 |

Specimen Number = MA23 Nominal Orientation = <123>

Test Temperature = 982°C (1800°F)

Deviation from Nominal Orientation = 5.1 degrees

Actual Orientation: Theta = 35.60 degrees
Psi = 10.76 degrees

Test Conditions

| Order of Test | Strain Rate (%/sec) | Nominal Strain Limits (%) | Number of Creep and Relaxation Tests |
|---|---|---|---|
| 1 | 0.1 | ± 0.3 | 0 |
| 2 | 0.1 | ± 0.3 | 8 |
| 3 | 0.01 | ± 0.3 | 0 |
| 4 | 1.0 | ± 0.3 | 0 |
| 5 | 0.01 | ± 0.3 | 0 |
| 6 | 0.1 | ± 0.4 | 0 |
| 7 | 0.1 | ± 0.5 | 0 |
| 8 | 0.001 | ± 0.5 | 0 |
| 9 | 0.1 | ± 0.5 | 10 |
| 10 | 1.0 | ± 0.5 | 0 |
| 11 | 0.1 | ± 0.65 | 0 |
| 12 | 0.1 | ± 0.4 | 0 |
| 13 | 0.1 | ± 0.3 | 3 |
| 14 | 0.0005 | ± 0.3 | 0 |

Specimen Number = JA69 Nominal Orientation = <100>

Test Temperature = 1038°C (1900°F)

Deviation from Nominal Orientation = 7.8 degrees

Actual Orientation: Theta = 6.87 degrees
Psi = 3.44 degrees

Test Conditions

| Order of Test | Strain Rate (%/sec) | Nominal Strain Limits (%) | Number of Creep and Relaxation Tests |
|---|---|---|---|
| 1 | 0.1 | ± 0.6 | 0 |
| 2 | 1.0 | ± 0.6 | 0 |
| 3 | 0.01 | ± 0.6 | 0 |
| 4 | 0.1 | ± 0.8 | 0 |
| 5 | 0.01 | ± 0.8 | 0 |
| 6 | 0.1 | ± 0.6 | 0 |
| 7 | 0.1 | ± 0.4 | 0 |
| 8 | 0.1 | ± 0.2 | 0 |
| 9 | 0.1 | ± 0.2 | 6 |
| 10 | 0.001145 | ± 0.6 | 0 |
| 11 | 0.0005 | -0.01 to +1.0 | 0 |

Specimen Number = LA62 Nominal Orientation = <111>

Test Temperature = 1038°C (1900°F)

Deviation from Nominal Orientation = 2.5 degrees

Actual Orientation: Theta = 42.57 degrees
Psi = 33.77 degrees

Test Conditions

| Order of Test | Strain Rate (%/sec) | Nominal Strain Limits (%) | Number of Creep and Relaxation Tests |
|---|---|---|---|
| 1 | 0.1 | ± 0.2 | 0 |
| 2 | 0.1 | ± 0.3 | 8 |
| 3 | 0.01 | ± 0.3 | 0 |
| 4 | 0.001 | ± 0.3 | 0 |
| 5 | 0.0001 | ± 0.3 | 0 |
| 6 | 1.0 | ± 0.3 | 0 |
| 7 | 0.1 | ± 0.4 | 0 |
| 8 | 0.1 | ± 0.5 | 0 |
| 9 | 0.1 | ± 0.3 | 0 |
| 10 | 0.1 | ± 0.2 | 0 |
| 11 | 0.1 | ± 0.1 | 0 |
| 12 | 0.1 | ± 0.1 | 7 |
| 13 | 0.01 | ± 0.1 | 9 |

Specimen Number = JA65 Nominal Orientation = <100>

Test Temperature = 1149°C (2100°F)

Deviation from Nominal Orientation = 6.8 degrees

Actual Orientation: Theta = 6.68 degrees
Psi = 0.34 degrees

Test Conditions

| Order of Test | Strain Rate (%/sec) | Nominal Strain Limits (%) | Number of Creep and Relaxation Tests |
|---|---|---|---|
| 1 | 1.0 | ± 0.3 | 0 |
| 2 | 0.1 | ± 0.3 | 0 |
| 3 | 0.01 | ± 0.3 | 0 |
| 4 | 0.001 | ± 0.3 | 0 |
| 5 | 0.00025 | ± 0.3 | 0 |
| 6 | 1.0 | ± 0.5 | 0 |
| 7 | 0.1 | ± 0.5 | 0 |
| 8 | 0.01 | ± 0.5 | 0 |
| 9 | 0.01 | ± 0.5 | 0 |
| 10 | 0.0005 | ± 0.5 | 0 |
| 11 | 1.0 | ± 0.7 | 0 |
| 12 | 0.1 | ± 0.7 | 0 |
| 13 | 0.01 | ± 0.7 | 0 |
| 14 | 0.000667 | ± 0.7 | 0 |
| 15 | 0.1 | ± 0.7 | 3 |

Specimen Number = JB44 Nominal Orientation = <100>

Test Temperature = 1079°C (1975°F)

Deviation from Nominal Orientation = . degrees

Actual Orientation: Theta = . degrees
Psi = . degrees

Test Conditions

| Order of Test | Strain Rate (%/sec) | Nominal Strain Limits (%) | Number of Creep and Relaxation Tests |
|---|---|---|---|
| 1 | 0.1 | 0.05 to +0.1 | 1 |
| 2 | 0.1 | 0.05 to +0.3 | 2 |
| 3 | 0.1 | 0.05 to -0.3 | 1 |

DISTRIBUTION LIST

Aerojet TechSystems
Attn: V Frick
Mgr,, Matl's Eng
Box 13222
Sacramento, CA 95813

W P A F B
Attn: Ted Nicholas
AFWAL/MLLN
WPAFB, OH 45433

Univ of Alabama
Attn: Dr. A. E. Carden
Dept Eng Mech
216 Hardaway Hall
University, AL 35486

University of Arizona
Attn: Dr. Paul H. Wirsching
Dept. Aero & Mech Eng
Tucson, AZ 85721

Battelle Columbus Lab
Attn: Brian Leis
505 King Avenue
Columbus, OH 43201

University of Cincinnati
Attn: Dr. Donald Stouffer
Rm 833 Rhodes Hall
Dept Eng Sci
Cincinnati, OH 45221

University of Dayton
Attn: Dr. Joseph Gallagher
Research Institute
Rm 563 Kettering Bldg
Dayton, OH 45469

Aerojet TechSystems
Attn: Walt Langhi
Mgr, Applied Mechanics
Box 13222
Sacramento, CA 95813

AiResearch Mfg Co
Attn: Richard Graves
Chief, Engrng Sciences
2525 W 190th St
Torrance, CA 90509

Allison Gas Turbine Oper.
Attn: Dr Ken Bain W8
Senior Metallurgist
Box 420
Indianapolis, IN 46206

Argonne Nat Lab
Attn: S. Majumdar
9700 S Cass Avenue
Argonne, IL 60439

University of California
Attn: Dr. Robert Ritchie
282 Heaof Mining Bldg
Berkley, CA 94720

University of Connecticut
Attn: Dr. Eric Jordan
Mech Eng Dept U-139
Storrs, CT 06268

DeLaval Turbine
Attn: Harry Gayley
Nottingham Way
Trenton, NJ 08602

AFOSR/NA
Attn: Nicholas Pagano
Mgr, Matl's & Structures
Bolling AFB
Washington, DC 20332

AiResearch Mfg Co
Attn: Dr. Tekal Nath
Mail T-42, Dept 93-3
2525 W 190th St
Torrance, CA 90509

Allison Gas Turbine Oper.
Attn: Mehmet Doner T27
Section Chief
Box 420
Indianapolis, IN 46206

AVCO - Lycoming Div
Attn: James Gardini
Matl's Lab
550 S Main St
Stratford, CT 06497

Case Western Reserve University
Attn: Prof. S. S. Manson
619 Glennan Bldg
10900 Euclid Avenue
Cleveland, OH 44106

Gen Dynamics Convair
Attn: A. Campbell
P. O. Box 80847
San Diego, CA 92138

Exxon Res & Eng Co
Attn: R. P. Gangloff
Box 45
Linden, NJ 07036

W P A F B
Attn: Jack Henderson
AFWAL/MLLN
Area B, Bldg 32
WPAFB, OH 45433

University of Akron
Attn: Prof. Padovan
Dept Civil Eng
Akron, OH 44325

Allison Gas Turbine Oper.
Attn: Stacy Thompson T27
Chief, Analy. Mech.
Box 420
Indianapolis, IN 46206

AVCO - Lycoming Div
Attn: Jerry Walters
550 S Main St
Stratford, CT 06497

University of Cincinnati
Attn: Dr. Jayaraman
Dept Matl's Sci & Met Eng
Cincinnati, OH 45221

Curtiss Wright
Attn: Jerome Mogul
Dir - Matl's Eng
1 Rotary Dr
Wood-Ridge, NJ 07075

F A A - New England Reg.
Attn: Dan Salvano
12 New England Exec Park
Burlington, MA 01803

Failure Analysis Assoc.
Attn: Dr. Jerrell Thomas
2225 E Bayshore Rd
Palo Alto, CA 94303

Gen Elec Co - AEBG
Attn: Dr. Len Beitch G-60
Mgr EM & LM
Evandale, OH 45215-6301

Gen Elec Co
Attn: Donald Mowbray
Bldg 55-219
1 River Rd
Schenectady, NY 12345

Georgia Inst of Tech
Attn: Prof. Dave McDowell
School Mech Engrng
225 North Ave
Atlanta, GA 30332

I I T Research Inst
Attn: Humphries
10 W 35th St
Chicago, IL 60616

NASA - LeRC
Attn: Dr. R. L. Dreshfield
Mail Stop 49-1
21000 Brookpark Rd
Cleveland, OH 44135

Garrett Turbine Eng Co
Attn: Joe Adams
111 S 34th St
Box 5217
Phoenix, AZ 85010

Gen Elec Co - AEBG
Attn: T. Cook G-60
Evendale, OH 45215-6301

DISTRIBUTION LIST (continued)

Gen Elec Co
Attn: Ted Russell G-25
Turbine Div
Schenectady, NY 12345

Johns Hopkins University
Attn: Prof. W. N. Sharpe
Chairman, Dept of Mech
123 LaTrobe Hall
Baltimore, MD 21218

Michigan State University
Attn: Dr. John Martin
MMM Dept
330 Engineering Bldg
E Lansing, MI 48824

NASA - LeRC
Attn: Dr. R. Ellis
Mail Stop 49-6
21000 Brookpark Rd
Cleveland, OH 44135

Garrett Turbine Eng Co
Attn: Harry Kington
111 S 34th St
Box 5217
Phoenix, AZ 85010

Gen Elec Co - AEBG
Attn: J. H. Laflen
Mail Drop G-60
Evendale, OH 45215-6301

Gen Elec Co - AEBG
Attn: Kennard Wright
Evendale, OH 45215-6301

University of Illinois
Attn: Prof. H. Sehitoglu
M&IE Dept
1206 W Green St
Urbana, IL 61801

Garrett Turbine Eng Co
Attn: Lee Matsch
111 S 34th St
Box 5217
Phoenix, AZ 85010

Gen Elec Co - AEBG
Attn: R. L. McKnight
Mail Drop G-60
Evendale, OH 45215-6301

Georgia Inst of Tech
Attn: Prof. S. Antolovich
Fracture & Fatigue Lab
Bunger - Henry Bldg
Atlanta, GA 30332

University of Illinois
Attn: Prof. D. Socie
Dept Mech Engrng
1206 W Green St
Urbana, IL 61801

NASA - LeRC
Attn: Dr. Robert Bill
Deputy Branch Mgr, MS 49-7
21000 Brookpark Rd
Cleveland, OH 44135

NASA - LeRC
Attn: Dr. A. Freed
Mail Stop 49-7
21000 Brookpark Rd
Cleveland, OH 44135

NASA - LeRC
Attn: Dr. Gary Halford
MS 49-7
21000 Brookpark Rd
Cleveland, OH 44135

NASA - LeRC
Attn: M. J. Verrilli
Mail Stop 49-7
21000 Brookpark Rd
Cleveland, OH 44135

NASA - LeRC
Attn: R&T Branch
MS 500-305
21000 Brookpark Rd
Cleveland, OH 44135

NASA Marshall Space Ctr
Attn: Gwyn Faile
EP42, Bldg 4610, Rm 5034
Huntsville, AL 35812

N A P C
Attn: A. Martino
P. O. Box 7176
Mgr, R&T Div
Trenton, NJ 08628

ORNL Box X
Attn: Dr. Robert Swindeman
Metals & Ceramics Div
Oak Ridge, TN 37830

PCC Inc
Attn: Dr. C. Kortovich
T/M-3357
23555 Euclid Avenue
Cleveland, OH 44117

NASA - LeRC
Attn: HOST Project Off. (2)
Mail Stop 49-7
21000 Brookpark Rd
Cleveland, OH 44135

NASA Marshall Space Ctr
Attn: Bryan McPherson
Huntsville, AL 35812

Northwestern University
Attn: Dr. Julia Weertman
Matl's Sci & Engrng
Evanston, IL 60201

ORNL Box X
Attn: J. McGowan
Oak Ridge, TN 37830

Pennsylvania State University
Attn: Dr. Sam Zamrik
121 Hammond Bldg
University Park, PA 16802

NASA - LeRC
Attn: M. A. McGaw
Mail Stop 49-7
21000 Brookpark Rd
Cleveland, OH 44135

NASA - LeRC
Attn: Report Control
MS 60-1
21000 Brookpark Rd
Cleveland, OH 44135

NASA - LeRC
Attn: Dr. R. L. Thompson
Mail Stop 49-6
21000 Brookpark Rd
Cleveland, OH 44135

NASA Marshall Space Ctr
Attn: Larry Salter
EP46, Bldg 4610
Huntsville, AL 35812

ORNL Box X
Attn: Dr. Charles Brinkman
Metals & Ceramics Div
Oak Ridge, TN 37830

O'Donnell & Assoc
Attn: Dr. W. O'Donnell
241 Curry Hollow Rd
Pittsburgh, PA 15232

Rensselaer Polytech Inst
Attn: Dr. Erhard Krempl
Mech & Aero Eng Dept
Troy, NY 12181

NASA - LeRC
Attn: Dr. R. V. Miner
Mail Stop 49-3
21000 Brookpark Rd
Cleveland, OH 44135

NASA - LeRC
Attn: J. F. Saltsman
Mail Stop 6-1
21000 Brookpark Rd
Cleveland, OH 44135

NASA Marshall Space Ctr
Attn: B. Bhat
Huntsville, AL 35812

NASA Sci & Tech Info (25)
Attn: Accessioning Dept
Box 8757
Balt/Wash Intn'l Airport
Maryland 21240

ORNL Box X
Attn: Joe Strizak
Metals & Ceramics Div
Oak Ridge, TN 37830

Ohio State University
Attn: Dr. Dan Mendelsohn
Dept Eng Mech - Boyd Lab
155 W Woodruff Ave
Columbus, OH 43210-1181

Rensselaer Polytech Inst
Attn: Prof. Norman Stoloff
Dept of Matl's Eng
Troy, NY 12181

Rensselaer Polytech Inst
Attn: Dr. David Woodford
Dept of Matl's Eng
Troy, NY 12181

Rocketdyne
Attn: Jim Newell AC10
6633 Canoga Avenue
Canoga Pk, CA 91304

Southwest Research Institute
Attn: Dr. Thomas Cruse
P. O. Drawer 28510
San Antonio, TX 78284

Southwest Research Institute
Attn: Dr. Jim Lankford
P. O. Drawer 28510
San Antonio, TX 78284

Teledyne CAE
Attn: Bryon L. Lewis
Box 6971
Toledo, OH 43612

University of Tennessee
Attn: Dr. Maurice Wright
Space Institute
Tullahoma, TN 37388

Williams Research
Attn: Tom Culbertson
2280 W Maple Rd
Walled Lake, MI 48088

Rocketdyne
Attn: Dr. Bob Jewett/AC10
6633 Canoga Avenue
Canoga Pk, CA 91304

Rolls Royce, Inc
Attn: Dr. Ashok Thakker
1895 Phoenix Blvd
Atlanta, GA 30349

Southwest Research Institute
Attn: Dr. Gerald Leverant
P. O. Drawer 28510
San Antonio, TX 78284

Stanford University
Attn: Prof. Alan K. Miller
Matl's Sci & Engrng
Stanford, CA 94305

Teledyne CAE
Attn: Tom Moyer
Box 6971
Toledo, OH 43612

Texas A&M University
Attn: Dr. W. L. Bradley
College Sta, TX 77843

Williams Research
Attn: R. Horn
2280 W Maple Rd
Walled Lake, MI 48088

Rocketdyne
Attn: Dr. D. Matejczyk/AC10
6633 Canoga Avenue
Canoga Pk, CA 91304

S U N Y
Attn: Dr. A. Rubinstein
Dept Mech Engrng
SUNY, Stony Brook
NY 11794-2300

Southwest Research Institute
Attn: Dr. U. S. Lindholm
P. O. Drawer 28510
San Antonio, TX 78284

Syracuse University
Attn: Dr. H. W. Liu
409 Link Hall
Syracuse, NY 13210

Teledyne CAE
Attn: Anil Nijhawan
Box 6971
Toledo, OH 43612

Texas A&M University
Attn: Dr. Walter Haisler
Aerospace Eng Dept
College Sta, TX 77843

Williams Research
Attn: R. L. Maxwell
2280 W Maple Rd
Walled Lake, MI 48088

Rockwell Int'l
Attn: Dr. Mike Mitchell
Rockwell Science Ctr
P. O. Box 1085
Thousand Oaks, CA 91360

University of Utah
Attn: Prof. Dave Hoeppner
Salt Lake City, UT

Sandia Labs
Attn: D. W. Lobitz
Div 1541
Box 5800
Albuquerque, NM 87115

Southwest Research Institute
Attn: Dr. K. S. Chan
P. O. Drawer 28510
San Antonio, TX 78284

Teledyne CAE
Attn: Hugh Gaylord
Mgr, Explor Dev Appl
Toledo, OH 43612

Teledyne CAE
Attn: Jerry Walcher
Box 6971
Toledo, OH 43612

| 1.REPORT NO. NASA CR-179594 | 2. GOVERNMENT AGENCY | 3.RECIPIENT'S CATALOG NO. |
|---|---|---|
| 4.TITLE AND SUBTITLE<br>Life Prediction and Constitutive Models for Engine Hot Section Anisotropic Materials | | 5. REPORT DATE<br>April 1987<br>6. PERFORMING ORG. CODE<br>533-04-11 |
| 7.AUTHOR(S)<br>G. A. Swanson, I. Linask, D. M. Nissley, P. P. Norris, T. G. Meyer and K. P. Walker | | 8. PERFORMING ORG. REPT. NO.<br>PWA-5968-47 |
| 9.PERFORMING ORG. NAME AND ADDRESS<br>UNITED TECHNOLOGIES CORPORATION<br>Pratt & Whitney, Engineering Division<br>400 Main St., East Hartford, CT 06108 | | 10. WORK UNIT NO.<br>11. CONTRACT OR GRANT NO.<br>NAS3-23939 |
| 12. SPONSORING AGENCY NAME AND ADDRESS<br>National Aeronautics and Space Administration<br>Lewis Research Center<br>21000 Brookpark Road, Cleveland, Ohio 44135 | | 13. TYPE REPT./PERIOD COVERED<br>Second Annual Status Report<br>14. SPONSORING AGENCY CODE |

15. SUPPLEMENTARY NOTES

Project Manager: R. C. Bill
NASA-Lewis Research Center, Cleveland, Ohio

16. ABSTRACT

This report presents the results of the second year of a program designed to develop life prediction and constitutive models for two coated single crystal alloys used in gas turbine airfoils. The two alloys are PWA 1480 and Alloy 185. The two oxidation resistant coatings are PWA 273, an aluminide coating, and PWA 286, an overlay NiCoCrAlY coating. To obtain constitutive and fatigue data, tests were conducted on uncoated and coated specimens loaded in the <100>, <110>, <111> and <123> crystallographic directions. Two constitutive models are being developed and evaluated for the single crystal materials: a micromechanics model based on crystallographic slip systems, and a macroscopic model which employs anisotropic tensors to model inelastic deformation anisotropy. Based on tests conducted on the overlay coating material, constitutive models for coatings also appear feasible and two initial models were selected. A life prediction approach has been proposed for coated single crystal materials, including crack initiation either in the coating or in the substrate. The coating initiated failures dominated in the tests at load levels typical of gas turbine operation. Coating life was related to coating stress/strain history which was determined from specimen data using the constitutive models.

| 17. KEY WORDS (SUGGESTED BY AUTHOR(S)) | 18. DISTRIBUTION STATEMENT |
|---|---|
| Life Prediction, Constitutive Models, Single Crystal Alloys, Anisotropic Materials, Gas Turbine Engine, Airfoils | General Release |

| 19. SECURITY CLASS THIS (REPT) | 20. SECURITY CLASS THIS (PAGE) | 21. NO. PGS | 22. PRICE * |
|---|---|---|---|
| Unclassified | Unclassified | | |

* For sale by the National Technical Information Service, Springfield, VA 22161